Protection of Multi-Inverter Based Microgrid Using Phase Angle Trajectory

Jerome Nsengiyaremye

Thesis submitted for the degree of

Doctor of Philosophy

Imperial College London

Department of Electrical and Electronic Engineering

Control and Power Research Group

June 2021

Declaration of Originality

I hereby declare that all the work reported in this thesis is my own, conducted in the Control and Power (CAP) Research Group, Department of Electrical and Electronic Engineering, Imperial College London from October 2017 to June 2021. The work of others has been properly acknowledged.

Jerome Nsengiyaremye

June 2021

Copyright Declaration

The copyright of this thesis rests with the author and is made available under a Creative Commons Attribution Non-Commercial No Derivatives licence. Researchers are free to copy, distribute or transmit the thesis on the condition that they attribute it, that they do not use it for commercial purposes and that they do not alter, transform or build upon it. For any reuse or redistribution, researchers must make clear to others the licence terms of this work.

To my family

Abstract

This thesis presents a simple, yet a clever way of using the current phase angle to develop low-bandwidth communication-assisted line protection strategies for medium and low voltage AC microgrids, particularly those with multi-inverter interfaced distributed generators. It is now a trend in both AC transmission and distribution segments of power network that inverters interface renewable energy to the system. Unlike synchronous generators the fault feeding, and control characteristic of these generators are different and mostly influenced by the topology, switching, control deployed in the power electronics interface. The limited and controlled fault current challenges the existing conventional protection schemes. Offering higher power supply reliability and system resilience than conventional radial distribution systems, multi-inverter based microgrids, particularly those with loop and mesh typologies, are characterised by bidirectional power flow. This further constrains traditional protections such that communication-less protection schemes become ineffective for such systems. So unit protection types, such as differential protection, become more technically suitable for such microgrids despite the necessity for a communication system.

In this thesis, two current direction based protection schemes for medium voltage islanded microgrids have been developed. The change in current flow direction in a line is detected using the cosine of the positive sequence current phase angle. Expressing the change and no-change of the flow directions as binary states, a low bandwidth communication based protection scheme is proposed comparing the binary states from local and remote ends of the line. To further enhance the scope and reliability of this scheme, a second protection scheme is proposed in Chapter 7 whereby the cosine function is combined with the rate of change of the slope of the phase angle (ROCOSP). This combination allows the detection and isolation of a fault even with the failure of the communication channel between relays protecting a faulted line. Furthermore, these scheme can work together and share the communication infrastructure as primary and backup protections. The performance of these schemes was assessed through simulations of microgrid models developed in Matlab/Simulink.

Acknowledgements

I would like to express my heartfelt gratitude to Prof. Bikash Chandra Pal, for giving me the opportunity to pursue the PhD degree under his supervision. Without his guidance, encouragement, patience and support, I would not achieve this milestone. It is an honour for me to have worked alongside and learnt from this generous, inspiring and exceptional researcher.

I would also like to deeply thank Prof. Miroslav M. Begovic of Texas A&M University for the insightful discussions we had throughout my research that have enhanced my understanding of power systems. I am appreciative of his valuable time and dedication offered to my research. His constructive and critical suggestions have improved my research and skills. I learnt a lot from his expertise and experience, both technically and professionally.

I would like to thank staff and colleagues at the Control and Power Research Group, especially, Adria, Firdous, Onyema, Nicolas, Georgios, Stratis, Kevin, Magne, Adeyemi, Sowmya, Naveed, Diptargha, Yifei, Malek, Husni, Linash, Ankur, Olayinka, Freddy, Daryl, and Jochen for contributing to a friendly working environment during my time at Imperial College.

Special thanks to the Commonwealth Scholarship Commission (CSC) and Imperial College London for the financial support for my PhD study.

I simply cannot find words to express my gratitude to my wife, Norbertine, my son, Jessy, and my daughters, Jessica and Jelia, whose constant loving support and sacrifice were pivotal to reaching this milestone.

I finally thank God for his grace.

Contents

Abstract **4**

Acknowledgements **5**

List of Abbreviations **16**

1 Introduction **18**

1.1 Background 19

1.2 Protection Parameter Choice Considerations 20

1.3 Cost Driver 21

1.4 Research Contributions and Dissemination 22

1.5 Outline of Thesis 24

2 Literature Review **25**

2.1 Active Distribution Networks 26

2.2 Microgrids and Operational Behaviour of IIDGs 27

2.2.1 Inverter Interfaced Distributed Generators (IIDGs) 28

2.3 Microgrid Protection 37

2.4 Conclusions 42

3 IIDGs and Microgrid Fault Behaviour **44**

3.1 Introduction 44

3.2 Behaviour in Grid-Connected Operation Mode 48

3.2.1 Three-phase fault 49

3.2.2 Single phase to ground fault 49

3.3 Behaviour in Islanded Operation Mode 54

3.3.1 Three-phase fault 54

3.3.2 Single phase to ground fault 55

3.3.3 The impact of feedforward compensation 56

3.4 The Comparison of System Fault Behaviour in Grid-Connected and Islanded Operation Modes 58

3.5 Conclusions 61

4 Current Phase Angle for Microgrid Protection **62**

4.1 Introduction 62

4.2 Advantages of Positive Sequence Current Phasor 64

4.3 Microgrid Line Characteristics and Detection of Change in Direction of Current Flow 64

4.4 Conclusions 70

5 Estimation of phasors **72**

5.1 Introduction 72

5.2 Numerical Relays 73

5.3 Sampling Theorem . . . 75
5.4 Phasor Representation of a Sinusoid . . . 77
5.5 Phasor Estimation Using Least-Square Technique . . . 78
5.6 Phasor Estimation Using Fourier Algorithms . . . 80
5.6.1 Discrete Fourier Transform . . . 81
5.6.2 Phasor estimation using full cycle DFT . . . 85
5.7 DFT Phasor Estimates Updates . . . 86
5.7.1 Non-recursive DFT method . . . 87
5.7.2 Recursive method . . . 88
5.8 Phasor Estimation Challenges in Real Power System . . . 90
5.9 Positive Sequence current Phasor Estimation . . . 93
5.10 Conclusions . . . 94

6 Protection Scheme Using Current Phase Angle Trajectory 95

6.1 Introduction . . . 95
6.2 Protection Operation Principle . . . 95
6.3 Low-Cost Communication System . . . 99
6.3.1 Practical considerations of low-cost communication system with the proposed protection scheme . . . 99
6.4 Simulation Scenarios and Results Discussion . . . 101
6.4.1 Microgrid study system and assumptions . . . 101
6.4.2 Simulation scenarios . . . 105
6.4.3 Simulation results and discussion . . . 106

6.5 Conclusions 113

7 Protection Scheme Using Phase Angle Trajectory and ROCOSP 114

7.1 Introduction 114

7.2 Disturbance Detection 115

7.3 Identification of the Faulted Line 117

7.4 Study Microgrid and Simulation Results 121

7.4.1 Detection of disturbance occurrence in the microgrid 125

7.4.2 Identification of the faulted line 127

7.5 Conclusions 134

8 Conclusions and Future Work 135

8.1 Summary of the Work 135

8.2 Future Work 136

8.2.1 Microgrid protection using current phase angle trajectory without communication system 136

8.2.2 Protection speed improvement using fractional cycle DFT estimation technique 136

8.2.3 The impact of energy resources variation on the behaviour of power electronic based power sources 137

8.2.4 Performance of current phase angle trajectory considering distribution automation systems 137

Bibliography 138

List of Tables

2.1 Comparison of protection schemes proposed in the literature 39

3.1 IIDGs parameters 45

3.2 Connections and line parameters of European MV Distribution network benchmark [107] 47

3.3 Load parameters of European MV Distribution network benchmark [107] 48

3.4 IIDGs and network behaviour in grid-connected and islanded operation modes . . . 60

6.1 Comparison of communication system delays of different message sizes 101

6.2 Microgrid system parameters 104

6.3 Performance of the proposed protection scheme for the Reference Scenario 108

6.4 Performance of the proposed protection scheme for Scenario 1 109

6.5 Performance of the proposed protection scheme for Scenario 2 110

7.1 Study microgrid parameters 124

List of Figures

2.1 Simplified representation of grid-connected power converters: (a) Grid-forming, (b) Grid-feeding, (c) and (d) GSGFm and GSGFd respectively [43, 44] 30

2.2 Fundamental structure of basic PLL: (a) dqPLL, (b) $\alpha\beta$PLL [63, 64]. With abc/dq - the transformation (Park transform) of three phase voltages (V_{abc}) to synchronous direct and quadrature components V_d and V_q, θ_{PLL} - estimated phase of the voltage signal, ω_{nom} - nominal voltage frequency, ω_{PLL} - estimated voltage frequency, $\Delta\omega$ - PI controller output signal 32

2.3 Basic structure of voltage source control 35

2.4 A model of a constant current-controlled inverter 35

2.5 Equivalent phase networks of a three-phase inverter 36

3.1 Microgrid study network [Adapted from [107] 46

3.2 IIDGs output current and voltage in grid-connected operation mode with a three-phase fault on Line 3-4 considering Delta-Wye transformer configuration: **(a)** IIDG 1 (PQ control loop with latched current limiting strategy) **(b)** IIDG 3 (constant current control strategy)) **(c)** IIDG 5 (PQ control loop with saturation current limiting strategy) 50

3.3 IIDGs output current and voltage in grid-connected operation mode with a three-phase fault on Line 3-4 considering Wye-Wye transformer configuration: **(a)** IIDG 1 (PQ control loop with latched current limiting strategy) **(b)** IIDG 3 (constant current control strategy)) **(c)** IIDG 5 (PQ control loop with saturation current limiting strategy) 51

3.4 IIDGs output current and voltage in grid-connected operation mode with a single-phase to ground fault on Line 3-4 considering Delta-Wye transformer configuration: **(a)** IIDG 1 (PQ control loop with latched current limiting strategy) **(b)** IIDG 3 (constant current control strategy)) **(c)** IIDG 5 (PQ control loop with saturation current limiting strategy) 52

3.5 IIDGs output current and voltage in grid-connected operation mode with a single-phase to ground fault on Line 3-4 considering Wye-Wye transformer configuration: **(a)** IIDG 1 (PQ control loop with latched current limiting strategy) **(b)** IIDG 3 (constant current control strategy)) **(c)** IIDG 5 (PQ control loop with saturation current limiting strategy) 53

3.6 IIDG 1 output and control signals in islanded operation mode with interfacing transformer in Delta-Wye configuration with a three-phase fault on Line 3-4 55

3.7 IIDG 1 output and control signals in islanded operation mode with interfacing transformer in Wye-Wye configuration with a three-phase fault on Line 3-4 56

3.8 IIDG 1 output and control signals in islanded operation mode with interfacing transformer in Delta-Wye configuration with a single phase to ground fault on Line 3-4 . 57

3.9 IIDG 1 output and control signals in islanded operation mode with interfacing transformer in Wye-Wye configuration with a single phase to ground fault on Line 3-4 . . 57

3.10 IIDG 1 output and control signals without a feedforward compensation in islanded operation mode with interfacing transformer in Delta-Wye configuration with a single phase to ground fault on Line 3-4 58

3.11 IIDG 1 output and control signals with a filtered feedforward compensation in islanded operation mode with interfacing transformer in Delta-Wye configuration with a single phase to ground fault on Line 3-4 59

4.1 Lumped π section model of a line/cable 65

4.2 Two IIDG system 66

4.3 Positive sequence equivalent circuit of the system in Fig. 4.2 66

4.4 Positive sequence equivalent circuit of the system in Fig. 4.2 with IIDGs replaced by synchronous generators 68

4.5 Comparison of positive sequence pre-fault and fault current phasors 69

4.6 Comparison of positive sequence pre-fault and fault current phasors with change of flow direction 70

5.1 Conceptual Diagram of a Relay 73

5.2 Relaying Computer Concept [113] 74

5.3 Time-domain aliasing illustration 76

6.1 Fault detection strategy: (a) principle (b) phasor estimation 98

6.2 Study microgrid system 102

6.3 Voltage source control 102

6.4 Voltage and current signals measured at PCC (at the output of the filter) for different fault conditions (three phase fault (3Φ), single phase to ground fault (Φ-G), and phase to phase fault (Φ-Φ)) 103

6.5 The cosine values computed by relays for a three-phase fault on Line L_{BE} 107

6.6 The illustration of current flow direction through the lines before and after a three-phase fault on Line L_{BE} 107

6.7 The cosine values computed by relays with a fault on Line L_{BE}: (a) solid line to ground fault; (b) line to ground fault with a fault resistance of 100 Ω; (c) solid line to line fault; (d) line to line fault with a fault resistance of 100 Ω 111

6.8 The cosine values computed by relays with a line to ground fault on Line L_{BE} at $t = 0.1\,s$ with: (a) IIDGs frequency of 49 Hz; (b) IIDGs frequency 45 Hz; (c) IIDGs frequency of 51 Hz; (d) IIDGs frequency 55 Hz 113

7.1 Example of a case with a tapped line (tap point B) 119

7.2 Coordination of Relays with the largest load at the tap point B 120

7.3 Coordination of Relays with the largest load at Bus A 120

7.4 Relay coordination for load switching event causing change of current flow direction seen by Relays 2 and 3 121

7.5 Four-bus loop-based microgrid 122

7.6 IIDG control structure 122

7.7 IIDGs voltage and current output during different types of fault 123

7.8 Simulation results for two different operating frequencies (50 and 52 Hz) for a load switching event at Bus B causing a change in current flow direction in the line protected by Relay 4: (a & e) cosine values computed by all relays; (b & f) phase angle difference between the two consecutive cycle estimates (degrees); (c & g) slope of the positive sequence current phasor angle (Hz); and (d & h) rate of change of the phase angle slope (ROCOSP in Hz/s) 126

7.9 Simulation results for a three-phase fault on Line L_{AB}: Cosine and ROCOSP values estimated by relays with operating frequency of: (a & b) 50 Hz; (c & d) 52 Hz; (e & f) 48 Hz 128

7.10 Current flow direction during normal operation (green) and during a fault on line L_{AB} (Orange) 129

7.11 Simulation results for a Phase A to ground fault on Line L_{BC}: (a) Cosine values estimated by all relays; (b) ROCOSP values estimated by master relays 130

7.12 Current flow direction during normal operation (green) and fault (orange) on Line L_{BC} 130

7.13 Simulation results for a fault on Line L_{EF}: (a) Cosine values estimated by all relays; (b) ROCOSP values estimated by master relays 131

7.14 Current flow direction during normal operation (green) and fault (orange) on Line L_{EF} 132

7.15 Cosine and ROCOSP values for a fault on Bus B in the microgrid constituting of: (a) purely resistive loads and only IIDGs; (b) purely resistive loads and only synchronous-based DGs; (d) inductive loads and only IIDGs; (e) inductive loads and only synchronous-based DGs; (c) Illustration of current flow direction during normal (green) and fault operating conditions (orange) 133

List of Abbreviations

$\alpha\beta PLL$	Stationery Reference Frame Phase-Locked Loop
AC	Alternating Current
ADN	Active Distribution Network
BER	Bit Error Rate
3EPLL	Three-Phase Enhanced Phase-Locked Loop
CT	Current Transformer
CTFS	Continuous Time Fourier Series
CTFT	Continuous Time Fourier Transform
d$\alpha\beta PLL$	Decoupled Stationary Reference Frame Phase-Locked Loop
DC	Direct Current
DDSRF-PLL	Decoupled Double Synchronous Reference Frame Phase-Locked Loop
DER	Distributed Energy Resource
DFT	Discrete Fourier Transform
DG	Distributed Generator/Generation
dqPLL	Synchronous Reference Frame Phase-Locked Loop
DSOGI-PLL	Double Second Order Generalized Integrator Phase-Locked Loop
DSRF-PLL	Dual Synchronous Reference Frame Phase-Locked Loop
DTFS	Discrete Time Fourier Series
DTFT	Discrete Time Fourier Transform
EPLL	Enhanced Phase-Locked Loop
EPMAFPLL	Enhanced Pre-filtering Moving Average Filter based Phase-Locked Loop
FFT	Fast Fourier Transform
FLL	Frequency-Locked Loop
GSGFd	Grid-Supporting Grid-Following/Feeding inverter

GSGFm	Grid-Supporting Grid-Forming inverter
HIHDO	Harmonic-Interharmonic-DC- Offset
IIDER	Inverter-Interfaced Distributed Energy Resource
IIDG	Inverter-Interfaced Distributed Generator/Generation
ISL	Instantaneous Saturation Limit
LF	Loop Filter
LL	Latched Limit
LPN-PLL	Low-Pass Notch filter Phase-Locked Loop
LSE	Least Squares Estimation
LV	Low Voltage
LVRT	Low Voltage Ride-Through
MAF	Moving Average Filter
MAFPLL	Moving Average Filter based Phase-Locked Loop
MV	Medium Voltage
PCC	Point of Common Coupling
PD	Phase Detector
PF	Power Factor
PI	Proportional Integral
PID	Proportional Integral Derivative
PLL	Phase-Locked Loop
PMAFPLL	Pre-filtering Moving Average Filter based Phase-Locked Loop
PV	Photovoltaic
ROCOF	Rate of Change of the Frequency
ROCOSP	Rate of Change of the Slope of the Phase angle
S/H	Sample and Hold
SG	Synchronous Generator
UART	Universal Asynchronous Receiver Transmitter
UK	United Kingdom
USA	United States of America
VCO	Voltage-Controlled Oscillator

Chapter 1

Introduction

Research on microgrid protection has recently received much interest as it plays an essential part to achieving the success of microgrid operation. Microgrid is one of the most promising approaches to (i) renewable energy integration in power system, (ii) power system flexibility and resilience, (iii) sustainability of power supply, and rural electrification, where investment in main grid expansion may not be justified. Furthermore, with the use of local energy sources, communities get to appreciate and develop a sense of preservation towards the environment we live in.

However, there is a two-faced challenge in developing and designing microgrid protection systems. On one hand, the cost of microgrid protection should be aligned with the expected cost of the protection system in a typical equivalent distribution network. Unfortunately, traditional protections used in distribution systems are not technically effective for microgrids due to multiple sources of fault currents with diverse behaviours in many cases, particularly limited and controlled fault currents from inverter-interfaced distributed generators (IIDGs). On the other hand, the cost of protection systems for power transmission infrastructure is very high and may not be economically viable relatively low-investment systems. Furthermore, in addition to uncommon behaviours of IIDGs during faults, line lengths of microgrids may not be sufficiently long to provide zoned protection, distance relays and traditional directional overcurrent relays are likely to fail [1].

The limits in the availability of suitable protection systems is one of major reasons, along with other operational challenges, that microgrids are not practically prevalent despite their obvious benefits. However, with deep understanding of the behaviour of renewable energy-based generators, particularly power electronic converters interfacing the source to the network, during normal and

fault operation states, and the impact such behaviour has on the whole microgrid, it may be possible to develop affordable protection systems. Current directionality feature based on monitoring current phase angle trajectory and low-cost communication systems are considered to potentially serve such a purpose. Affordable and robust microgrid protection systems could not only be used in distribution systems with IIDGs but also may inspire the development of novel and more low-cost protection systems for power transmission infrastructure, particularly systems encompassing power electronic-based power sources.

1.1 Background

Microgrid is not a brand new concept. It dates back to the beginning of power system industry in the end of 19^{th} century. The first one was introduced by Thomas Edison in 1882 at his Manhattan Pearl Street Station, which combined heat and power. Four years latter, Edison's firm had installed 58 Direct Current (DC) microgrids. Although they have not always been called microgrids, these represent an early example of systems where a group of loads and distributed energy resources can be controlled as a single electrical system.

While university campuses have been using microgrids for decades and shown that microgrids can be compatible with local utility grids and provide benefits to both the campuses and the larger grids, a series of natural disasters in 2011-2012 in the United States and Japan heightened interest in microgrids, when microgrid operators, Princeton University in the US and Sendai Microgrid in Japan, showcased how microgrid technology kept power on when the central grid failed during both Sandy Storm and Great East Japan Earthquake respectively. Over the past two decades, microgrid concept has attracted a lot of attention of researchers in power systems. With imminent high penetration level of Distributed Energy Resources (DERs) - mainly inverter interfaced DERs (IIDGs) - into traditional distribution networks (medium and low voltage), microgrids have been regarded as a promising approach to these local energy resources integration [2–10]. With this approach, the capability of microgrids to operate in grid-connected and islanded modes, offers an opportunity to enhance reliability, flexibility, security and energy efficiency of power supply [3–6, 8, 11]. Successful demonstration of microgrid projects have showcased promising practical implementation of this concept. It is worth mentioning some representative examples of microgrids around the world: Illinois Institute of Technology Microgrid, USA [12]; Isle of Eigg Microgrid (off-grid), UK [13]; Sendai Microgrid, Japan [14], and Gaidouromantra microgrid in Kythnos island, Greece [15].

Despite the potential of enabling the exploitation of local renewable energy resources for electricity supply to remote areas, as autonomous generation systems, or for integration to local distribution systems, microgrid concept implementation has not been straightforward. Integrated in the main grid, microgrids can operate in grid-connected or islanded mode, which enhances the grid power supply reliability. Ensuring dual-mode operation, development of new protection schemes, ensuring stable operation during faults and disturbances as well as the development of new voltage and frequency control techniques have impeded large-scale uptake of microgrids [3, 16, 17]. The cause of these issues is the complex and different behaviour of IIDGs from conventional synchronous generators. This unlikely behaviour mostly originates from their low inertia, variable internal voltage source, limited synchronisation capability and low fault current contributions [18]. The designing and understanding of protection schemes for power system requires a comprehensive understanding of its normal operation and control, the fault models of its components and the impact of the behaviour of each component and their interaction with the rest of the system. A great deal of research has been undertaken on the above three aspects for microgrid protection and new protection schemes have been proposed. However, there is still a lack of widely recognised and established microgrid protection strategy. This thesis will present microgrid protection systems using low-cost communication system; providing the IIDGs behaviour during faults seen from the inverter output and from the microgrid network; introducing a current directionality estimation concept using current phase angle trajectory, intended for specific applications such as line protection of multi-IIDGs based microgrids. Unlike most schemes proposed in the literature that attempt to adapt conventional distribution or transmission-based protections to microgrids - which tend to limit them to specific scopes such as microgrid topology, and inverter control strategy, among others [1, 19] - the choice of the protection parameters under this research recognizes fault behaviour of IIDGs such as controlled, limited and relatively balanced fault currents.

1.2 Protection Parameter Choice Considerations

While microgrid protection has attracted a big deal of research, the majority of protection schemes proposed in the literature tend to adapt conventional protection schemes to establish their effectiveness. Despite this effort, it seems that this approach might not be appropriate as the effectiveness of a protection scheme depends on the operational conditions of the system to be protected. On the other hand, other proposed protection schemes that might effectively work are based on complex algorithms that require many input parameters from both current and voltage measurements.

This level of parameter requirement leads to high cost that might not be reasonably acceptable in distribution systems investment decision.

Research studies recently undertaken based on data mining have identified a list of parameters that may be appropriate for microgrid protection [20–22]. It has been revealed that symmetrical components of voltage and current signals contain significant information for fault discrimination, particularly positive and negative sequence components [20, 21]. Furthermore, the latter parameters together with power factor angle top the feature list for fault localisation [21].

Consequently, one can conclude that both positive and negative sequence components of the current contain significant information useful for both fault detection and localisation. With positive sequence component feature having an advantage of existing for all types of faults, this makes it a potential microgrid protection parameter, and it is the one adopted in this research work.

While the above features can detect and localise the fault, to achieve 100% accuracy is difficult especially for fault localisation in islanded microgrid. Fortunately, [20] provide an answer to the question whereby it is demonstrated that differential quantities can provide high level of accuracy for protection than quantities measured at only one end of the line. This increases the suitability of positive sequence current phasors for multi-inverter microgrid protection. Nevertheless, recalling that IIDGs generate fault current restricted to a maximum value close to the rated current, one can derive that the phase angle of the current phasor contains most of the fault information.

1.3 Cost Driver

The cost of a protection system depends on the cost and number of measurement devices and relays required to protected a line as well as the cost of communication system for communication-assisted protection strategies.

Considering that this research has adopted currents measured from both ends of the line (local and remote ends), only current transformers (CTs) and microprocessor-based relay are required at each end. There is no requirement for voltage measurements, which limits the cost to only CTs. The main question lies on the cost of communication system.

It is a conventional principle that the communication system infrastructure should meet the protection algorithm communication requirements. This is evident in most communication-assisted

protection schemes proposed in the literature where the communication system is not comprehensively covered by assuming that the communication infrastructure that meets the requirements is available. However, in distribution system and microgrids, this assumption does not seem appropriate due to the cost limitation. Therefore to address this issue, an opposite analysis approach to the conventional approach should be adopted. This means that the proposed protection algorithm output data size should be as optimally minimum as possible to allow the use of low-bandwidth communication infrastructure.

The overall cost of a communication system comprises the cost of the communication equipment (physical link and interfaces), the installation cost (work and labor), the required installation time, and its reliability. The cost comparison analysis of existing communication systems for protection including fiber optics, power line carrier, leased telephone lines, licensed microwave radio and unlicensed microwave radio has shown that the latter practically being by far the cheapest technology for transmission lines of less than 21 miles in length [23]. Its low cost is due to the nonrequirement of right of way, low installation cost, low cost of labor (no specialized expertise), and short installation time [23–26]. A detail assessment of the possibility of using such a communication system with protection schemes proposed in this work is provided in Chapter 6. It is important to highlight that fiber optic communication technology is the most expensive compared with rest. It is approximately 40, 65, 85 and 430 times expensive per mile for a 20 mile-link of power line carrier, leased telephone line, licensed radio and unlicensed radio respectively [23]. This low-cost communication technologies are characterised by low bandwidth. They are mostly used for teleprotection but fall short for most other protection schemes such as differential protections with high-bandwidth communication requirement.

1.4 Research Contributions and Dissemination

Most of the proposed protection schemes in the literature for inverter based microgrids try to adapt conventional transmission based protection schemes leading to their application limitation as demonstrated by recent studies. The choice of the protection parameter - the positive sequence current phase angle - under this thesis stemmed from the insight provided by different literature on the search for potential and suitable features for protection of distribution systems with power electronic based power sources using data mining techniques. The analysis of such different features such as positive and negative sequence voltage and current magnitudes, power factor angle and differential feature has led to the identification of the positive sequence current phase angle as the protection parameter

that can be more appropriate for islanded microgrids. The reasons behind this choice are provided in Chapter 4. This analysis can be the basis for identifying and deriving more suitable protection features from the current phase angle.

The major contribution and, to a certain extent, the primary novelty of the work in this thesis has been the estimation of current directionality change in a line using two new concepts: 'the cosine' of the current phase angle and 'the rate of change of the slope of the phase angle (ROCOSP)'. The directionality of the current in a line has traditional been based on the comparison of current phase angle and the voltage as a polarising quantity. This is because in transmission systems both current and voltage measurement devices are available and their cost can be justified. However, in distribution systems voltage measurement devices do not exist at every single node. So based on the literature on only current fault direction estimation, the cosine and ROCOSP concepts were developed to detect a change in current flow direction using only the current signal.

Another major contribution is the development of two line protection strategies based on the cosine and ROCOSP, that recognises not only typical fault characteristics of IIDGs but also the lack of detailed IIDG fault models by considering general operation states of the system such as current directionality. Furthermore, to ensure that the proposed protection strategies do not required high-bandwidth communication systems that are associated with high cost, minimum size information extraction from three-phase currents in the form of binary states has been established with a case study of unlicensed microwave radio, a low-cost communication technology.

The following publications have arisen from this work:

- J. Nsengiyaremye, B. C. Pal and M. M. Begovic, "Microgrid Protection Using Low-Cost Communication Systems," *in IEEE Transactions on Power Delivery,* vol. 35, no. 4, pp. 2011-2020, Aug. 2020, doi: 10.1109/TPWRD.2019.2959247.
- J. Nsengiyaremye, B. C. Pal and M. M. Begovic, "Low-Cost Communication-Assisted Line Protection for Multi-Inverter Based Microgrids," *in IEEE Transactions on Power Delivery,* doi: 10.1109/TPWRD.2020.3039176.

1.5 Outline of Thesis

The work presented in this thesis describes development of microgrid protection strategies using current phase angle trajectory approach and will be organised as follows:

- Chapter 1 has introduced the background of microgrid concept and provided protection parameter choice considerations and cost requirements for the proposed protection strategy. It also addressed author's original contributions.
- Chapter 2 will provide a literature review of protection systems starting with the control and behaviour of inverter-interfaced distributed generators (IIDGs) during normal and fault conditions.
- Chapter 3 will demonstrate the behaviour of the IIDGs and their impact on the rest of the system using simulations of a case study with Specific control assumptions.
- Chapter 4 will discuss the choice of positive sequence current phase angle as a parameter for microgrid protection adopted.
- Chapter 5 will discuss the estimation of phasors, from which the current phase angle is derived. The challenges related to phasor estimation in real power systems are also discussed and how they can be overcome.
- Chapter 6 will provide the concept of phase angle trajectory and a protection scheme based on this concept.
- Chapter 7 will build on the protection scheme in Chapter 6 to develop a more powerful scheme that can operate even when there is a failure of the communication channel between relays protecting a faulted line. This protection scheme can work as a main protection on its own or a back-up to the one proposed in Chapter 6.
- Chapter 8 summarises the work discussed in this thesis and provides suggestions for future research.

Chapter 2

Literature Review

In this chapter, a literature review on IIDGs, microgrids, and their associated protection schemes proposed in the literature will be presented. This review will be divided into four sections:

1. Active distribution networks. In this section, the transition from passive distribution networks to active distribution systems will be documented. This aims to provide the operational requirements of active distribution systems and operational challenges brought by the integration of DGs in conventional protection practices.

2. Microgrids and operational behaviour of IIDGs. In this section, a review on islanded microgrids will be provided. This aims to provide the difference between a grid-connected system and islanded network. The latter's characteristics will be highlighted as well as different IIDGs operational behaviour during normal operation and during disturbances and the limitation of conventional protection schemes.

3. Microgrid protection. Here, a review of microgrid protection will be provided along with the context and limitation of different proposed protection schemes in the literature.

4. Conclusions. Under this section, a summary of this chapter will be provided and reasons why there is still a need for new microgrid protection schemes.

2.1 Active Distribution Networks

Traditional distribution systems have been characterised by power flowing from secondary substation to the consumption point (unidirectional power flow). This goes along with the traditional radial topology that had dominated distribution networks; medium voltage and low voltage. With such a configuration, distribution system protection against overcurrent and short-circuit has been straightforward using current magnitude i.e. fuses and overcurrent relays.

With the integration of distributed generation, distribution power systems are no longer passive in nature but have become active and the long-established planning, operation, and protection practices have become ineffective in active distribution networks (ADN) due to the departure from traditional radial topology and different fault behaviour, which totally change the type of protection that is possible to use.

To keep conventional operational practices, in the recent past, distributed generators (DGs) have traditionally been controlled and protected based on self-preservation approach in fault conditions [27]. In the past this was ideal as DGs were required to instantly disconnect from the network when a fault occurred in the system. Such operation of DGs would allow overcurrent protections to operate based on their conventional setting and grading approach. However, with the increase in penetration level, DGs are required to remain connected during faults for a certain period of time depending on their category [27]. This fault ride through capability requirement obliges distribution network operators to review their protection strategies. The challenges on traditional distribution protections are more significant from DGs connected to medium voltage (MV) systems as the impact of DGs connected to very low single-phase voltage levels is limited, even negligible for faults far from the DG [28]. Nevertheless, the aggregated impact of these generators should not be ignored.

The integration of DGs not only affects distribution system protections but also may compromise transmission system protections and the operation of other system components such as circuit breakers, lines, and transformers [29]. For example, if the capacity of DGs connected upstream the fault location is large, the fault current may cause high thermal and mechanical stress on a transformer, busbars and lines. Furthermore, the current may exceed the breaker's capacity. On the other hand,if the capacity of the DGs connected downstream of the fault location is large, the fault current contribution from the grid will relatively decrease compared to the situation with no DG. This may result in protection misoperation, delays in fault detection and fault clearance or miscoordination of protections [29].

For example, recent power cut incidents, major and minor, reported in UK power systems involved DGs due to the wrong setting of their loss of mains protection i.e. ROCOF and Vector shift protections [30, 32, 35]. The incident of May 2016 is worth mentioning whereby around 400 MW of distributed generation was disconnected from the system [30]. However, with misoperation of vector shift and ROCOF protections in a series of incidents, Vector shift protections were banned and the ROCOF settings were revised from 0.125 Hz/s to 1 Hz/s with a delay of 0.5 s in G59 version 3 amendment 3 for IIDGs $> 5MW$ and in the new standard (G99) for all categories of IIDGs ($> 0.8kW$) to ensure system security. There are still concerns on the ROCOF protection settings, however, as phase jump resulting from faults may cause sharp change in ROCOF values, which does not mean necessarily the islanding condition, particularly in small networks [30,33]. This is emphasised by recent incident in UK, where over 1 million customers were affected by a major power disruption that occurred across England and Wales and some parts of Scotland with about 500 MW of DGs disconnected. Also, noise, off-nominal frequencies and interharmonics may cause erroneous ROCOF measurements that may jeopardize the ROCOF relay reliability [33].

2.2 Microgrids and Operational Behaviour of IIDGs

Microgrid concept has not only been seen as one of strategies for power system decarbonisation through local renewable energy integration but also as a promising approach to power system resilience. The need for power system resilience has been accentuated by worldwide catastrophic events such as bushfires in Australia, floods in United Kingdom, storms in Americas, earthquakes in the pacific region that caused blackouts affecting millions of customers. With most of the renewable energy resources locally available, along with the availability of cost-effective power electronic conversion technology, the formation of distribution islands encompassing a group of loads and DGs that can be controlled and operated as a single unit has become more realistic than before and can help mitigate the adverse impact of the extreme events [34]. This is particularly true when the islanded microgrid encompasses a different mix of power generation technologies and underground cables, which makes the system more resilient and robust. This has been demonstrated by the Princeton University microgrid in the United Stated and Sendai Microgrid in Japan, that kept power on when the central grids failed during Sandy Storm and Japan Earthquake respectively. It is most likely, therefore, that many distribution feeders will evolve into microgrids that could be operated in grid-connected or islanded mode to enhance the system resilience and service reliability.

The need of operating microgrids on-grid or off-grid constrains further the design of distribution

system protections as faults become much harder to detect, particularly in islanded mode of operation [35]. With a variety of DG types and a wide range of control strategy possibilities that can be adopted in those DGs, their interaction among DGs and with the rest of the system devices such as power transformer, and the grounding method, create a complexity of constraints that render the design of generic protections for distribution systems with DGs challenging. The change in topology of distribution feeders from radial to transmission-like topology does not guarantee the application of transmission-based protection systems [1]. Not only they are challenged by different DG fault behaviours, but also by short lines and low voltage characteristics limit their applicability. That is the reason why the current practice is to design protection systems based on a case-by-case basis [36].

2.2.1 Inverter Interfaced Distributed Generators (IIDGs)

While the operation of synchronous generators (SGs) is a well-established practice, the one for power electronic based power sources, IIDGs in this case, is not, particularly during disturbances. This is because the behaviour of these generators depends on the behaviour of the power electronic converter interfacing the resource to the network. The design requirements of these devices depends mainly on the guidelines set by interconnection codes and the specific manufacturer's design. Establishing these guidelines has been a learning experience for power system community. This can be seen from steady changes made since the first integration of IIDG in power system [37]. The changes in performance guidelines have resulted in changes in design and models of power electronic converters accordingly. For example, with fast dynamics of power system dominated by IIDG, current grid-following inverter-based power sources technology cannot alone maintain system stability, support system recovery and system resilience. This has brought new functional requirements: grid-forming inverter-based power source technology [38]. Recalling that a power system can be in either of the following operational states: normal, alert, emergency, blackout, or restoration [39], to achieve resilient power system, a deep understanding of the behavior of existing IIDG technologies and the power system required performances in each of the states is key. This can be achieved through the development of accurate individual and aggregate dynamic models of IIDGs taking into account the interactions between these devices and the rest of the power system. However, modelling and simulating a system encompassing multiple technologies (including legacy inverters) and a large number of controllable devices has been a challenge. This can be said for dynamic models of wind farms, PV systems, and other systems with aggregated elements in the wider power system.

Despite this conundrum caused by steady changes in performance guidelines resulting in a variety

of IIDG technologies and a lack of established practice (leading to lack of accurate IIDGs' fault models), there are essential characteristics of IIDGs that are well known and are different from the ones of SGs:

- IIDGs cannot sustain high fault currents due to low thermal withstanding capability of power electronic components [18]
- IIDGs offer fast dynamics due to high control bandwidth and low inertia or even null [40]
- the behaviour of IIDGs during either of the above-mentioned operational states depends on the power converter control strategy(e.g. IIDGs do not provide the same fault current phasors as SGs.) [1]

State of the art of IIDGs' control in microgrid system

A control strategy of a microgrid depends on DGs embedded within its network whereby each has its own primary control particularly, the IIDGs which are designed according to their functional requirements and operating conditions within the microgrid [41–44]. According to their control and operational function, IIDGs can be grouped into four categories viz. grid-forming, grid-feeding, grid-supporting-grid-forming (GSGFm), and grid-supporting-grid-feeding (GSGFd) DGs [43–45]. As their name suggest, grid-forming DGs form the voltage and frequency within the microgrid operating in islanded mode. These DGs, in steady state, are modelled as an ideal voltage source with a low output impedance [43, 44]. However, they are not suitable for parallel operation with other grid-forming DGs or with the grid. In this case, GSGFm DGs are appropriate [44]. While the voltage magnitude (V) and frequency (ω) references are directly set by the operator for basic grid-forming IIDGs, droop controls ($P-\omega$ and $Q-V$) are used to generate the references from measured active (P) and reactive power (Q) for GSGFm IIDGs. The remaining categories; grid-feeding and GSGFd DGs use the bus voltage of the system (grid/microgrid) to which they are connected as a reference signal for synchronisation purposes [47–49]. These DGs are modelled as ideal current source connected to the grid in parallel with high impedance [43,44]. The basic grid-feeding requires P and Q references for current control from the operator while GSGFd IIDGs adjust these references through $\omega - P$ and $V - Q$ droop controls, whereby V and ω are extracted from the bus voltage signal to which they are connected. Figure 2.1 illustrates the four types of basic control structure as given in [43,44]. In the figure, the parameters with * refer to a reference inputs while parameters without it are provided from measurements or calculated directly from measurements.

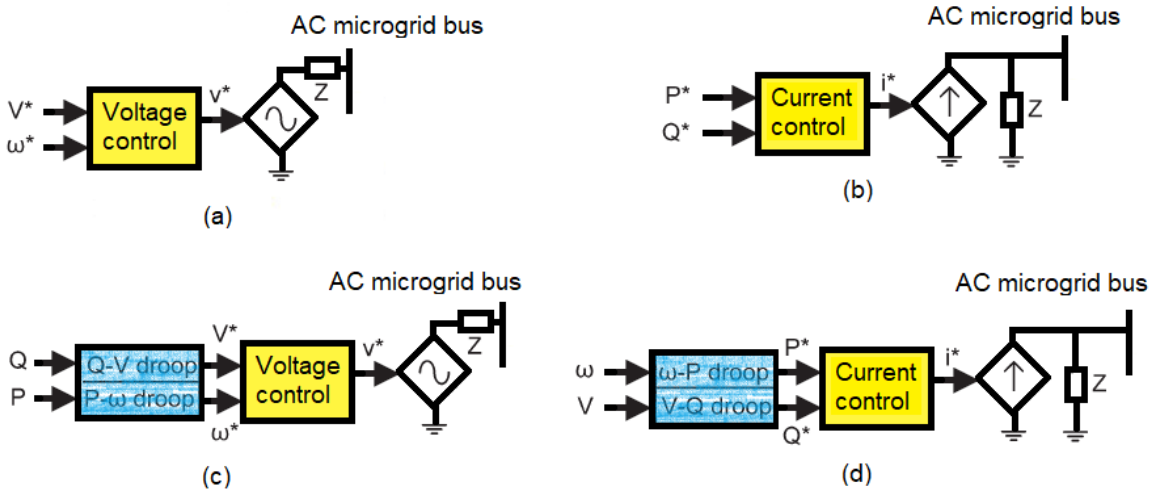


Figure 2.1: Simplified representation of grid-connected power converters: (a) Grid-forming, (b) Grid-feeding, (c) and (d) GSGFm and GSGFd respectively [43, 44]

A typical inverter's primary control consists of two control loops namely inner and outer control loops [47, 50–52]. The former is often a current control loop which controls the current injected into the grid/microgrid while the outer control loop is either for voltage control for grid-forming IIDGs or power control for grid-feeding IIDG types [52]. The outer loop generates the current reference signal to the inner controller. The reference signals for voltage or power controllers as previously mentioned are either set by the IIDG operator (fixed or variable through droop control) or provided from a remote dispatcher (microgrid operator or distribution network operator) [53]. Due to low thermal inertia of semiconductors making the inverters, the output current of IIDGs is limited to less than two times the rated current [20, 54]. This is implemented in the control of the inverters using current limiting strategies. The most two popular strategies are the instantaneous saturation limiting strategy (ISL) and latched limiting strategy (LL). However, due to these strategies limitations in some situations like fault ride through, researchers have proposed other strategies [53, 54].

The control of IIDG can be implemented in either of the following three reference frames: natural or *abc* reference frame, stationary or $\alpha\beta$ reference frame, and synchronous or *dq* reference frame [43, 52, 54]. The control implemented in *abc* and $\alpha\beta$ use Proportional Resonant (PR) controller while the design of a *dq* control uses a Proportional Integral (PI) controller [55, 56]. PI controller being also referred to as a conventional controller due to its technology maturity, the control in *dq* domain has dominated the inverters on the market. However, the reference frame plays a key role in the behaviour of the IIDG, particularly in fault conditions. The behaviour of IIDGs in fault conditions is discussed in the next section and chapter. The control of IIDGs as above-

mentioned may require the voltage magnitude and frequency references from the microgrid/grid, particularly the grid-feeding and GSGFd IIDGs. The control in $\alpha\beta$ reference frame requires a frequency locked loop (FLL) to accurately acquire the microgrid/grid frequency. The dq control, on the other hand, requires the voltage phase angle to transform the voltage and current signals from abc to dq reference domain [55, 56]. The reference frame clearly influences the synchronisation of the IIDG to the microgrid or distribution system through its control [43]. With the dq reference frame widely adopted in practice, the PLL has also dominated the literature and can be designed in either of the three reference frames [57–59]. For example, the Enhanced PLL (EPLL), Dual Synchronous Reference Frame PLL (DSRF-PLL), and Double Second Order Generalized Integrator PLL (DSOGI-PLL) are respectively implemented in abc, dq, and $\alpha\beta$ domains.

The choice of a suitable synchronisation scheme, however, not only depends on the reference frame of the IIDG control but also on the application requirements. For example, DSRF-PLL has been adopted widely in three-phase systems as it can accurately and fast estimate the phase and frequency [60]. Its negative aspect lies in its complexity in estimation process and sensitivity to phase-angle of microgrid/grid voltage [60]. DSOGI-PLL can be used in single-phase and three-phase systems and has registered good performance in generic grid conditions, but poor estimation of voltage phase and frequency in presence of harmonic distortions [58]. The EPLL performs well in all conditions but its slow dynamics make it unsuitable for applications requiring fast response such as synchronisation [61]. Therefore, there are important performance characteristics for PLL design that should be fulfilled for good performance of an IIDG. The main ones are fast dynamic response in fault conditions, fast processing time (simple structure), and accurate performance in abnormal conditions such as unbalanced faults, harmonics, interharmonics, DC offset, phase jumps, and frequency variations [56]. Basic PLL techniques dqPLL and $\alpha\beta$ PLL [62] present fast dynamic response and very simple structure but fall short on the required accuracy during abnormal conditions such as unbalanced fault, harmonics and interharmonics, and DC offset [63, 64]. The fundamental structure of dqPLL and $\alpha\beta$ PLLs are given in Fig. 2.2.

A great deal of research has been undertaken over the years to improve the performance of these basic techniques during abnormal conditions [56]. However, in most of the cases the improvements have come to the detriment of dynamic response speed and simplicity. Among the proposed improved techniques, two classes of techniques have been identified namely pre-filtered (or pre-calculated or pre-loop filter) and loop filter modification (in-loop filter) methods [63, 64]. According the performance analysis study of different advanced PLL technologies conducted in [63, 64], the former class is implemented in the phase detector to provide rejection capability to unbalanced fault oscilla-

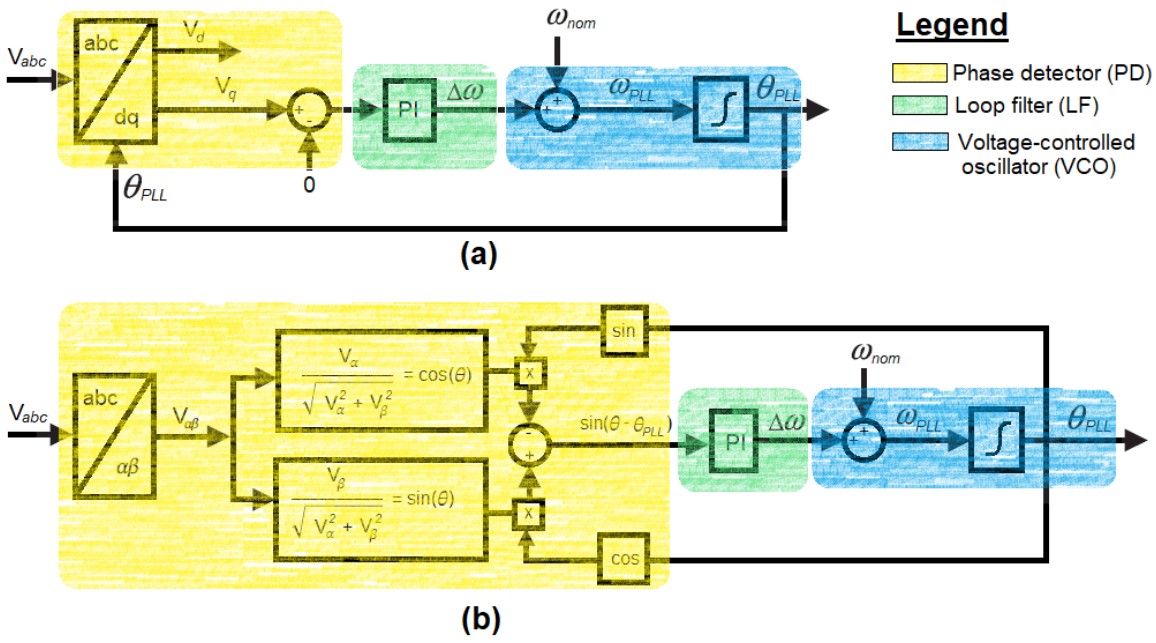


Figure 2.2: Fundamental structure of basic PLL: (a) dqPLL, (b) $\alpha\beta$PLL [63, 64]. With abc/dq - the transformation (Park transform) of three phase voltages (V_{abc}) to synchronous direct and quadrature components V_d and V_q, θ_{PLL} - estimated phase of the voltage signal, ω_{nom} - nominal voltage frequency, ω_{PLL} - estimated voltage frequency, $\Delta\omega$ - PI controller output signal
, and abc/$\alpha\beta$ - the transformation (Clarke transformation) of three phase voltages (V_{abc}) to stationary reference frame components V_α and V_β.

tions and harmonics but degrades the dynamic response speed of the PLL while the latter class is implemented in the loop filter (LP) to improve the PLL's dynamics [64].

Among the prevalent pre-filtered methods in the literature, the first improvement to basic dqPLL is the Decoupled Double Synchronous Reference Frame PLL (DDSRF-PLL) proposed by Rodriguez et al. in [65]. The principle of this technique is the extraction and decoupling of positive and negative sequence components implemented in dq reference frame. The equivalent technique implemented in $\alpha\beta$ reference frame is the Dual Second-Order Generalized Integrator (DSOGI) PLL whereby instantaneous positive sequence components are extracted and used to track the phase. These techniques perform accurately during unbalanced faults but present large frequency overshoot when disturbances occur [64]. While these technique remove oscillations caused by the imbalance such as 2^{nd} order harmonic component, removing other harmonics would require targeted harmonic filters which can affect the PLL's dynamic response speed. Furthermore, they lose their accuracy in the presence of interharmonics and DC offset [66].

To reduce the frequency overshoot that usually lead to the violation of frequency limits of the grid code, further improvement were brought to basic PLLs, particularly to build upon DDSRF-PLL technique [67]. The main examples among these are Hybrid $d\alpha\beta$PLL, Decoupled network-based $\alpha\beta$PLL, Proportional Integral Derivative (PID)-based PLL, Adaptive or notch filtering techniques FFT-PLL and LPN-PLL, and Three-Phase Enhanced PLL (3EPLL) [64]. While some of the improvements have resulted in low frequency overshoot and good performance under certain harmonic components, they also detrimentally affect the dynamic response speed and the simplicity of the basic PLL structure. Furthermore, their performance is not satisfactory in the presence of interharmonics and DC offset.

The improvement to basic PLL techniques has not only focused on the PD process of the PLL but also on the loop filtering process to improve the dynamic response speed without causing frequency overshoot and in some cases eliminate harmonic voltage distortions [64]. Among these techniques the main ones are based on modifying the PI controller by adaptively adjusting the controller's parameters, and Frequency Phase Decoupling $d\alpha\beta$PLL and its variants. The two latter techniques seem to provide very good dynamic response speed and low frequency overshoot. However, as all the PLL techniques discussed so far, harmonic and interharmonic distortion as well as DC offset compromise their accuracy.

With the increase in harmonic and interharmonic distortion level in modern power system, it is becoming imperative to develop PLLs that are immune to voltage distortion. The most recognised technique in the literature to handle this issue is the moving average filter (MAF). This filtering technique has been applied to either PD or LF process. The basic MAFPLL has been proposed as an improvement to dqPLL. This PLL is simple in structure and performs satisfactorily in the presence of imbalance, harmonics, interharmonics (partially), DC offset, and phase jumps. However, it presents slow dynamic response and poor performance in off-nominal frequency conditions [64]. More advanced MAF based PLL techniques have been proposed for appropriate performance in all above-mentioned conditions with improved dynamic response speed. Among these advanced proposed PLLs are Pre-filtering Moving Average Filter (PMAFPLL), Enhanced PMAFPLL (EPMAFPLL), EPMAFPLL Type 2, and $\alpha\beta$-enhanced PMAF ($\alpha\beta$EPMAFPLL) with EPMAFPLL and $\alpha\beta$EPMAFPLL present the best overall performance with improved dynamic response speed [56].

It can be said that researchers have the technical basis on which they can build and bring practical improvements to the above proposed PLL techniques to ensure simplicity and much faster dynamic response during disturbances. In this line, authors in [56] propose a Harmonic-Interharmonic-DC-

Offset (HIHDO) PLL with improved performance in all conditions with faster dynamic response than advanced MAF-based PLL techniques.

With all these said, it is clear that with such a number of PLL techniques, recalling that PLL technology can be digitally implemented, there are a variety of PLL technologies that could be implemented in an inverter.

The synchronised techniques discussed above are required by IIDGs integrated in distribution systems as grid-feeding units [43]. In a microgrid however, all types of IIDGs can be found in a microgrid. For a microgrid solely based on IIDGs to have dual capability to operate in grid-connected and islanded mode, it must comprise at least a grid-forming or voltage-source-based grid-supporting IIDG. Otherwise, the only possible operation is grid-connected mode. Alternatively, at least a synchronous-based DG can be embedded in the microgrid to form the voltage in the system. When multiple grid-forming IIDGs are installed in the microgrid, a power sharing strategy is required either in the primary control if droop-based strategy is used or as part of the microgrid control when communication based-control technique such as master-slave is used [41, 47, 48, 50]. This control scheme ensures even distribution of load among the DGs in parallel. While droop-based controls are simple, secure and do not require communication infrastructure, their implementation would require the adoption of ad-hoc devices since most of the inverters available on the market are not equipped with droop controllers [68].

The behaviour of inverters in fault conditions

At the inception of a fault, the immediate reaction of an inverter is a current peak of short duration which is caused by the output filter [69]. This sudden spike is due to large signal response requirement that temporarily takes the inverter control loop out of operation [70]. For legacy inverters (grid-feeding inverters with no low voltage fault ride through capability), tests have shown that the peak fault current varies between 2 to 3 times for three-phase inverters [71]. This fault current lasts between 1 and 5 ms. This fault duration range is the same for single phase inverters while the peak current magnitude varies between 4 to 5 times. On the other hand, it has been shown in the same report that with low voltage fault ride through capability, these inverters can continue to generate limited fault current for 7 to 10 cycles. The fault current of IIDGs is limited due to the low thermal inertia of semiconductor switches making the inverter. This limitation of the output current is ensured by the inverter control strategy. Fig. 2.3 below illustrates the position of the current limiting process in the basic structure of inverter control.

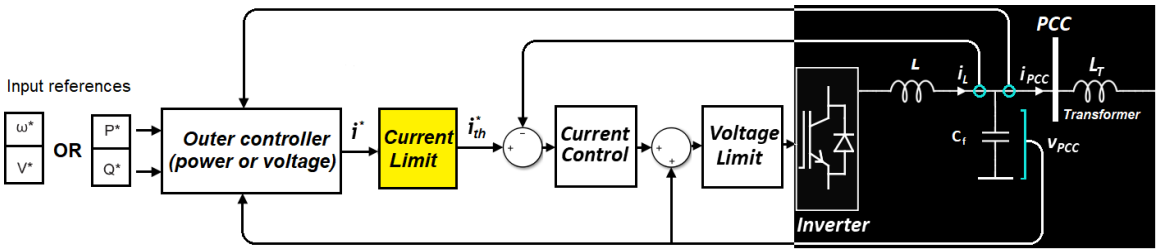


Figure 2.3: Basic structure of voltage source control

When a fault occurs, the current is limited to protect the inverter's electronic components. The current limiting strategy is activated when the current reference from the outer control loop (PQ control for grid-feeding or Voltage control loop for grid-forming inverters) is greater than a predefined threshold. This threshold can be surpassed when a fault occurs in the the power system (grid or microgrid). In such a situation, the outer loop is broken and the inverter behaves like a constant current source [72, 73]. This can be represented with the equivalent circuit depicted in Figure 2.4. Constant current-controlled IIDGs are used to deliver constant current to the grid and only require current reference. The reference is constant and makes the IIDG to maintain the same current output regardless of the operation state of the system (normal or subject to fault) and the reference frame in which the control is implemented. The inverter output voltage of such an inverter is automatically adjusted to provide balanced current.

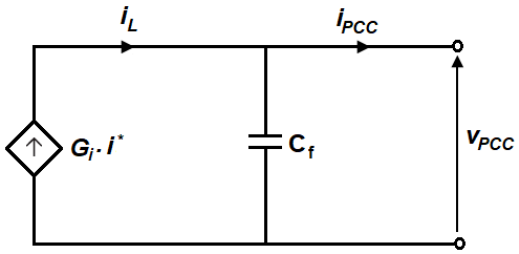


Figure 2.4: A model of a constant current-controlled inverter

The behaviour of inverters that use outer loop to provide current references to the current controller such as PQ-controlled (grid-feeding) and V/f-controlled (grid-forming) inverters is different depending on the current limiting strategy adopted and the reference frame in which the control of the inverter is implemented [73, 74].

In contrast to constant current controlled inverter, the output current of the PQ- or V/f-controlled inverter is impacted by the voltage sags or swells [73, 74]. When a fault occurs the inverter output current can be significantly high and should be limited to prevent inverter components damage.

When current limiter is triggered, these inverters fault behaviour is as the one of constant current controlled. It is important to highlight, however, that PQ-/voltage-controlled inverter's inner current control and current limiter can be implemented in any of the previously mentioned reference frames and depending on a fault type, particularly unbalanced faults whereby one or two phases may only be current-limited. In [74], Plet et al. developed inverter models in different reference frames under different faults types. Figure 2.5 provides the models in synchronous, and natural reference frames.

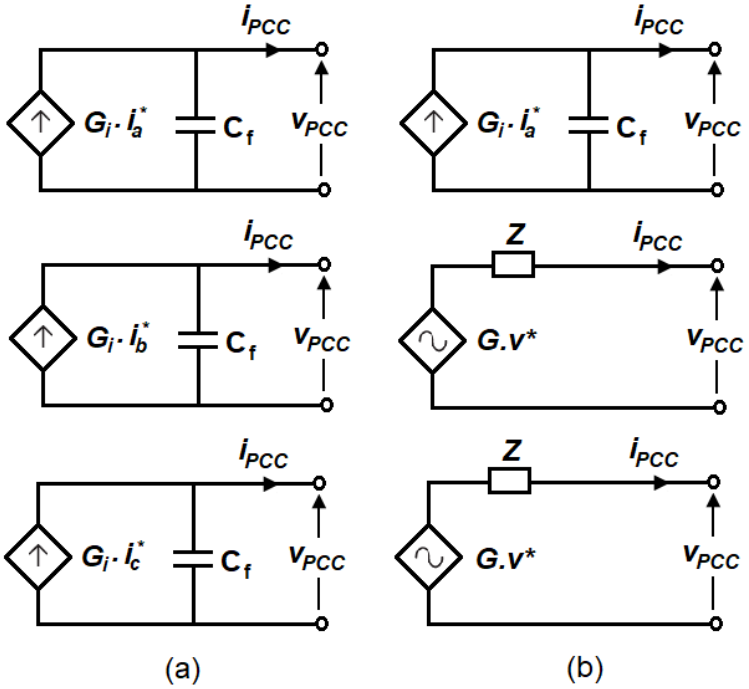


Figure 2.5: Equivalent phase networks of a three-phase inverter: (a) with any type of fault with control in synchronous reference frame/stationary reference frame (the current references were converted from (dq) and ($\alpha\beta$) to (abc) OR a three-phase fault with control in Natural reference frame; (b) with a single phase to ground fault with control in Natural reference frame (note that for phase to phase fault, only 2 phases will be current-limited) [74]
. With G – Overall inverter control transfer function; Z(s) - Load impedance; i_{PCC} - Load current; v^* - Reference voltage; V_{PCC} - Filter capacitor voltage; C_f – Filter Capacitor; G_i - Current controller loop transfer function, i^* - Reference maximum inductor current.

From the above, it can be seen that the fault current from an IIDG depends explicitly on the reference frame in which its current control and limiter are implemented. The inverter control implementation in natural reference frame abc offers an advantage over dq and $\alpha\beta$ as each phase is controlled independently, which allows injection of fault current into only faulty phases. However,

this would not be of more importance in meshed systems where loads can be supplied from other buses.

There are two popular current limiting strategies and used in practice namely instantaneous and latched limiting strategies that have been used to limit current during faults or overcurrent conditions to protect inverters. However, they have been criticised due to some drawbacks. The use of instantaneous current limiter results in voltage and current distortion, overvoltage and inaccurate current limiting in dq and $\alpha\beta$; while the latched current limiter experiences these drawbacks in some cases.

As its name suggests, instantaneous current limiting strategy works as a saturation as soon as the current references reaches the threshold. The latched limiting strategy, on the other hand, as soon as the references generated by the outer loop reach the threshold, the pre-defined internal references are generated and used. This breaks the outer control loop making the inverter a current source during faults.

2.3 Microgrid Protection

From the perspective of existing and well-established practices in grid operation, the integration of IIDGs in traditional grid distribution system does not affect much its operation due to the robustness of the grid as long as the volume of DG is less than 20%. On the other hand, this penetration compromises its protection scheme, which is typically based on overcurrent and time grading techniques, due to IIDGs' relatively low contribution to fault current, in comparison to conventional synchronous-based generation, and bidirectional power flow between the grid and the DGs [75]. This makes the conventional overcurrent protection based schemes not only ineffective in the distribution system with IIDG(s) but also in IIDG-based microgrid operating in off-grid mode [2, 76].

As shown in the previous section, the behaviour of an inverter subsequent to fault inception depends significantly on its control strategy. When a fault occurs, the current is not only limited but also it is controlled. While the former depends on the threshold, the latter depends on the strategy adopted to generate current references, which have a significant impact on the protection requirements.

A good deal of recent research on new microgrid protections has been reported in literature, and due to the number of challenges involved each assumes a certain topology, operating conditions, and

source types, location and size [19,36] . This is because each of these factors result in non-negligible impact on fault current levels in microgrids. One suggested way is to use directional feature of overcurrent relays and adapt their settings according to microgrid state or topology [78–81]. This adaptive technique is implemented through local measurements or a central unit [7]. The main issues with these protection schemes are a compulsory prior knowledge of all possible microgrid configurations and running heavy computational simulations each time, a configuration is changed [82]. Another proposition is the use of distance protection schemes which are based on admittance or impedance relays [83]. This technique can be used in MV and LV but cannot detect effectively phase to phase and earth faults [7]. Moreover, they present inability to detect high impedance faults, errors in admittance measurements, increasing tripping time and loss of accuracy due to harmonics and transients. A third group of new protection schemes is based on voltage measurements and Park transformation [10]. The main problem with this method is the very small differences in voltage drops between relays at both end of short lines, calculation complexity due to conversion of measurements from abc to dq frames and network structure dependence. A fourth category, which is most appreciated in literature, is the category of differential protection-based techniques [22,84–90]. They are accurate in detecting faults [54]. This better performance is obtained from their non-sensitivity to bidirectional power flow, changing current levels, number of DGs connected, microgrid operation mode and weak infeed [7]. These schemes can be used also to protect meshed microgrids and can allow plug-and-play and low voltage ride through requirements [12]. However, the cost associated with their communication system requirements impedes their uptake [91].

All the aforementioned schemes use either voltage or current waveforms, voltage or current symmetrical components, or differential quantities of the systems to detect faults [54]. Other proposed fault detection techniques are transient-based which capture transients' signature at IIDG's control level [54, 92]. However, these schemes are limited to detection of fault in the system. Table 2.1 provides a summary of the proposed schemes in the literature as discussed above with a highlight of their advantages and disadvantages.

Looking at the above extensive literature, one can conclude that the proposed schemes for control and protection of microgrid can easily allow practicability of microgrids. However, despite the recent significant research interest, there is no commercially available protection relay for microgrids [1, 93, 94]. Furthermore, results from studies undertaken on the relationship between microgrid control strategies, dynamic stability [54, 74, 93] and popular fault detection methods show that designing and operating a microgrid which can be in various operation modes (grid-connected, islanded, various network configurations) can create real challenges in the protection system which

Table 2.1: Comparison of protection schemes proposed in the literature

Protection scheme	**Advantages**	**Disadvantages**
Adaptive Protection	• Dynamic change features in settings between relays • Communication improves the speed of operation • Can be effective in grid-connected and islanded mode of operation	• Expensive due to communication infrastructure • It is complex and involves heavy computational simulations and can compromise real-time operation • Communication dependant which can impact reliability
Directional Overcurrent Protection	• Effective in bidirectional current flow conditions • Good selectivity • Can allow local or central implementation	• Expensive as it requires voltage and current measurement devices • Prior knowledge of all possible system configurations
Voltage measurements	• Effective fault detection	• Coordination issues for short lines • Requirement of voltage measurement devices • Network structure dependence • May not detect high impedance faults

Distance Protection	• Can provide fast operation • Can be suitable for both grid-connected and islanded operation modes	• Expensive as it requires voltage and current measurement devices • They may not be effective for short line and high level of integration of IIDGs due to its sensitivity to IIDG fault contribution. • Inability to detect high impedance faults • Loss of accuracy due to harmonics and transients
Differential Protection-based techniques	• High fault detection accuracy • Immune to bidirectional power flow, changing current levels, number of IIDGs, system topology, and operation mode	• Expensive communication system • Communication dependent • Requirements for synchronised measurements for long lines • Traditional differential protection may fail in islanded mode of operation

needs to address not only reduced fault currents from multiple feeds but also various levels of fault current. The argument for this issue can be that the control strategies have been developed according to typical behaviour of power electronics while most of the proposed protection schemes have been based on finding solutions to the limitations of conventional protection schemes. For example, in [54], it has been shown that fault detection based on voltage waveform feature or voltage/current symmetrical components, both popular detection techniques, cannot always be reliable depending on microgrid's IIDG topology, current limiting strategy and reference frame.

On the other hand, few protection schemes have been proposed in the literature and not often exhaustively discussed, particularly their coordination with the back-up protection. This is essential as a system should always be protected even when the main protection has failed.

In [95], the authors proposed a protection strategy (main and back-up) for medium voltage microgrids. However, the strategy is limited to radial networks. In [96] directional overcurrent relay is proposed with the relay settings obtained from an optimisation algorithm to ensure optimal coordination between primary and back-up relays. However, it only considered synchronous distributed generators (DGs). In [97] a dual setting directional overcurrent relay is proposed with the primary protection being communication-less and the back-up being communication-assisted (low bandwidth). However, the study considers as well only synchronous DGs in islanded mode of operation. In [98] authors looked at the economic aspect of dual setting directional overcurrent relays and proposed a coordination of a mix of convectional and dual setting relays. In this study, the primary and back-up protection functionalities are integrated in a single relay programmed in two directions namely forward/primary and reverse/back-up. However, this category dual setting directional overcurrent protection schemes require prior knowledge of the system configuration [99].

Other techniques are based on inverter control to detect faults [54, 92, 100, 101]. In [100] overcurrent relays are used with the coordination implemented in the inverter control whereby the current limiting strategy is modified for the inverter to adaptively inject current proportional to the distance from the fault. This strategy is only applicable to inverter-only microgrids. This limitation also applies to the protection scheme proposed in [101] whereby directional overcurrent relays are used with the IIDER controller modified to inject harmonic currents detectable by the relays. [54, 92] have proposed fault detection using inverter output signals using transient monitoring function and transient content of inverter output respectively. However, these schemes are only limited to fault detection.

Another category of protection strategies used for looped and meshed islanded microgrids is differential-based protection schemes. They have been recognised to be effective for islanded microgrids [1, 7, 19, 95, 102, 103]. However, like all communication-assisted protection schemes, differential-based protection schemes have also been criticised for their high cost and reliance on communication system whose failure may compromise their correct operation.

On the other hand, however, it has also been pointed out that schemes which do not require communication infrastructure may not protect microgrids from all types of faults or may experience delays that can be prevented by communication [89, 95]. Also, it has been recognised that commu-

nication can prevent miscoordination that can happen in dual setting directional overcurrent relays between primary and back-up protections [104]. Therefore, a low cost solution to the possibility of the communication failure is essential.

One approach to this is a back-up communication means to the main one [19, 95]. The back-up communication is usually implemented using a different channel or an alternative communication path when a communication network is used. Another approach is a separate back-up protection.

To date, there is no commercially available protection relay for microgrids [1, 94]. With all the challenges previously discussed it is clear that designing an effective back-up protection is as challenging as the main one as well as the coordination between them. For example in [87], a differential current line protection is backed up with a comparative voltage strategy. This back-up protection is not as effective as the primary protection as it may isolate a larger part of the system, leading to the loss of load unnecessarily. Also, in [84], an under-voltage and an overcurrent protection schemes were proposed as a back-up protection to a differential protection. However, as discussed, these back-up schemes are likely to fail in multi-inverter islanded microgrid. In [12], a differential protection for loop-based microgrids is proposed with an overcurrent relay as a back-up in grid-connected and in islanded modes. As previously explained, overcurrent relay in islanded mode is likely to fail in inverter-based microgrids due to low fault currents.

2.4 Conclusions

In this chapter active distribution networks, IIDGs types and various control strategies and their behaviour during fault conditions have been extensively reviewed. Also, a number of microgrid protection schemes found in the recent literature has been reviewed highlighting the advantages and limitations.

From the literature review, it is clear that there is a great deal of open questions about the integration of IIDGs in power systems that require answers, particularly the recommended models for different types of inverters and their control strategies for various power system studies and applications. It can be said that the variety of inverter control strategies found in the literature reflects a possibility of a large number of inverters control strategies on the market. With operation guidelines in grid codes of various countries keeping on improving and changing, the operation of microgrids, even national grids with a large of number of inverter will require careful adoption of new practices

keeping in mind the variety of inverter technologies.

With microgrid protection schemes that have been proposed so far in the literature, the obvious conclusion is that there is still a lack of practical microgrid relays. This thesis proposes protection strategies that can be applied to any types of microgrid, particularly multi-inverter based-microgrids without the knowledge of detailed models of inverters and system elements, yet taking into account the main typical characteristics of inverters such as low and controlled fault currents.

Chapter 3

IIDGs and Microgrid Fault Behaviour

3.1 Introduction

The behaviour of IIDGs during disturbances and their models have been extensively discussed in the literature review. This chapter will build on the literature review and provide the background on the behaviour of the IIDGs, the microgrid, and the grid-feeder in general during various disturbances using simulations of a case study. The understanding of these behaviours will inform us on the requirements of protection strategies for multi-inverter microgrids discussed in the subsequent chapters. In this chapter the IIDG's operation mode (grid-connected or islanded), control and current limiting strategy, and the interfacing transformer configuration are considered. It is important to highlight that though the discussions have been based on simulations, this thesis considers the practical operational aspect and the availability of technologies on the present market. For example, while theoretically, grid-forming inverter should be able to behave like a synchronous machine during fault conditions (generating zero- and negative-currents) it is important to highlight that there is no commercially available three-phase grid-forming inverter that guarantees such a requirement [77]. This is because most of inverters on the market adopt three-wire configuration and are controlled in dq reference frame for cost saving and technology maturity reasons [77]. With the control in dq reference frame, three-wire inverters to generate negative sequence currents would require designing PI controllers taking into account dynamics of the AC system which may be uncertain, time varying,

Table 3.1: IIDGs parameters

	IIDG1	**IIDG2**	**IIDG3**	**IIDG4**	**IIDG5**	**IIDG6**
Rated power (kVA)	1000	300	250	150	100	250
Rated voltage (V)	520	260	260	260	120	260
DC bus voltage (V)	1000	500	500	500	250	500
Fundamental frequency (Hz)	50	50	50	50	50	50
Switching frequency (kHz)	5	5	5	5	5	5
Filter inductance (mH)	0.106	0.0884	0.106	0.177	0.061	0.106
Filter resistance (mΩ)	0.270	0.225	0.270	0.144	0.676	0.270
Filter capacitance (mF)	0.589	0.706	0.589	0.353	1.1	0.589
Damping resistance (mΩ)	81.0	52.2	62.6	104.4	33.6	62.6
Current control proportional	1.667	1.389	1.667	2.779	0.962	1.667
Current control integral	4.247	3.539	4.247	7.079	2.262	4.247
Voltage control proportional	0.924	-	-	-	-	-
Voltage control integral	0.00	-	-	-	-	-
Step-up Transformer Parameters						
Rated power (kVA)	1200	500	300	200	150	300
Rated primary voltage (kV)	0.520	0.260	0.260	0.260	0.120	0.260
Rated secondary voltage (kV)	20	20	20	20	20	20
Winding inductance (mH)	0.052	0.022	0.026	0.043	0.013	0.026
Winding resistance (mΩ)	0.541	0.225	0.270	0.451	0.144	0.270

non-linear, and of high order [105].

Recognising that there is no currently recognised practical fault model that can describe the characteristics of grid-forming inverters [106], the grid-forming inverters used in this thesis are of three-wire configuration. They are controlled in *dq* reference frame with the inverters dynamics decoupled from the AC system using voltage feed-forward compensation. As there are always questions on how control can affect protections, it is important to highlight that the use of other control techniques than these may require protection scheme retesting.

This chapter is divided into two sections: (i) the behaviour of IIDGs in grid-connected operation

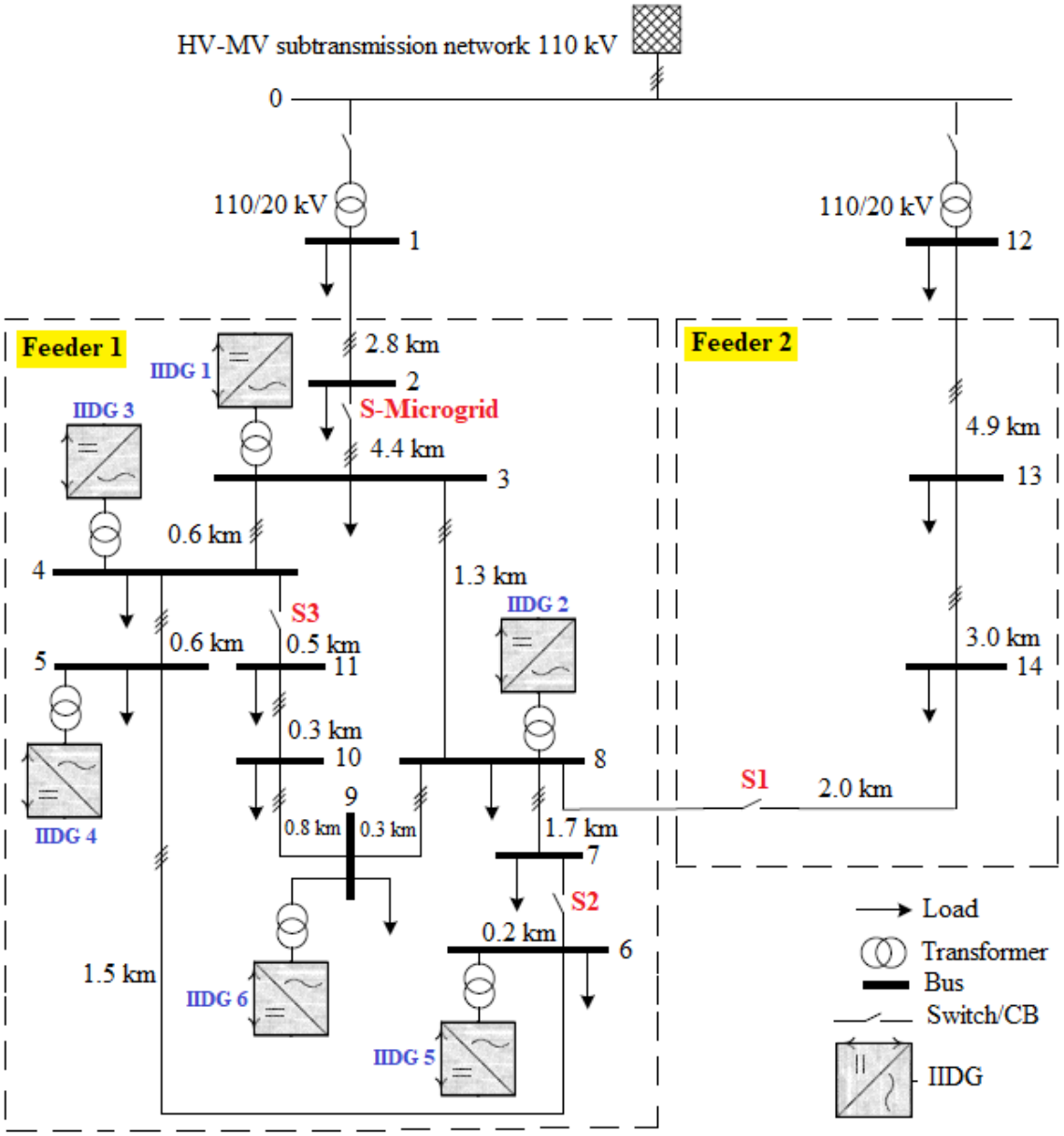


Figure 3.1: Microgrid study network [Adapted from [107]

Table 3.2: Connections and line parameters of European MV Distribution network benchmark [107]

Line segment	Node from	Node to	R'_{ph} [Ω/km]	X'_{ph} [Ω/km]	B'_{ph} [μS/km]	R'_0 [Ω/km]	X'_0 [Ω/km]	B'_0 [μS/km]	l [km]	Installation
1	1	2	0.501	0.716	47.493	0.817	1.598	47.493	2.82	underground
2	2	3	0.501	0.716	47.493	0.817	1.598	47.493	4.42	underground
3	3	4	0.501	0.716	47.493	0.817	1.598	47.493	0.61	underground
4	4	5	0.501	0.716	47.493	0.817	1.598	47.493	0.56	underground
5	5	6	0.501	0.716	47.493	0.817	1.598	47.493	1.54	underground
6	6	7	0.501	0.716	47.493	0.817	1.598	47.493	0.24	underground
7	7	8	0.501	0.716	47.493	0.817	1.598	47.493	1.67	underground
8	8	9	0.501	0.716	47.493	0.817	1.598	47.493	0.32	underground
9	9	10	0.501	0.716	47.493	0.817	1.598	47.493	0.77	underground
10	10	11	0.501	0.716	47.493	0.817	1.598	47.493	0.33	underground
11	11	4	0.501	0.716	47.493	0.817	1.598	47.493	0.49	underground
12	3	8	0.501	0.716	47.493	0.817	1.598	47.493	1.30	underground
13	12	13	0.510	0.366	3.172	0.658	1.611	1.280	4.89	overhead
14	13	14	0.510	0.366	3.172	0.658	1.611	1.280	2.99	overhead
15	14	8	0.510	0.366	3.172	0.658	1.611	1.280	2.00	overhead

mode and (ii) their behaviours in islanded mode of operation. To this purpose, the CIGRE European MV distribution network benchmark [107] is adopted. As shown in Figure 3.1, six IIDGs: IIDG 1 (1000 kVA), IIDG 2 (300 kVA), IIDG 3 (250 kVA), IIDG 4 (150 kVA), IIDG 5 (100 kVA), and IIDG 6 (250 kVA) have been added to the network on Buses 3, 8, 4, 5, 6 and 9 respectively.

The network main parameters such as line and load parameters are provided in Table 3.2 and Table 3.3 respectively. Other details about it can be found in [107]. The IIDGs parameters are provided in Table 3.1.

This network provides the flexibility of studying an MV feeder as a microgrid in different configurations (radial, loop or mesh) and in different modes of operation (grid-connected or islanded). This chapter will only consider the multi-generator radial topology i.e. both S2 and S3 are open. In grid connected mode of operation, all IIDGs and loads are connected with S1 open. In islanded mode, the S-Microgrid is opened and some loads are disconnected from the microgrid for the IIDGs to satisfy the demand. It is important however, to note that the islanding transition from grid-connected to islanded mode is out of the scope of this work. Each state is investigated individually.

Table 3.3: Load parameters of European MV Distribution network benchmark [107]

Node	Apparent Power, S [kVA]		Power Factor, pf	
	Residential	Commercial / Industrial	Residential	Commercial / Industrial
1	15300	5100	0.98	0.95
2	---	---	---	---
3	285	265	0.97	0.85
4	445	---	0.97	---
5	750	---	0.97	---
6	565	---	0.97	---
7	---	90	---	0.85
8	605	---	0.97	---
9	---	675	---	0.85
10	490	80	0.97	0.85
11	340	---	0.97	---
12	15300	5280	0.98	0.95
13	---	40	---	0.85
14	215	390	0.97	0.85

3.2 Behaviour in Grid-Connected Operation Mode

The network as in given in Fig. 3.1 is simulated in Matlab/Simulink environment. To provide insight on different fault behaviours of IIDGS due to control and current limiting strategy adopted, the IIDGs have been modelled as follows:

- **IIDG 1 and IIDG 2** - Power control loop with latched current limiting strategy
- **IIDG 3 and IIDG 4** - Constant current control strategy
- **IIDG 5 and IIDG 6** - Power control loop with saturation current limiting strategy

As previously stated, radial feeder topology with S1, S2 and S3 all open. A fault is simulated on Line 3-4 (line linking Buses 3 and 4). Two cases are investigated: (i) a three phase fault with 1 Ω fault resistance and (ii) a single phase (Phase A) to ground. For each case, simulation is done for Delta-Wye and Wye-Wye interfacing transformer configuration.

3.2.1 Three-phase fault

With a three-phase fault on Line 3-4, it is expected that no zero sequence and negative sequence currents are generated as it is a balanced fault. The simulation results of this case with the transformer configurations Delta-Wye and Wye-Wye are identical due to the balanced currents as shown in Fig. 3.2 and Fig. 3.3 respectively.

The behaviour of different IIDGs with respect to their respective current limiting strategies are as expected. It can be seen that the latched limiting strategy limits the current magnitude to 1.2 p.u. (see Fig. 3.2a and Fig. 3.3a). It is important to note that with the maximum limit set in dq reference frame, only the positive sequence current is limited to that value. In case the signal is unbalanced, the maximum phase current can be larger than the limit due to other sequence components. An example of such a case is provided in islanded operation mode. From the figures, it can be seen that the latched limiting control behaves better than saturation limiting control (see Fig. 3.2 (c) and Fig. 3.3 (c)) as the latter experiences distortion (frequency and magnitude variations) due to the instability in I_q current reference. This is due to the influence of the power control loop on the references and the wide range of possible values I_d and I_q references can take [-1.2, 1.2]. This also means that the inverter output phase current magnitude can be larger than the limit even with no imbalance.

On the other hand, the latched limiting strategy use predefined current references, $I_d = 1.0$ and $I_q = -0.67$, in this case. This means that the inverter output current magnitude is limited to 1.2 p.u. as the output is balanced and I_d and I_q are individually limited to a single value not a range of values.

For the constant current controlled IIDGs (see Fig. 3.2b and Fig. 3.3b), the output current remains the same as the pre-fault current ($I_d = 1.0$, $I_q = 0$) as there is no influence of the voltage in their control, except the decoupling feedforward compensation, which is the source of the transients just after the fault inception.

3.2.2 Single phase to ground fault

With the occurrence of a single phase to ground fault on Line 3-4, there is a significant difference between the inverter output current and the transformer output current due to the transformer winding configuration (see Fig. 3.4 and Fig. 3.5). It can be seen that with Delta-Wye configu-

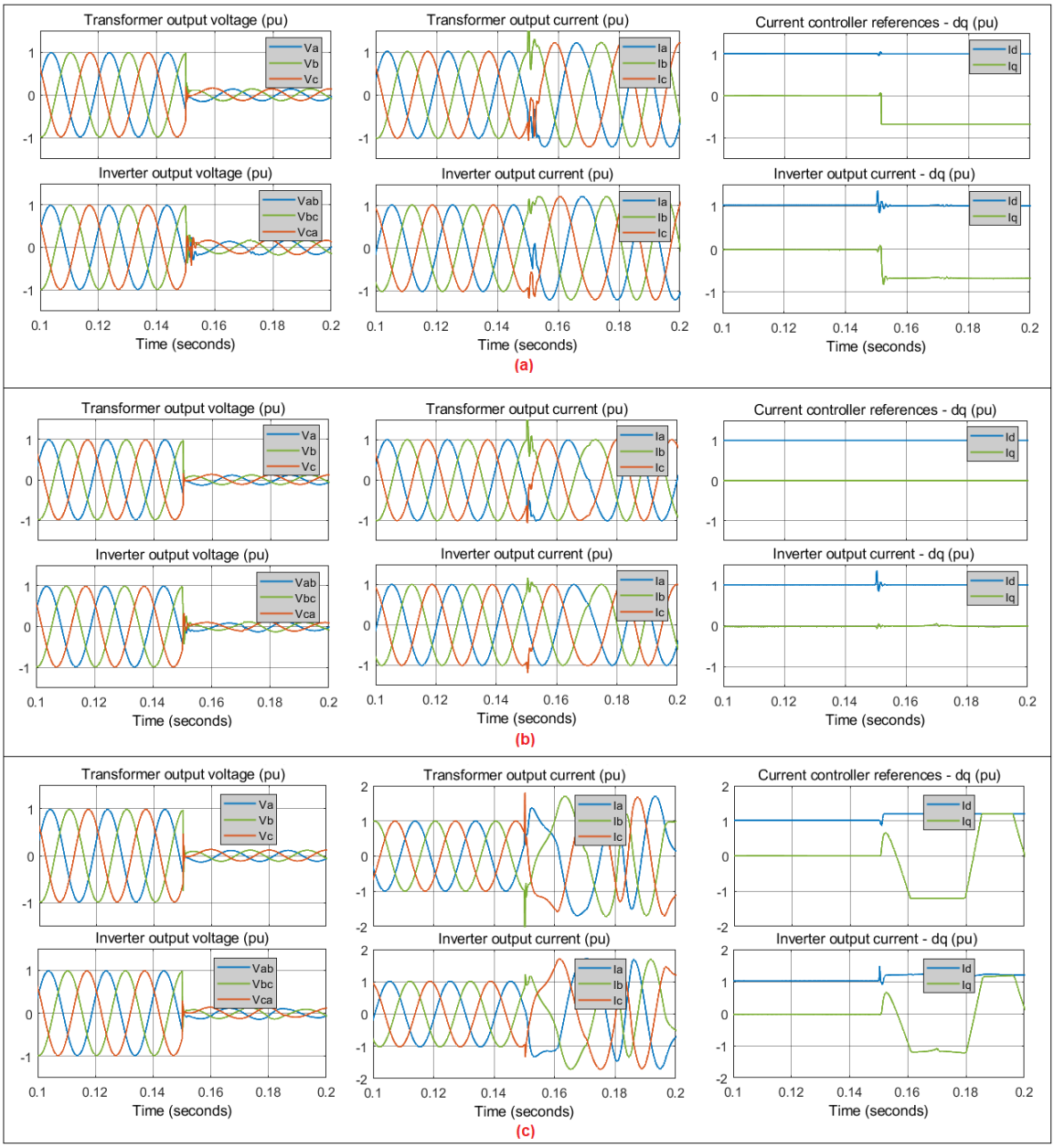


Figure 3.2: IIDGs output current and voltage in grid-connected operation mode with a three-phase fault on Line 3-4 considering Delta-Wye transformer configuration: **(a)** IIDG 1 (PQ control loop with latched current limiting strategy) **(b)** IIDG 3 (constant current control strategy)) **(c)** IIDG 5 (PQ control loop with saturation current limiting strategy)

ration, the balanced inverter output currents is transformed into unbalanced currents due to the zero sequence current circulating in the primary windings. It can be verified that the equality of

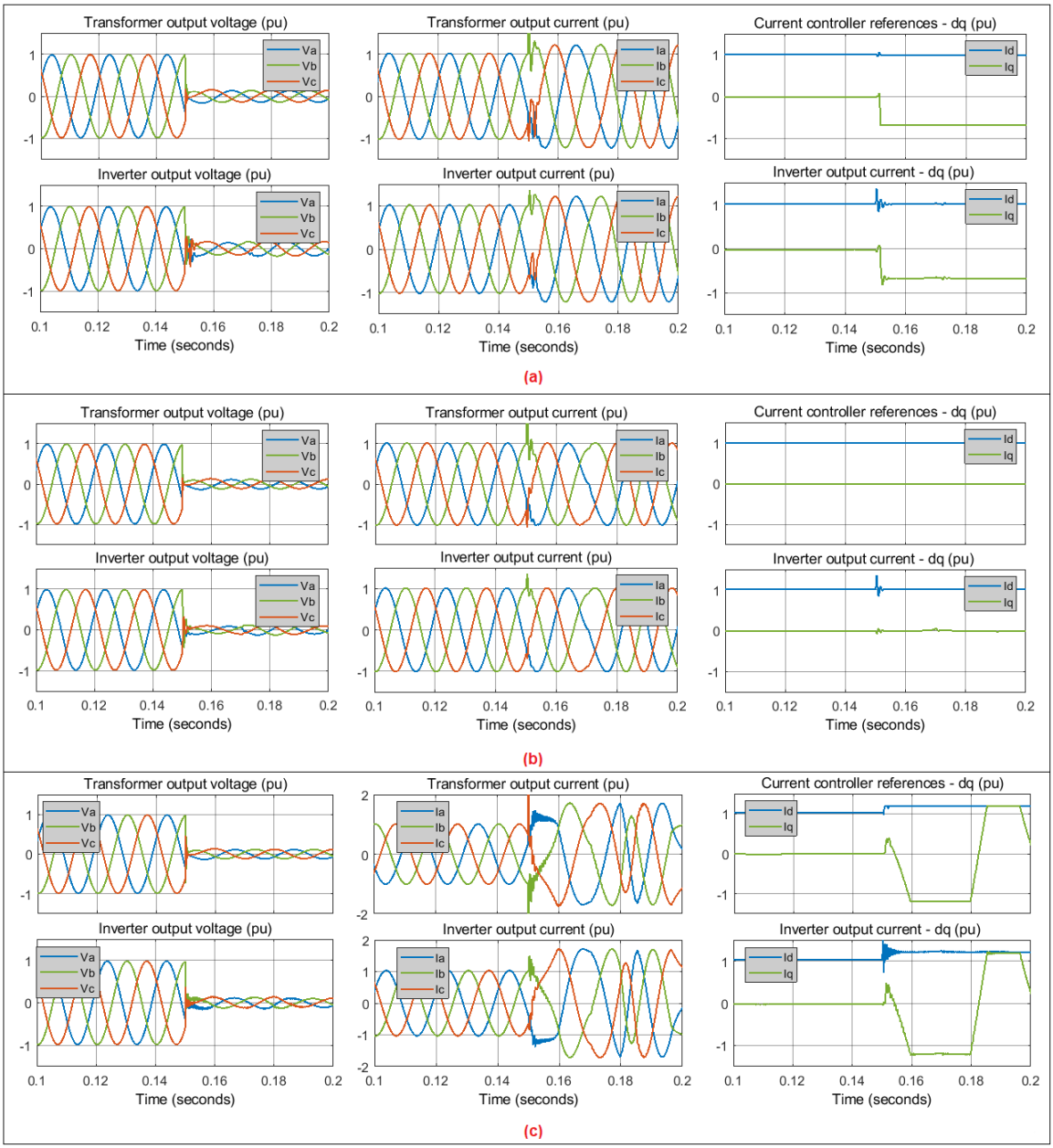


Figure 3.3: IIDGs output current and voltage in grid-connected operation mode with a three-phase fault on Line 3-4 considering Wye-Wye transformer configuration: **(a)** IIDG 1 (PQ control loop with latched current limiting strategy) **(b)** IIDG 3 (constant current control strategy)) **(c)** IIDG 5 (PQ control loop with saturation current limiting strategy)

currents in delta winding currents and their respective secondary Wye winding currents times the transformation factor still holds.

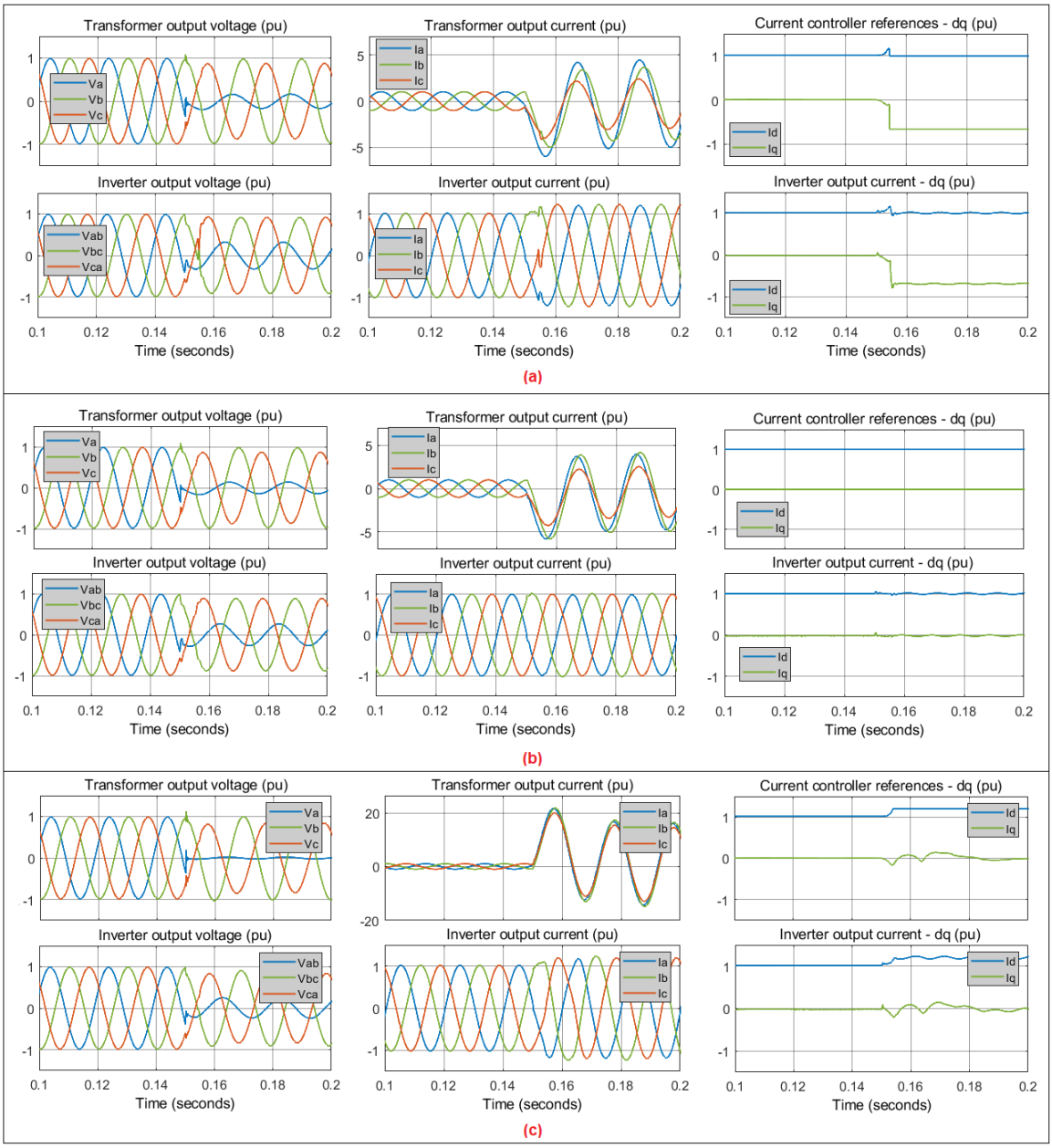


Figure 3.4: IIDGs output current and voltage in grid-connected operation mode with a single-phase to ground fault on Line 3-4 considering Delta-Wye transformer configuration: **(a)** IIDG 1 (PQ control loop with latched current limiting strategy) **(b)** IIDG 3 (constant current control strategy)) **(c)** IIDG 5 (PQ control loop with saturation current limiting strategy)

An obvious difference between the three-phase fault and the single phase fault is in the behaviour of the IIDGs with PQ control loop with the saturation current limit whereby in this case (single phase

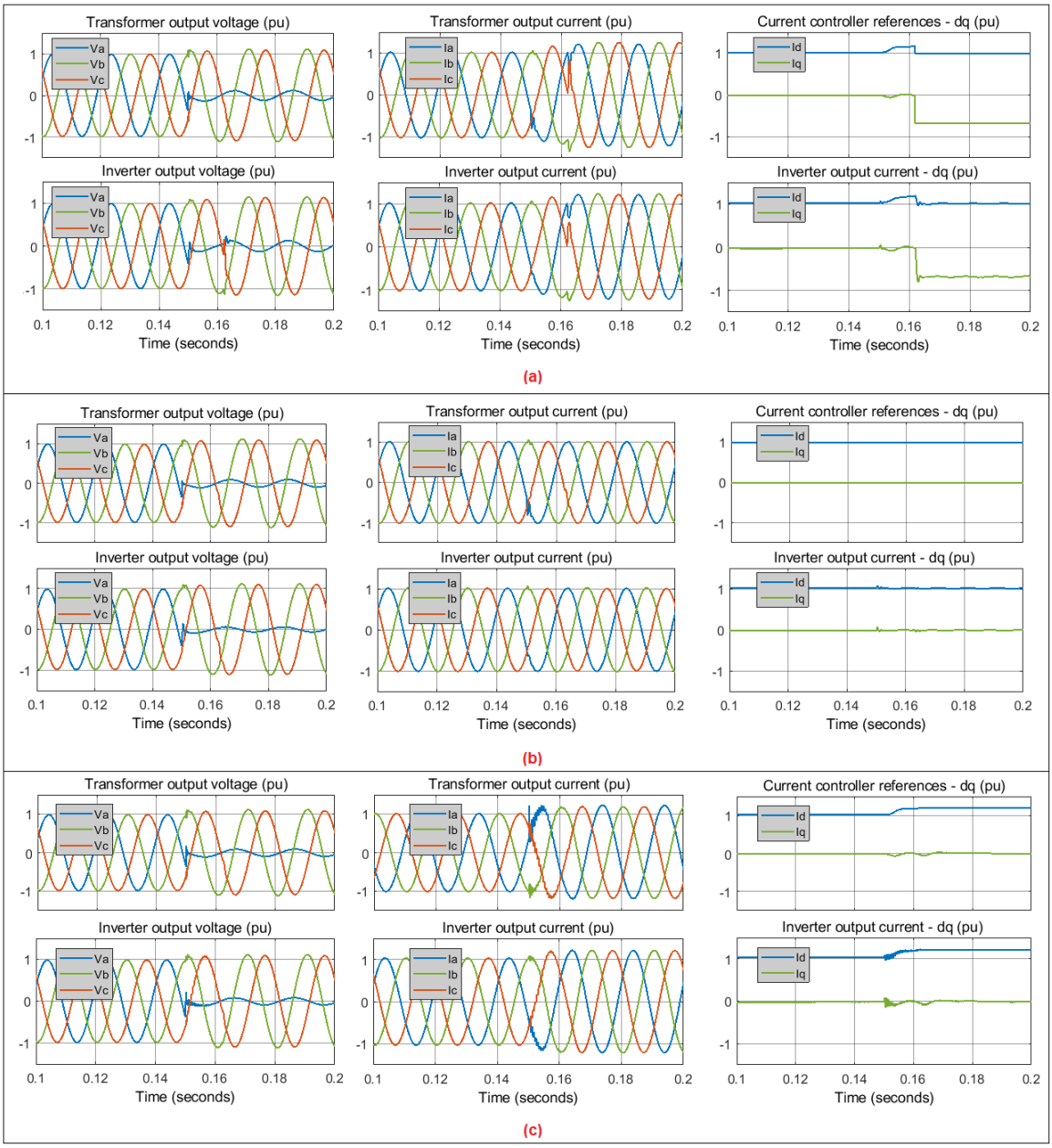


Figure 3.5: IIDGs output current and voltage in grid-connected operation mode with a single-phase to ground fault on Line 3-4 considering Wye-Wye transformer configuration: **(a)** IIDG 1 (PQ control loop with latched current limiting strategy) **(b)** IIDG 3 (constant current control strategy)) **(c)** IIDG 5 (PQ control loop with saturation current limiting strategy)

fault) the I_q reference generated by the PQ control loop is stable (zero) making the inverter output phase current magnitude limited to 1.2 p.u.. The signal is also less distorted. It can be further

said that the distortion is much less for a single phase fault with Wye-Wye transformer winding configuration as there are no circulating zero sequence currents through the winding.

3.3 Behaviour in Islanded Operation Mode

As mentioned in the introduction of this chapter, the islanded operation mode considers only the load the IIDGs can satisfy. Loads on Buses 4, 5, 8, 10, 11, and the commercial/industrial load on Bus 3 are disconnected while the rest of the network parameters unchanged. With all switches open (including the S-microgrid) the multi-generator radial based microgrid is simulated in Matlab/Simulink environment.

Each of the IIDGs is controlled in the synchronous reference frame using PI controller. A master-slave power sharing control strategy is adopted whereby the IIDG 1 is the master that forms the voltage and frequency of the microgrid, and share the current references i_{th} generated by its voltage controller to the current controllers of the slave IIDGs. The current reference of each IIDG is limited to 120% of the rated current based on latched limiting strategy as one of the most popular strategies [108].

As done for the grid-connected analysis investigated above, a fault is simulated in the middle of Line 3-4. Two cases are investigated: (i) a three phase fault with 1 Ω fault resistance and (ii) a single phase (Phase A) to ground. For each case, simulations are run for Delta-Wye and Wye-Wye interfacing transformer configuration.

The use of the master slave power sharing strategy allows the provision of the master behaviour as a representation of all IIDGs as the current reference signals shared to them from the master voltage controller are the same in p.u.. Also the frequency signal is shared along with the current reference for *abc* to *dq* transformation and vice-versa. There is no need for a PLL.

3.3.1 Three-phase fault

A three-phase fault is simulated on Line 3-4. The behaviour of the IIDGs under this case for both Delta-Wye and Wye-Wye transformer winding configurations are therefore identical as shown respectively in Fig. 3.6 and Fig. 3.7.

As expected, only positive sequence currents are generated. It can be clearly seen that the IIDGs

output currents perfectly track the current references from the voltage controller during normal operation and those pre-definded ($I_d = 1.0$ and $I_q = -0.67$) when the 1.2 pu threshold is reached. The current references are shown in the second sub-figure on the left side of Fig. 3.6 and Fig. 3.7. Those represented with pink and green colours are generated by the voltage control loop while the black and blue ones are pre-defined when a fault occurs.

The inverter output voltages on the other hand cannot be controlled to their references as the control loop is broken by the current limiting process.

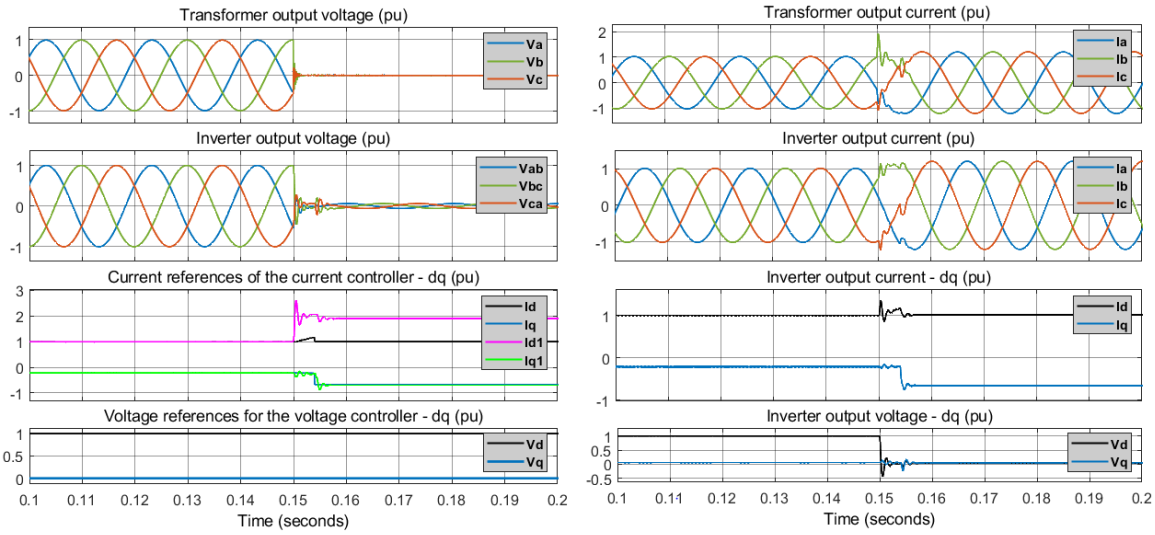


Figure 3.6: IIDG 1 output and control signals in islanded operation mode with interfacing transformer in Delta-Wye configuration with a three-phase fault on Line 3-4

3.3.2 Single phase to ground fault

When a single phase to ground fault is simulated on Line 3-4, the output currents generated by IIDGs are identical for both transformer winding configurations as shown in Fig. 3.8 and Fig. 3.9. As above-mentioned, the IIDGs are controlled to generate only positive sequence currents during fault conditions. It can be clearly seen that the IIDGs output currents track the current references from the voltage controller during normal operation and those pre-definded ($I_d = 1.0$ and $I_q = -0.67$) when the 1.2 pu threshold is reached. It can be seen from the dq components of the inverter output currents that the current reference tracking is not perfect after the fault occurrence. This is because the feedforward compensation cannot ideally decouple the dynamics of the inverter from those of the system leading to small oscillations in the current PI controller input. The feedforward compensation

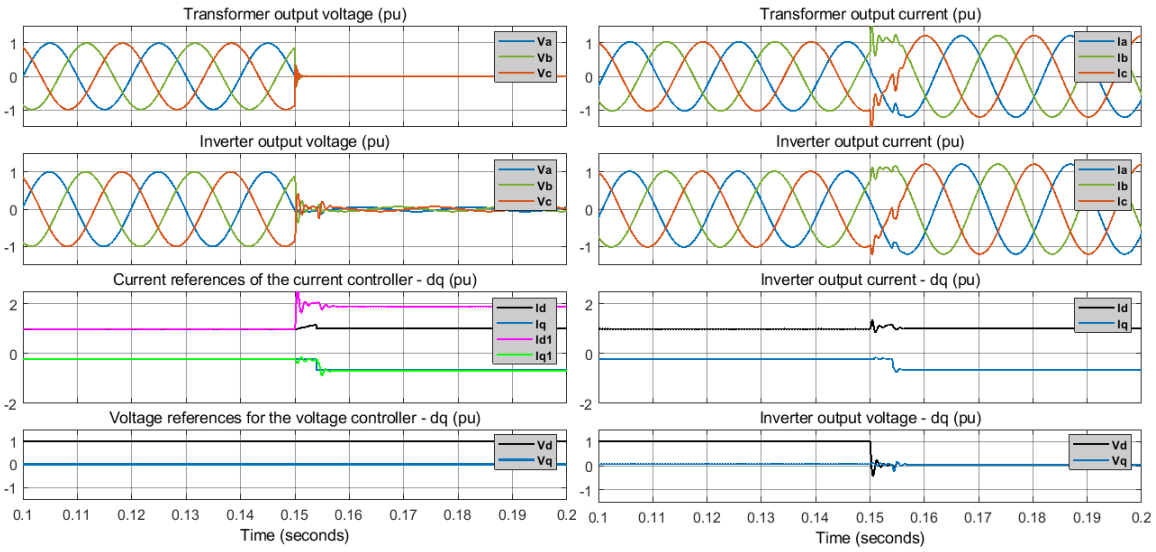


Figure 3.7: IIDG 1 output and control signals in islanded operation mode with interfacing transformer in Wye-Wye configuration with a three-phase fault on Line 3-4

signal is the dq components of the inverter output voltage.

The inverter output voltages as shown in the figures cannot be controlled to their references as the voltage control loop is broken by the current limiting process during a fault.

Another significant difference can be noticed in the transformers' output currents. With Delta-Wye configuration, the currents are unbalanced as previously explained due to the circulating zero sequence currents while the currents for the Wye-Wye configuration case are balanced.

3.3.3 The impact of feedforward compensation

As stated in the introduction of this chapter, the control of inverters in dq reference frame to generate balanced currents during faults can depend on the controller's parameters and feedforward compensation. The latter decouples the system dynamics from the inverter's dynamics. This gives the inverter the capability for disturbance and the start-up transients rejection [105]. Fig. 3.10 and Fig. 3.11 provides simulation results of the case of single phase to ground fault on Line 3-4 without and with a filtered feedforward compensation respectively.

Without a feedforward compensation, the inverter output current is significantly unbalanced leading to the reduction in output voltage magnitudes. With a filtered feedforward compensation signal,

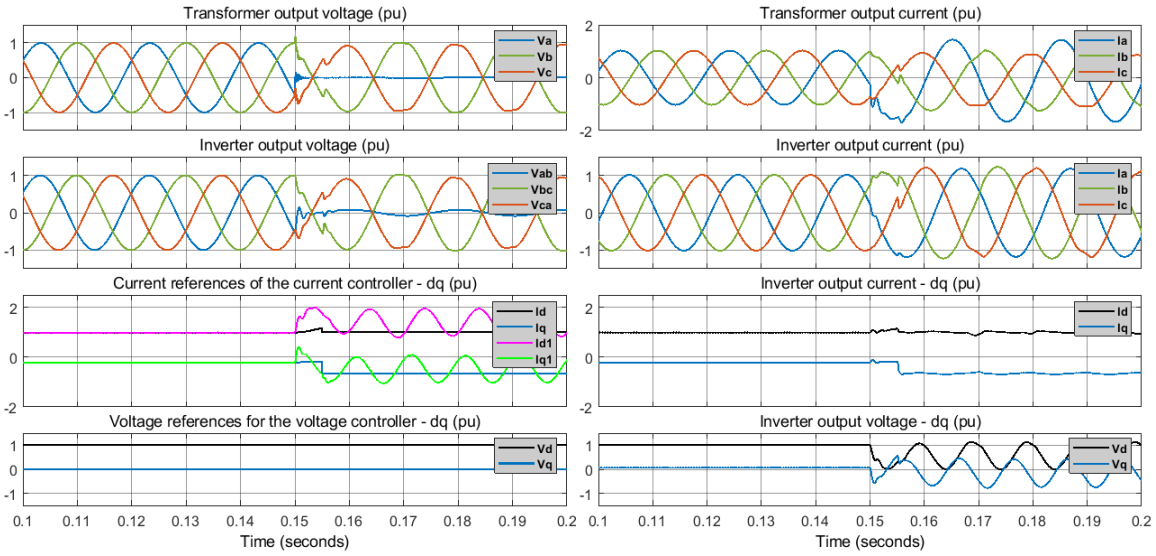


Figure 3.8: IIDG 1 output and control signals in islanded operation mode with interfacing transformer in Delta-Wye configuration with a single phase to ground fault on Line 3-4

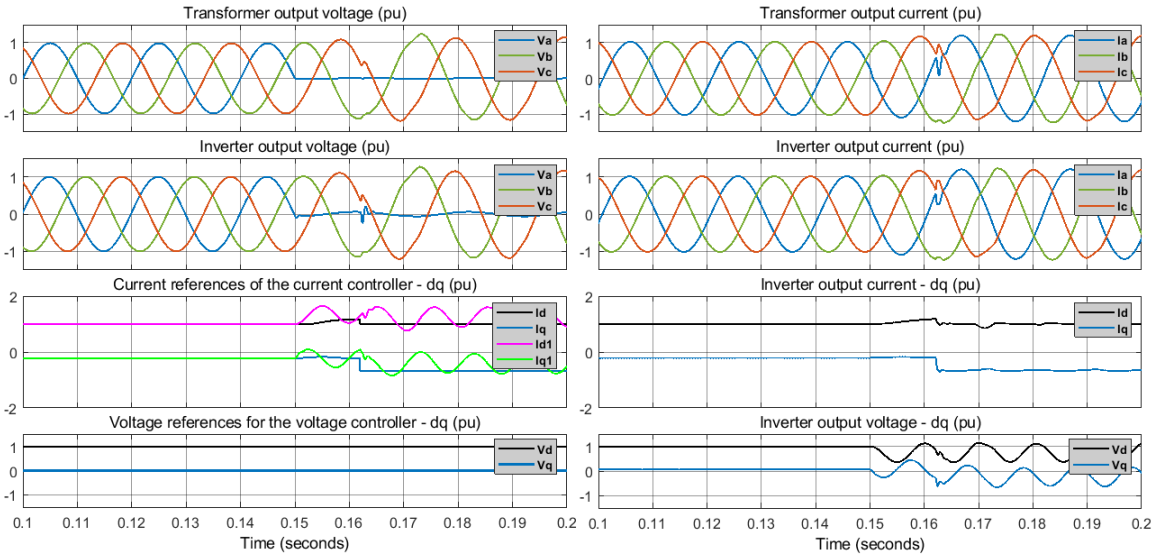


Figure 3.9: IIDG 1 output and control signals in islanded operation mode with interfacing transformer in Wye-Wye configuration with a single phase to ground fault on Line 3-4

the imbalance in the inverter output current exists but less than that without it. Also, the voltage magnitude reduction is less.

Although it can be said from these results that *dq* controlled grid-forming inverters can generate negative sequence currents, it is important to notice significant oscillations in the *dq* components

of the inverter output currents. This means that the decoupling of the system dynamics from the inverter system's was not really achieved, which led to current PI controllers not to be able to stably track the references. So, without or with a highly filtered feedforward compensation signal, the current controller design becomes a laborious task, making it more difficult for grid-forming inverters controlled in *dq* reference frame to generate negative sequence components [105].

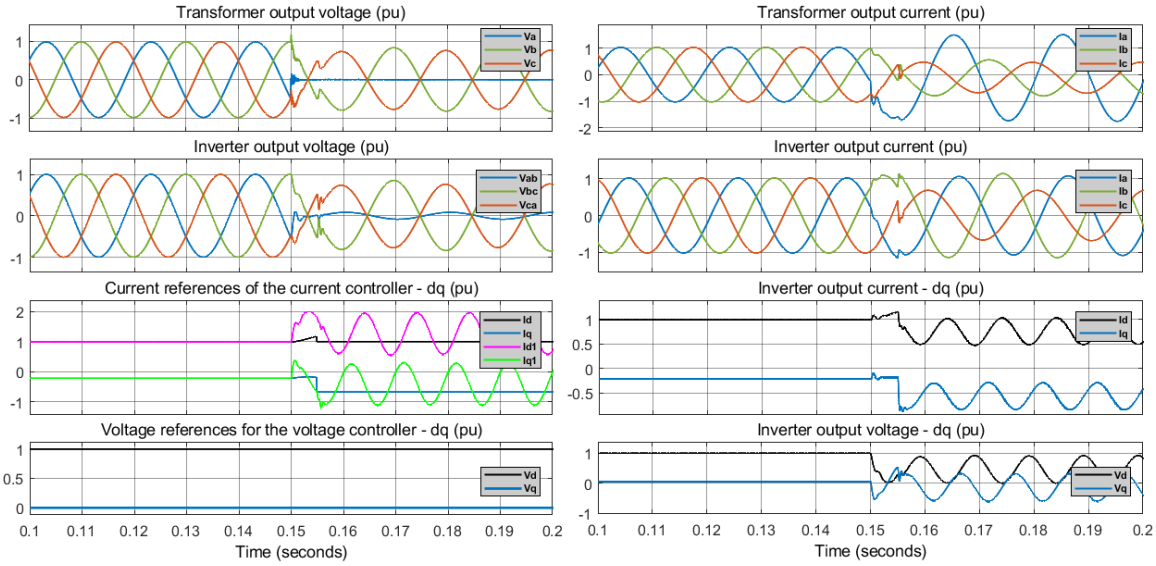


Figure 3.10: IIDG 1 output and control signals without a feedforward compensation in islanded operation mode with interfacing transformer in Delta-Wye configuration with a single phase to ground fault on Line 3-4

3.4 The Comparison of System Fault Behaviour in Grid-Connected and Islanded Operation Modes

To establish and compare the impact of the inverter behaviours on the system in both grid-connected and islanded operation modes, in Table 3.4, sequence currents for different simulation cases discussed in the previous sections are provided for all lines connected on Bus 3.

It can be seen that while the inverters behave identically in both operation modes, it is not the case for the system. As expected the fault currents in grid-connected operation mode are far larger. This itself means that a protection scheme that is designed to operate in both operation modes cannot directly use the current magnitudes.

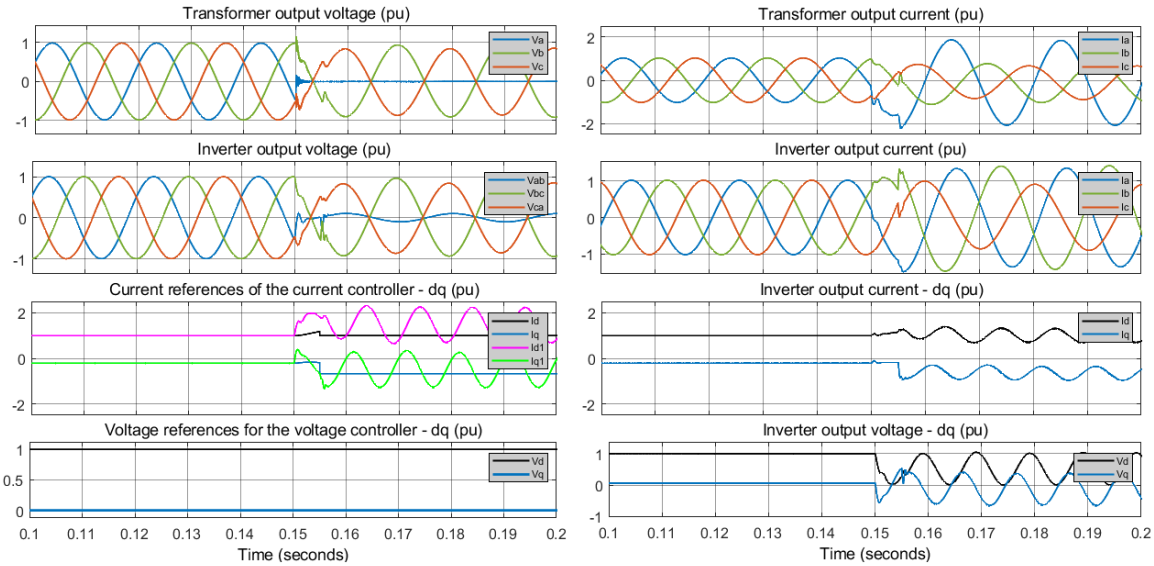


Figure 3.11: IIDG 1 output and control signals with a filtered feedforward compensation in islanded operation mode with interfacing transformer in Delta-Wye configuration with a single phase to ground fault on Line 3-4

Another difference is seen in significant negative and zero sequence currents in the network line currents due to the imbalance created by the fault. There is also a difference in negative and zero sequence values depending on the winding configuration of the IIDGs interfacing transformer. The negative sequence current values are larger when all IIDGs are interfaced with transformers configured in Delta-Wye while the associated zero sequence current values are lower. This also creates a challenge on conventional protection relays using sequence components.

Table 3.4: IIDGs and network behaviour in grid-connected and islanded operation modes

	Grid-connected				Islanded			
Transf. config.	**Delta-Wye**		**Wye-Wye**		**Delta-Wye**		**Wye-Wye**	
Fault type	**3ph**	**A-G**	**3ph**	**A-G**	**3ph**	**A-G**	**3ph**	**A-G**
IIDG 1 current (p.u)	1.0	1.0	1.0	1.0	1.0	1.0	1.0	1.0
	1.2	1.2	1.2	1.2	1.2	1.2	1.2	1.2
	0.0	0.0	0.0	0.0	0.0	0.0	0.0	0.0
	0.0	0.0	0.0	0.0	0.0	0.0	0.0	0.0
IIDG 1 Transf. current (A)	42	42	42	42	42	42	42	42
	50	50	50	50	49	49	49	49
	0.0	1.4	0.0	1.0	0.0	2.3	0.0	1.6
	0.0	150	0.0	0.9	0.0	16	0.0	0.8
Line 2-3 current (A)	100	100	100	100	–	–	–	–
	1836	756	1836	566	–	–	–	–
	0.3	698	0.3	508	–	–	–	–
	0.0	201	0.0	485	–	–	–	–
Line 3-4 current (A)	50	50	50	50	2.8	2.8	2.8	2.8
	1893	764	1893	566	76	39	76	27
	0.7	725	0.7	528	0.0	37	0.0	25
	0.0	517	0.0	519	0.0	35	0.0	25
Line 3-8 current (A)	67	67	67	67	29	29	29	29
	12	32	13	40	27	4.5	27	14
	1.0	32	1.1	23	0.0	30	0.0	20
	0.0	170	0.0	40	0.0	18	0.0	21
Load current-Bus 3 (A)	22	22	22	22	11	11	11	11
	3.0	14	3.0	16	0.1	6.7	0.1	8.9
	0.0	7.8	0.0	5.7	0.0	6.6	0.0	4.4
	0.0	4.1	0.0	9.8	0.0	0.2	0.0	4.5

Note: The black, red, blue and orange coloured values in the table represent pre-fault current, positive sequence fault current , negative sequence fault current , and zero sequence fault current respectively.

3.5 Conclusions

This chapter has presented an initial analysis for a selected number of inverter control approaches and current limiting techniques. Two types of faults have been simulated and key aspects have been discussed. In grid-connected, different control and current limiting strategies were simulated and results were as expected. In the islanded or isolated operation mode, the grid-forming control and current limiting strategy were discussed and the impact of the feedforward compensation on the behaviour of the inverter during fault conditions. Finally, results from grid-connected and islanded operation mode have been discussed.

From the discussions in this chapter, phase currents or sequence currents magnitudes cannot be used directly as protection parameters as the levels are significantly different in grid-connected and islanded operation mode. Also, this chapter has given an insight on the the lack of grid-forming actual fault models since the literature on inverter fault behaviour only provide models that can be representative of the devices as it is quite often difficult to get the data from the manufacturers.

Subsequent chapters in this thesis focus on the development of protection strategy for islanded multi-inverter based microgrids. With challenges obtaining the data from the manufacturers to obtain the equivalent models much attention is paid on the typical known inverter fault characteristics to develop the protection schemes.

Chapter 4

Current Phase Angle for Microgrid Protection

4.1 Introduction

This chapter discusses the challenges related to the choice of protection parameters for islanded multi-inverter based microgrids and the literature background on potential parameters. An analysis of positive sequence current phase angle as a potentially appropriate protection parameter is provided. The chapter also provides the background on the characteristics of electric lines, overhead lines and cables, used in microgrids and their impact on the current flowing through the lines.

While microgrid protection field has attracted a big deal of research, most of the proposed protection schemes in the literature for inverter based microgrids have tried to adapt conventional protection schemes to establish their effectiveness. Despite this effort, it seems that this approach might not be appropriate as the effectiveness of a protection scheme depends on the operational conditions of the system to be protected. On the other hand, other proposed protection schemes that might effectively work are based on complex algorithms that require many input parameters from both current and voltage measurements. This amount of parameters requirement leads to high cost that might not be acceptable for distribution system's investment.

The lack of appropriate microgrid protection relays due to this techno-economic challenge has pushed

the use of sub-transmission and transmission based protection schemes in distribution systems embedded with IIDGs and multi-inverter microgrid systems [1]. Despite the use of these proven conventional transmission protection schemes, their application to distribution systems embedded with IIDGs and multi-inverter microgrid systems suffers technical limitations, particularly when a high number of IIDGs are integrated into the system, as comprehensively demonstrated in [1] except differential protection.

Differential protection schemes; however, in their conventional form necessitate sophisticated and significantly expensive communication systems to allow the exchange of signals between relays at both ends of the line. Unfortunately, communication-less protection schemes have proved to be ineffective for multi-inverter microgrids due to bidirectional power flow, and limited and controlled fault currents generated by the voltage source converters interfacing the energy source to the network. Therefore, to conserve the reliability brought by differential protection schemes, there is a need to reduce the cost requirement associated with their conventional form.

The cost reduction leads to the second question on how can one achieve a minimum data size to be exchanged between remote and local line relays in order to allow the usage of a low bandwidth communication system without jeopardising the effectiveness of the protection scheme.

It has been almost a conventional principle that the communication system infrastructure should meet the protection algorithm communication requirements. This is evident in most communication-assisted protection schemes proposed in the literature where the communication system is not comprehensively covered by assuming that the communication infrastructure that meets the requirements is available. However, in distribution system and microgrids, this approach does not seem to work. Therefore to address the question in this study, an opposite analysis approach to the conventional one is adopted. This means that the proposed protection algorithm output data size should be as minimum as possible to allow the use of low bandwidth communication infrastructure such as power line carrier and unlicensed microwave radio.

The minimum data size possible is the binary bit. This means that the protection parameter should be translated in an event based information. This adds a challenging twist to the first study question on whether an event information extracted from a single parameter could effectively protect distribution systems embedded with IIDGs and multi-inverter microgrid systems.

4.2 Advantages of Positive Sequence Current Phasor

The conceptual operation of multi-inverter distribution systems and microgrids is mainly influenced by inverter control, particularly during faults. This is one of the main reason conventional protection schemes fail to effectively protect such systems.

Research studies recently undertaken based on data mining have identified appropriate parameters for microgrid protection [20–22]. It has been revealed that symmetrical components of voltage and current signals contain significant information for fault discrimination, particularly positive and negative sequence components [20, 21]. Furthermore, [21] shows that the same sequence current components and the power factor angle are the most appropriate quantities for fault localisation.

Consequently, one can conclude that both positive and negative symmetrical components of the current contain significant information useful for both fault detection and localisation. Positive sequence components have an advantage as they exist for all types of faults. This advantage helps us to select a parameter on which a protection scheme is developed in this study.

While the above features can detect and localise the fault, achieving 100% accuracy is difficult especially for fault localisation in islanded microgrid. Nevertheless, [20] has demonstrated that differential quantities can provide high level of accuracy than just local features from measurements at only one end of the line. This makes the idea of developing a protection scheme using both positive sequence current phasors and differential features a compelling one for multi-inverter microgrid protection.

4.3 Microgrid Line Characteristics and Detection of Change in Direction of Current Flow

The transfer of electrical power from generating station to consumers is done through overhead lines and cables. These conductors are characterised by four main parameters namely series resistance (R) and inductance (L); shunt capacitance (C) and conductance (G). Although these basic parameters are the same for both overhead lines and cables, their values are different due to their different structures. These values form the basis for line/cable modeling depending on the conductor length and application. While the values of series resistance and inductance of the conductor are always taken into account for line/cable modelling, the shunt conductance and capacitance are not. The

series resistance and inductance are basically due to intrinsic characteristics of the conductor; the conductor resistivity and structure (and distance between other conductors in case of three phase system) respectively. These characteristics measure the capability of the line/cable to transport power.

On the other hand, the shunt conductance and capacitance values depend only on external interactions. The shunt conductance is reflected in the leakage currents along insulator to the ground while the capacitance depends the distance between conductors and line/cable insulator properties [109]. The effect of these external interactions are neglected in some cases. For example, the effect of shunt conductance is neglected in power lines due to very small values of leakage currents.

In medium voltage , the equivalent circuit of a three phase line or cable will depend on the above parameters. However, as discussed their values depend on the line or cable performance which depends on application. Similar to conventional medium or low voltage distribution systems, microgrids are characterised by short lines/cables. Though it is unlikely that underground cables are found in medium voltage microgrids due to their cost, it is possible they can still be used in some sections of the network. They also can be found in existing distribution feeders.

While the equivalent circuit of short overhead lines (conventionally less than 80 km) is usually characterised by only series resistance and inductance with shunt parameters neglected, the effect of high shunt capacitance of the cables cannot be neglected unless the cable length is significantly shorter. This may be the case for microgrids [7].

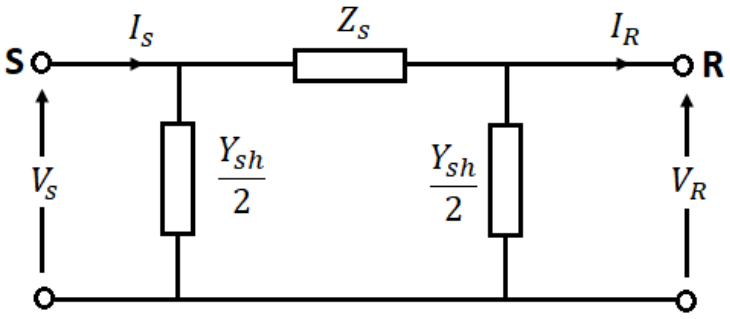


Figure 4.1: Lumped π section model of a line/cable

Typically, short lines are modelled using π model as shown in Fig. 4.1. The series resistance and inductance are represented by the series impedance Z_s and shunt capacitance by shunt admittance Y_{sh}. The model is considered as a four terminal system where the sending and receiving ports are respectively denoted by “S” and “R”.

Considering a two-source system illustrated in Fig. 4.2, a power line L_{AB} protected by Relays 1 and 2 at its both ends are assumed. It is also assumed that both relays have the same monitoring direction. Practically this is achieved by ensuring that their respective current transformers circuits are polarized at the two ends.

During normal operational conditions or for an external fault, the three-phase currents measured at the remote end are almost in phase with their local counterparts. Consequently, the local and remote positive sequence currents calculated by the respective relays have the same direction. This is illustrated in Fig. 4.2. The figure illustrates also the current flow direction in case of an internal fault whereby the current flows into the fault point from both ends of the line.

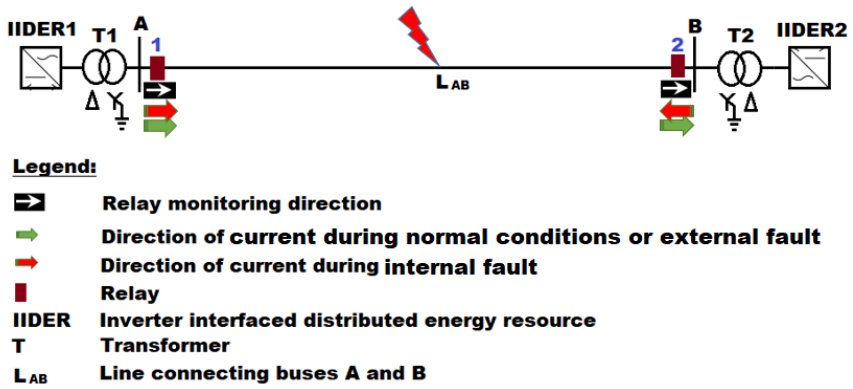


Figure 4.2: Two IIDG system

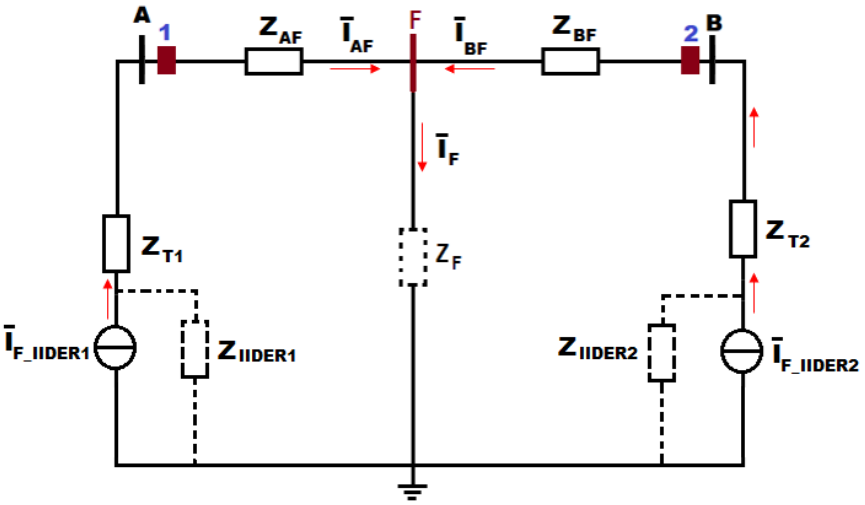


Figure 4.3: Positive sequence equivalent circuit of the system in Fig. 4.2

Assuming a three-phase fault on Line L_{AB} occurred at point F, the positive sequence equivalent

circuit of the system in Fig. 4.2 is given in Fig. 4.3. The transformers are represented by their respective positive sequence impedances Z_{T1} and Z_{T2} while the impedances of the right and left parts of the Line L_{AB} with respect to the fault point position are Z_{AF} and Z_{BF} respectively. In the circuit, the inverter interfaced distributed energy resources (IIDGs) are represented by positive sequence current sources in parallel with their respective internal positive sequence impedances [110–112]. Since the internal impedances are much larger than other impedances, they are ignored. It is a standard that the values of the positive sequence current generated by the inverter for each type of fault are provided by the manufacturers [112].

The total fault current $\bar{I}_F$ is given by the sum of currents flowing towards the point F. The bar sign indicates the phasor value.

$$\bar{I}_F = \bar{I}_{AF} + \bar{I}_{BF}$$

From the figure, it is clear that the faults currents $\bar{I}_{AF}$ and $\bar{I}_{BF}$ depend mainly, if not totally, on the fault currents generated by the IIDGs.

$$\bar{I}_{AF} = \bar{I}_{F_IIDG1} \quad \text{and} \quad \bar{I}_{BF} = \bar{I}_{F_IIDG2} \tag{4.1}$$

The expression (4.1) demonstrates the effect of the behaviour of the inverter based generator during fault. Replacing the IIDGs by conventional synchronous generators (SGs) in the given system, the equivalent circuit of the system becomes quite different as shown in Fig. 4.4. In the circuit, the SGs are represented by their internal positive sequence impedances Z_{SG1} and Z_{SG2}, and an equivalent voltage source at the fault location. From Fig. 4.4 it can be clearly seen that the fault currents depend mainly on the circuit impedance.

With the fault currents in inverter-based microgrid depending mainly on the inverters control, the directional feature of the current in the system becomes an interesting aspect. In order to analyse this aspect, the phasor representation of the currents is considered.

Assuming $\bar{I}_{pre} = I_{pre}\angle\phi$ to be the positive sequence current phasor during normal operational conditions. With no reference, the angle ϕ can be in any angle quadrant. For analysis purposes, the voltage phasor $V_{pre}\angle 0$ is assumed. In such a case, ϕ will be in the 4^{th} quadrant if a slightly inductive system load is considered while keeping in mind that the recommended power factor (PF) is close to 1.

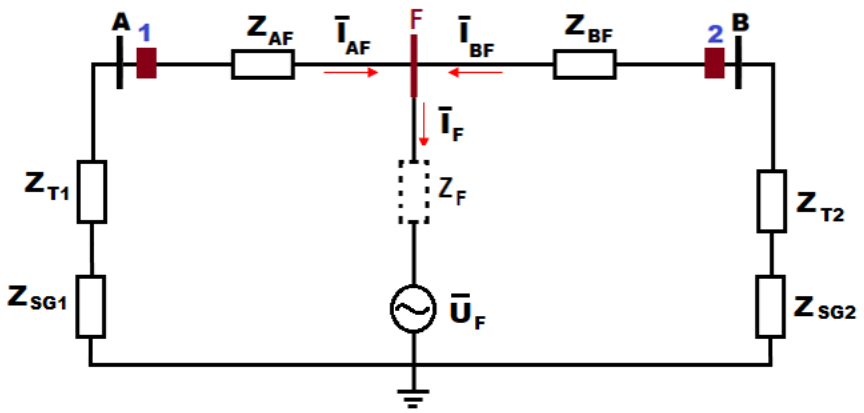


Figure 4.4: Positive sequence equivalent circuit of the system in Fig. 4.2 with IIDGs replaced by synchronous generators

For an internal fault, as mentioned, the fault currents flow towards the fault location from both ends. This means that one end experiences a change in current flow direction while the other stays unchanged. Considering the LVRT capability, the maximum angle difference between pre-fault and fault currents occurs when fault currents generated by the IIDGs are much more reactive. Therefore the following two cases are analysed:

- **CASE 1:** IIDGs generate reactive current and the flow direction remains unchanged
- **CASE 2:** IIDGs generate reactive current and the flow direction changes.

For each case, the phase angle of the positive sequence current is analysed for changed flow direction and for unchanged flow direction.

CASE 1: The analysis of this case is based on phasor diagram, as shown in Fig.4.5. During normal operation, the current generated by IIDGs is more active i.e. the current phase angle is close to zero. When reactive current is generated by IIDGs, which is usually the case for LVRT capability requirement, the fault current in the line will be more inductive i.e. the phase angle of the current ϕ' moves towards (but always less than) $-\frac{\pi}{2}$ radians. Mathematically,

$$\phi' < \frac{\pi}{2} \tag{4.2}$$

From (4.2) it can be concluded that when the flow direction of the positive sequence current is

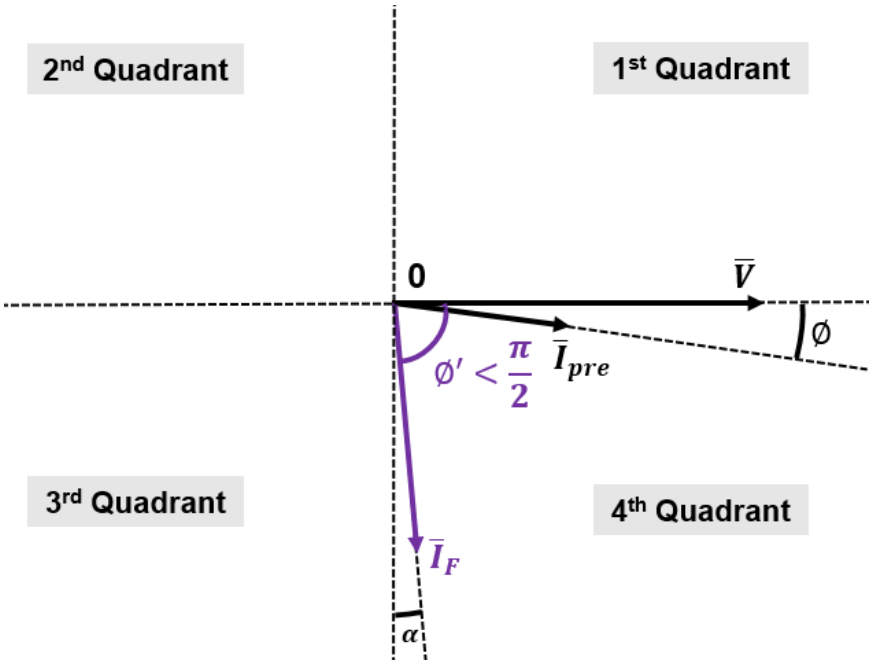


Figure 4.5: Comparison of positive sequence pre-fault and fault current phasors

unchanged, the fault and pre-fault current phasors lie in the same quadrant. This case is the same for an external fault.

CASE 2: The analysis of this case is illustrated in Fig. 4.6. Starting the analysis with the impact of change in flow direction, when the current direction changes without a change in PF, the phase angle becomes out of phase at about π rad i.e. the phasor becomes symmetrical to the pre-event phasor with respect to zero origin of the complex plane. Consequently, the phasor lies in the quadrant symmetrically opposite to the pre-event quadrant with respect to zero origin.

Taking into account both the impact of change in direction and fault occurrence, the fault current phasor will lag the pre-fault current with maximum angle difference of less than $-\frac{\pi}{2}$. Equivalently, the fault current phasor lies in the same quadrant as the phasor obtained considering only the flow direction.

$$\phi + \pi - \phi' < \frac{\pi}{2} \tag{4.3}$$

From (4.2), it can be concluded that when the flow direction of the positive sequence current changes due to fault, the fault and pre-fault current phasors lie in opposite quadrant with respect to zero

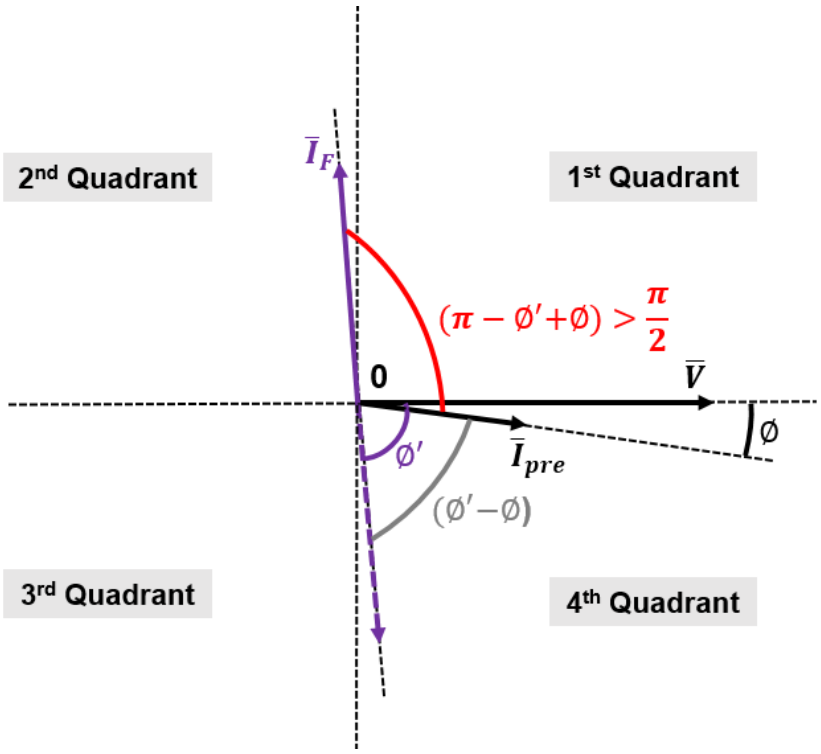


Figure 4.6: Comparison of positive sequence pre-fault and fault current phasors with change of flow direction

origin of the complex plane.

4.4 Conclusions

In this chapter, the phase angle of the current has been discussed as a parameter for microgrid protection, particularly multi-inverter based microgrids. The advantages of choosing the phase angle have been highlighted in this chapter, particularly the phase angle of the positive sequence current for three-phase systems. With reliability being essential for protection applications, differential features have been identified as an essential factor whereby two phase angle values from two points in the system can be compared for fault detection and localisation. While this feature, in this chapter, has been considered for local and remote ends of the line, this can be extended to a busbar whereby the phase angle values of the currents flowing through the lines connected to the busbar are compared. An application of such a comparison is discussed in one of the proposed schemes in Chapter 7. It is important to highlight that the comparison of features requires a communication channel between

the local and remote relays. Therefore, a minimal size message is ideal considering the cost of the communication system. This aspect is discussed in the subsequent chapters, particularly in Chapter 6.

Chapter 5

Estimation of phasors

5.1 Introduction

This chapter provides the mathematical background around phasor estimation. As discussed in the previous chapter, the focus of this thesis is to derive the appropriate protection parameters from positive sequence currents. The main parameter is the value of the positive sequence current phase angle. The computation algorithm of this parameter can be done in microprocessor based relays. In such relays, analog current signals are sampled and transformed into digital signals before being processed by the microprocessor for decision making.

In this particular case, the decision making is derived from the positive sequence current phasor estimates from the measured three-phase currents signals. To obtain the estimates, a phasor estimation algorithm is necessary in the microprocessor software. There exist many algorithms for phasors estimation. Among them are the least squares-based algorithms, Fourier algorithms, differential-equations algorithms, Kalman filter algorithms and Walsh functions algorithms [113]. The former two algorithms are the most used in power system relaying and are only discussed in this thesis.

Before discussing these phasor estimation algorithms, it is important to lay down a brief description of the concept of microprocessor based relay also known as numerical relay or digital relay. Numerical relays use software programs to estimate parameters, phasors in this case, required for the protection purposes. Typically, the numerical relay programs are built based on digital signal processing whereby the input current/voltage signal is sampled before it is processed [114].

5.2 Numerical Relays

A relay is defined as a logical element which processes the inputs (mostly voltages and currents) from the system/apparatus and issues a trip decision if a fault within its jurisdiction is detected [46]. Fig. 5.1 illustrates its concept.

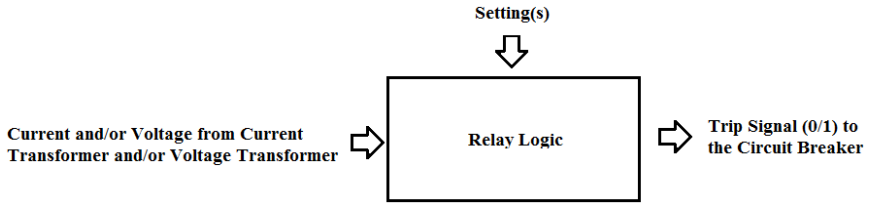


Figure 5.1: Conceptual Diagram of a Relay

The relay technology has evolved over a century from electromechanical relays through solid State relays to numerical relays. The first generation, the electromechanical relays, use the principle electromechanical energy conversion for decision making. The solid-state relays use logical operations based on analog circuit to generate the output. These relays offer self-checking ability, low burden to the instrumental transformers, improved dynamic performance characteristics, high seismic withstand capacity and space saving. Despite their advantages over the electromechanical relays, they have been superseded by numerical relays. Numerical relays, also called computer relays, are microprocessor-based relays that make decision using software algorithm to process the input signal(s). These relays offer additional advantages to solid states 'ones. The most important are reflected in their cost, lower burden (very low impedance), ease at system integration and digital environment, and functional flexibility and adaptive relaying, less immune to variation of individual components, the use of communication cables rather than long lead wires, storage capacity (pre- and post-fault data). Numerical relays are adaptive as they allow minimisation of compromises that normally have been represented by conventional relays (electromechanical and solid state relays of the order of few cycles – memory cost), time stamping of data, simple interfacing with instruments transformers (e.g. zero sequences computation inside the processor rather than additional wiring to instruments transformers), reduced maintenance and possible uniform hardware design for different protective relaying purposes (the function is determined by software than hardware). These compromises are economy and performance, dependability and security, complexity and simplicity, speed and accuracy, credibility and conceivability. Numerical relaying can conceptually be illustrated in Fig. 5.2.

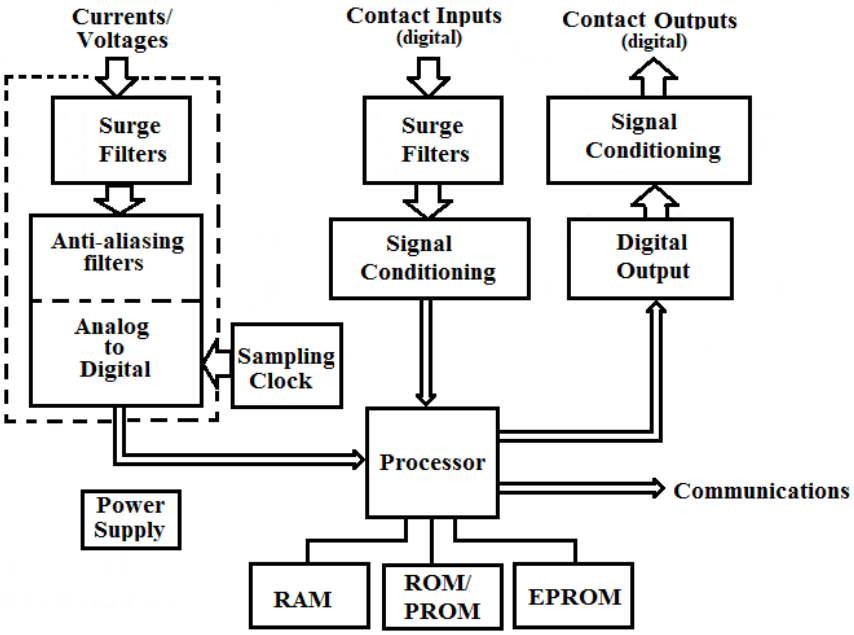


Figure 5.2: Relaying Computer Concept [113]

The current and/or voltages signals as well as the signals indicating circuit breakers contact status (from other relays or other element in the system), are input to the relay. These signals (current and/or voltage) which are measured by instrument transformers are usually analog signals and are converted to voltage signal suitable for analog to digital conversion; typically to a full-scale value of ± 10 volts. While current signals can be converted to suitable voltage signals using resistive shunt or an auxiliary current transformer, voltage signals can be scaled down using resistive potential divider or an auxiliary voltage transformer. The relay should also be protected from surges created by faults or switching events using surge filters or optical isolation. The output signal from the surge filter is again filtered and sampled. The sampling process is characterised by a sampling frequency. This frequency indicates the choice of the filters cut-off frequency, which is usually less than half the sampling frequency to satisfy the Nyquist criterion. These filters, which are usually analog are called anti-aliasing filters. It is important to note that the sampling is performed by a sample and hold (S/H) circuit at intervals defined by the sampling clock. At the specific instant determined by the sampling clock, the S/H circuit converts the analog signal value to digital. There are two types of analog to digital conversion techniques. One is known as successive approximation technique, which uses sampling frequency of few kHz. Another one is delta-sigma technique which uses high sampling rate (referred to as oversampling) in the region of tens of kHz. The latter technique requires an anti-aliasing filter with high cut-off frequency and a digital decimation filter to convert the sampled

data to a lower sampling rate suitable for relaying applications. This technique offers simplicity and is less expensive [2]. Moreover, it provides a stable anti-aliasing filtering ensuring the same phase shift and attenuation for all the analog input signals. The digital signals produced are then processed in the microprocessor. This relay part is responsible for the execution of the relay program. These samples input to the microprocessor are fed to the Random-Access Memory (RAM), where they are held as they are processed. The relay algorithm is stored in the Read Only Memory (ROM) or Programmable Read Only Memory (PROM). The Erasable PROM (EPROM) stores the data that can be erased such as setting parameters that can be changed depending on the relaying algorithm built. This memory can also store other information input to or output from the microprocessor depending on its size.

5.3 Sampling Theorem

As mentioned sampling of the input waveform is the starting point of any digital signal process. The sampling of many analog inputs, such as three-phase signals, can be simultaneous or non-simultaneous. With the latter requiring linear interpolation to generate approximate simultaneous samples from non-simultaneous ones, it may require longer time to compute [113]. **This makes simultaneous sampling preferable and is assumed in this document.**

Turning to the question of sampling theorem, a time continuous periodic function $x(t) = sin(2\pi f_0 t)$ (with f_0, its frequency) is considered for analysis. Assuming a sampling interval t_s (i.e. the sampling frequency $f_s = \frac{1}{t_s}$, the sampled values of the function are given by

$$x(n) = sin(2\pi f_0 n t_s + 2\pi m) \tag{5.1}$$

where n is an integer and m, an integer multiple of n i.e. $m = kn$, k an integer.

Considering the periodic aspect of the given function, (5.1) can be written as

$$x(n) = sin\Big[2\pi n t_s (f_0 + k f_s)\Big] \tag{5.2}$$

where m is an integer multiple of n i.e. $m = kn$; k an integer.

Analysing the expressions (5.1) and (5.2), it is clear that functions $x_1(t) = sin(2\pi f_0 t)$ and $x_2(t) = sin\Big[2\pi(f_0 + k f_s)t\Big]$ can have the same sampled values. This occurs when the sampling time interval is

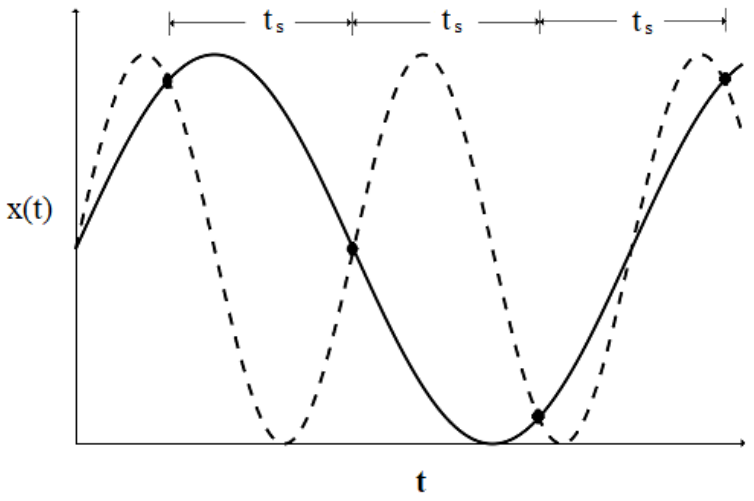


Figure 5.3: Time-domain aliasing illustration

very large. Fig. 5.3 illustrates this effect, whereby the samples can represent two periodic functions of different frequencies. This effect characterising the inability to distinguish the frequency of the waveform function is called aliasing.

To understand this effect well, it is then important to consider the analysis of the waveform in the frequency-domain. In a general form, a sampled waveform of x(t) with sample interval t_s is given by

$$x_s(t) = x(n) = x(t) \sum_{n=-\infty}^{\infty} \delta(t - nt_s) = \sum_{n=-\infty}^{\infty} x(nt_s)\delta(t - nt_s); \quad n = 0, \pm 1, \pm 2, \pm 3, ... \tag{5.3}$$

where $\delta(t)$ is the impulse function also called Dirac function or a distribution function and is used as a sampling function.

The frequency version of the function can be derived from the time sampled values using the frequency-convolution theorem. The expression (5.3) is the product of the continuous time function and the sequence of impulses function. Assuming $\Delta(t)$ a time sampling function consisting of infinite sequence impulses separated by time interval t_s and $\Delta(f)$ its Fourier transform, it can be established from the Fourier transform pair (5.4) that when the sample interval t_s is increased (i.e. sampling frequency decreased), the interval of the impulses of $\Delta(f)$ decreases. When this decrease is high, the convolution with the function $X(f)$ might result in an overlapping waveform. This overlap causes distortion of the resulting waveform, which reflects the aliasing effect.

$$\Delta(t) = \sum_{n=-\infty}^{\infty} \delta(t - nt_s) \Longleftrightarrow \Delta(f) = \frac{1}{t_s} \sum_{n=-\infty}^{\infty} \delta(f - \frac{n}{t_s}); \quad n = 0, \pm 1, \pm 2, \pm 3, ... \tag{5.4}$$

In relaying and many other scientific applications, it is necessary to have samples that can represent the replica of the original continuous function. For this to happen, aliasing should be avoided. This is achieved by choosing the sampling frequency f_s at least twice the highest frequency component f_c of the Fourier transform of the continuous function $x(t)$ (i.e. the sampling frequency that eliminates the convolution overlaps) as given in expression (5.5). This is known as the sampling theorem.

$$f_s = \frac{1}{t_s} \geq 2f_c \tag{5.5}$$

The theorem states that if the Fourier transform of a function x(t) is zero for all frequencies greater than a certain frequency f_c, then the continuous function $x(t)$ can be uniquely determined from a knowledge of its sampled values. The frequency f_c is known as the cut-off frequency. This means that the signal is band-limited, as it has no frequency beyond f_c. The sampling frequency $f_s = 2f_c$ represents the maximum interval between samples for which the theorem is respected. This frequency is known as the Nyquist frequency or folding frequency.

In practice, even a band-limited signal will contain noise. The noise is usually of high frequency and can be aliased to lower frequency. With aliasing phenomenon, it may not be possible to reconstruct the correct frequency domain information, as discussed above. To avoid aliasing errors, it is customary to filter the signal to a bandwidth of half the sampling frequency. Such a filter is known as an anti-aliasing filter.

5.4 Phasor Representation of a Sinusoid

Mathematically AC voltage and current signals are represented by a sinusoidal function. Any sinusoidal function can be represented in the form of a phasor.

Assuming a constant and continuous sinusoidal function $x(t)$ with peak amplitude X_m, a frequency f, and a phase angle ϕ can be defined as $x(t) = X_m cos(2\pi ft + \phi)$. If the signal is sampled at a frequency $f_s = Nf$ (N, an integer), the samples are given by the following discrete function $x(n)$:

$$x(n) = X_m cos(n\theta + \phi) \tag{5.6}$$

where $n = 1, 2, 3, ...N-1$, θ the sampling angle given by $2\pi/N$.

The phasor representation of the sinusoid is given by the expression in (5.7) [115]:

$$\bar{X} = \frac{X_m}{\sqrt{2}} e^{j\phi} = \frac{X_m}{\sqrt{2}} [cos\phi + jsin\phi] = \bar{X}_r + j\bar{X}_i \tag{5.7}$$

where, $\bar{X}_r$ and $\bar{X}_i$ are the real and imaginary parts of the phasor respectively.

Applying Ptolemy's cosine sum identity, the expression in (5.6) becomes

$$x(n) = X_c cos(n\theta) + X_s sin(n\theta) \tag{5.8}$$

where, $X_c = X_m cos\phi$ and $X_s = X_m sin\phi$.

Transforming from a sum of two trigonometric functions to a single function yields

$$x(n) = \sqrt{(X_c)^2 + (X_s)^2} cos(n\theta - \alpha) \tag{5.9}$$

where, $\alpha = tan^{-1}(\frac{X_s}{X_c})$.

Comparing (5.6) and (5.9), the following is obtained:

$$X_m = \sqrt{(X_c)^2 + (X_s)^2} \quad \text{and} \quad \phi = -\alpha = -tan^{-1}\left(\frac{X_s}{X_c}\right) \tag{5.10}$$

Therefore, it can be derived from (5.7) and (5.10) an expression that can be used to estimate the phasor values from sample values:

$$x(n) = \sqrt{2}\bar{X}_r cos(n\theta) - \sqrt{2}\bar{X}_i sin(n\theta) \tag{5.11}$$

5.5 Phasor Estimation Using Least-Square Technique

The least squares estimation (LSE) method is based on measurement redundancy to reject the noise component of the signal. This is a proven principle and is referred to as measurement redundancy.

Ideally, to accurately estimate the unknowns, the number of samples should be higher than the number of unknowns.

Considering K samples ($N > K > 2$) of the sinusoidal signal in (5.11) with a noise component $e(n)$, the phasor estimation problem can be formulated using (5.11) as follows:

$$\begin{bmatrix} x_n \\ x_{n-1} \\ . \\ x_{n-K+1} \end{bmatrix} = \sqrt{2} \begin{bmatrix} cos(n\theta) & -sin(n\theta) \\ cos[(n-1)\theta] & -sin[(n-1)\theta] \\ . & . \\ cos[(n-K+1)\theta] & -sin[(n-K+1)\theta] \end{bmatrix} \begin{bmatrix} \bar{X}_r \\ \bar{X}_i \end{bmatrix} + \begin{bmatrix} e_n \\ e_{n-1} \\ . \\ e_{n-K+1} \end{bmatrix} \tag{5.12}$$

The noise component models real life measurement and signal conditioning inaccuracies as well as errors from voltage/current measurement devices and analog to digital (A/D) converters. They are typically represented by zero mean Gaussian distribution. Redundancy in measurements serves to filter out the noise. The introduction of the noise component renders the system non-linear. Since there is no exact solution to (5.12), the system's solutions can be approximated using least squares estimated technique.

The expression (5.12) can be written in a simple generalised matrix format

$$b = Ax + e \tag{5.13}$$

The objective of LSE is to minimise the noise so that the vector b is as close to Ax as possible. The noise vector minimisation is obtained by minimising its Euclidean norm or preferably the square of its Euclidean norm to simplify calculations. This norm is the sum of the squares of its elements as in (5.14). To do so, the gradient of the objective function is set to zero, as in (5.15), to obtain the minimum value of the function from which the least squares estimates are determined.

$$O(x) = (b - Ax)^T (b - Ax) \tag{5.14}$$

$$\nabla O(x) = A^T Ax - A^T b = 0$$

$$A^T Ax = A^T b \tag{5.15}$$

The least squares estimates are therefore given by

$$x = [A^T A]^{-1} A^T b \tag{5.16}$$

Applying (5.16) to (5.12), the phasor estimates using least squares estimation are given by

$$\begin{bmatrix} \bar{X}_r \\ \bar{X}_i \end{bmatrix} = \frac{1}{\sqrt{2}} \begin{bmatrix} \sum_{k=n-K+1}^{n} cos^2(k\theta) & \sum_{k=n-K+1}^{n} sin(k\theta)cos(k\theta) \\ \sum_{k=n-K+1}^{n} sin(k\theta)cos(k\theta) & \sum_{k=n-K+1}^{n} sin^2(k\theta) \end{bmatrix}^{-1} \begin{bmatrix} \sum_{k=n-K+1}^{n} cos(k\theta).x(k) \\ \sum_{k=n-K+1}^{n} sin(k\theta).x(k) \end{bmatrix} \tag{5.17}$$

The estimation of phasors based on LSE uses all matrix elements, resulting in very complex calculations. Despite the possibility of using few samples, the computation complexity is a major disadvantage for this technique. Furthermore, the frequency response of this algorithm does not reject all harmonics and dc offset as well as any other noises which do not have zero mean.

5.6 Phasor Estimation Using Fourier Algorithms

In the previous section, it has been highlighted that LSE algorithm are characterised by a certain number of samples defining the length of the data window. With Fourier-based algorithms, the data window length is defined by its time span. For a fixed data window time span, the higher the sampling frequency, the higher the number of samples in the data window. As highlighted above for the least squares technique, the number of samples in this data window should always be higher than two samples. This is equally emphasised by the sampling theorem.

Fourier series and transforms have proved to be powerful mathematical tools for signal analysis. They include continuous time Fourier series (CTFS), discrete time Fourier series (DTFS), continuous time Fourier transform (CTFT), discrete time Fourier transform (DTFT), discrete Fourier transform (DFT), and fast Fourier Transform (FFT). However, each of these tools is applied depending on the application. Power system numerical relaying field is based on using microprocessors whose storage and computation process is inherently discrete i.e. they can only handle discrete signals (in time or frequency domain). This practical requirement of numerical relays limits the application of the Fourier tools to DFT and FFT, since they can handle discrete inputs and yield discrete outputs.

The Fourier transform is at the heart of signal phasor estimation; and both DFT and FFT are practical methods for calculating the Fourier transform. The DFT is used when a small number of samples (4 to 20) [113] are considered. When the number of samples is very high or when many signal frequency components are considered, the FFT is used. In power system protection relaying, very few applications require the use of FFT as usually only few samples of the fundamental frequency are required [113]. In this study, the fundamental frequency phasor estimation is the subject, which makes the DFT more appropriate.

5.6.1 Discrete Fourier Transform

The DFT can be considered as a special continuous Fourier transform which is suitable for digital computation for a better understanding of the relationship between CTFT and DFT [114]. It is given by the Fourier transform calculated at discrete steps in the frequency domain, just as the input signal is sampled at discrete instants in the time domain [115].

The Fourier transform of a continuous time function x(t) is obtained mathematically by applying the Fourier integral to it as follows:

$$X(f) = \int_{-\infty}^{+\infty} x(t) e^{-j2\pi ft} dt$$

If this integral exists for every value of frequency f, then $X(f)$ is defined as the Fourier transform of x(t). The existence of the integral is defined by conditions well documented in the literature [114] and functions used in real life, especially power system relaying are well-defined functions that meet these conditions.

While the parameter t represents variable time, f represents variable frequency. Thus, the Fourier transform is a frequency-domain representation of a time-domain function. Using the inverse Fourier transform, the time-domain function can be recovered from the frequency-domain function.

$$x(t) = \int_{-\infty}^{+\infty} X(f) e^{j2\pi ft} df$$

The pair x(t) and X(f) is known as Fourier transform pair. The pair relationship is expressed as follows in some literature.

$$x(t) \Longleftrightarrow X(f)$$

Mathematically, the DFT can be established from the continuous Fourier transform by performing the following three consecutive main steps: (1) time-domain sampling, (2) windowing, and (3) frequency-domain sampling [114].

(1) Time-domain sampling: Assuming a time continuous function $x(t)$ sampled at time interval t_s chosen such that there is no aliasing effect and using the time sampling function $\Delta(t)$, the sampled values of the function are given by

$$x(t)\Delta(t) = \sum_{n=-\infty}^{\infty} x(nt_s)\delta(t - nt_s); \quad n = 0, \pm 1, \pm 2, \pm 3, ... \tag{5.18}$$

(2) Windowing: The windowing process or truncation can mathematically be expressed by multiplying the sampled function by a windowing function such as a rectangular function as given in (5.19).

$$x(t)\Delta(t)w(t) = \left[\sum_{n=-\infty}^{\infty} x(nt_s)\delta(t - nt_s)\right] w(t) = \sum_{n=0}^{N-1} x(nt_s)\delta(t - nt_s) \tag{5.19}$$

where T_0 is the duration of the windowing function; $N = \frac{T_0}{t_s}$, the number of samples lying within the data window; and $w(t)$, the windowing function given by

$$w(t) = \begin{cases} 1, & \text{if - } \frac{t_s}{2} < t < T_0 - \frac{t_s}{2}. \\ 0, & \text{otherwise.} \end{cases}$$

The windowing function w(t) limits the number of samples from 0 to (N-1). It is chosen such that a sample value does not coincide with each end point of the windowing function. Otherwise, it may cause time-domain aliasing.

The Fourier transform of the sampled and windowed waveform can be obtained by the convolution of Fourier transforms of the three functions $X(f)$, $\Delta(F)$, and $W(f)$:

$$x(t)\Delta(t)w(t) \Longleftrightarrow X(f) * \Delta(F) * W(f) \tag{5.20}$$

The last step is the mathematical representation of the sampling of Fourier transform of the sampled and windowed function. This is done by multiplying the Fourier transform of the expression (5.20) by the frequency sampling function. The frequency sampling function is given by

$$\Delta'(f) = \sum_{n=-\infty}^{\infty} \delta(f - \frac{k}{T_0})$$

As provided in the pair relationship (5.4), the inverse transform of $\Delta'(f)$ is given by

$$\Delta'(t) = T_0 \sum_{n=-\infty}^{\infty} \delta(t - kT_0)$$

In time domain the convolution of the sampled windowed function and $\Delta'(t)$ is given by

$$\Big[x(t)\Delta(t)w(t)\Big] * \Delta'(t) = \left[\sum_{n=0}^{N-1} x(nt_s)\delta(t - nt_s)\right] * \left[T_0 \sum_{n=-\infty}^{\infty} \delta(t - kT_0)\right]$$

$$= T_0 \sum_{n=-\infty}^{\infty} \left[\sum_{n=0}^{N-1} x(nt_s)\delta(t - nt_s - kT_0)\right] \tag{5.21}$$

The function given by equation (5.21) is a periodic function of period T_0 and consists of N samples. Let $\tilde{x}(t)$ be the function given by (5.21). It is important to remember that the Fourier transform of this function is the DFT. Since $\tilde{x}(t)$ is a periodic function, the DFT consists of a series of equidistant impulses.

$$\tilde{X}\Big(\frac{m}{T_0}\Big) = \sum_{k=-\infty}^{\infty} \alpha_m \delta(f - mf_0); \qquad f_0 = \frac{1}{T_0} \tag{5.22}$$

where

$$\alpha_m = \frac{1}{T_0} \int_{-\frac{t_s}{2}}^{T_0 - \frac{t_s}{2}} \tilde{x}(t) e^{\frac{-j2\pi mt}{T_0}} dt; \quad m = 0, \pm 1, \pm 2, \pm 3, ... \tag{5.23}$$

Replacing $\tilde{x}(t)$'s expression from (5.21) in (5.23) yields

$$\alpha_m = \frac{1}{T_0}\int_{-\frac{t_s}{2}}^{T_0-\frac{t_s}{2}} T_0 \sum_{n=-\infty}^{\infty}\sum_{n=0}^{N-1} x(nt_s)\delta(t-nt_s-kT_0)e^{\frac{-j2\pi mt}{T_0}}dt$$

Since the integration is only over one period, the summation on k can be removed, and have $k=0$. This yields

$$\begin{aligned}\alpha_m &= \int_{-\frac{t_s}{2}}^{T_0-\frac{t_s}{2}} \sum_{n=0}^{N-1} x(nt_s)\delta(t-nt_s)e^{\frac{-j2\pi mt}{T_0}}dt \\ &= \sum_{n=0}^{N-1} x(nt_s)\int_{-\frac{t_s}{2}}^{T_0-\frac{t_s}{2}} e^{\frac{-j2\pi mt}{T_0}}\delta(t-nt_s)dt \\ &= \sum_{n=0}^{N-1} x(nt_s)e^{\frac{-j2\pi mn}{N}} \qquad (5.24)\end{aligned}$$

Finally, the Fourier transform of $\tilde{x}(t)$ is given by

$$\tilde{X}\Big(\frac{m}{Nt_s}\Big) = \sum_{k=-\infty}^{\infty}\sum_{n=0}^{N-1} x(nt_s)e^{\frac{-j2\pi mn}{N}} \qquad (5.25)$$

There are only N distinct values for which (5.25) can be evaluated and with $\tilde{X}\Big(\frac{m}{Nt_s}\Big)$ being a periodic function with a period of N samples, the expression (5.25) becomes

$$\tilde{X}\Big(\frac{m}{Nt_s}\Big) = \sum_{n=0}^{N-1} x(nt_s)e^{\frac{-j2\pi mn}{N}} \qquad (5.26)$$

The expression (5.26) is the desired DFT of N input samples taken at intervals t_s. Its inverse $x(nt_s)$, called inverse discrete Fourier transform (IDFT) is given by

$$x(nt_s) = \frac{1}{N}\sum_{n=0}^{N-1} \tilde{X}\Big(\frac{m}{Nt_s}\Big)e^{\frac{j2\pi mn}{N}} \qquad (5.27)$$

The DFT pair is therefore established below

$$x(nt_s) = \frac{1}{N}\sum_{n=0}^{N-1} X\Big(\frac{m}{Nt_s}\Big)e^{\frac{j2\pi mn}{N}} \Longleftrightarrow X\Big(\frac{m}{Nt_s}\Big) = \sum_{n=0}^{N-1} x(nt_s)e^{\frac{-j2\pi mn}{N}} \qquad (5.28)$$

The factor $\frac{1}{N}$ in the time-domain function depends on the respective factor in the frequency domain. Generally, the Relation (5.28) is written as follows:

$$x(n) = C_1 \sum_{n=0}^{N-1} X(m) e^{\frac{j2\pi mn}{N}} \Longleftrightarrow X(m) = C_2 \sum_{n=0}^{N-1} x(n) e^{\frac{-j2\pi mn}{N}} \tag{5.29}$$

where $C_1 C_2 = \frac{1}{N}$. C_1 and C_2 can take any value as long as their product is $\frac{1}{N}$. For example, in (5.28), $C_1 = \frac{1}{N}$ and $C_2 = 1$. However, for relaying application, the following values are recommended: $C_1 = \frac{2}{N}$ and $C_2 = \frac{1}{2}$. This choice simplifies the computation in phasor estimation.

5.6.2 Phasor estimation using full cycle DFT

Let us consider the discrete signal of (5.6) with $x(n) = X_m cos(n\theta + \phi)$ ($n = 1, 2, 3, ...N-1$ and θ the sampling angle given by $2\pi/N$). Applying (5.29), the fundamental frequency DFT of this signal is given by

$$X(1) = \frac{2}{N} \sum_{n=0}^{N-1} x(n) e^{-jn\theta} \tag{5.30}$$

Applying the Euler formula of the exponential factor of the summation term (5.30) becomes

$$X(1) = \frac{2}{N} \sum_{n=0}^{N-1} x(n) cos(n\theta) - j\frac{2}{N} \sum_{n=0}^{N-1} x(n) sin(n\theta) \tag{5.31}$$

From (5.32) the cosine and sine sums can be demarcated in the form of $X(1) = X_c(1) - jX_s(1)$ where

$$X_c(1) = \frac{2}{N} \sum_{n=0}^{N-1} x(n) cos(n\theta) \quad \text{and} \quad X_s(1) = \frac{2}{N} \sum_{n=0}^{N-1} x(n) sin(n\theta) \tag{5.32}$$

Recalling that a phasor magnitude of a signal is equal to the root mean square (RMS) of peak amplitude of that signal, the given signal can be expressed as follows:

$$x(n) = \sqrt{2}|\bar{X}| cos(n\theta + \phi) \tag{5.33}$$

Replacing $x(n)$ with (5.33) in (5.32) yields

$$X_c(1) = \frac{2}{N}\sum_{n=0}^{N-1}\Big[\sqrt{2}|\bar{X}|cos(n\theta+\phi)\Big]cos(n\theta) \quad \text{and} \quad X_s(1) = \frac{2}{N}\sum_{n=0}^{N-1}\Big[\sqrt{2}|\bar{X}|cos(n\theta+\phi)\Big]sin(n\theta) \tag{5.34}$$

Applying the Ptolemy's identity to $X_c(1)$ of (5.34) yields

$$X_c(1) = \frac{2}{N}\sqrt{2}|\bar{X}|\sum_{n=0}^{N-1}\Big[cos(\phi)cos^2(n\theta) - \frac{1}{2}sin(\phi)sin(2n\theta)\Big] \tag{5.35}$$

Since the summation of the term $sin(2n\theta)$ over one period is equal to zero and the average of the term $cos^2(n\theta)$ over a period is equal to $\frac{1}{2}$; then

$$X_c(1) = \sqrt{2}|\bar{X}|cos(\phi) \tag{5.36}$$

Similarly, it can be verified that

$$X_s(1) = \sqrt{2}|\bar{X}|sin(\phi) \tag{5.37}$$

From (5.7), (5.32), (5.36), and (5.37) it can be established that the phasor $\bar{X} = \bar{X}_r - j\bar{X}_i$ of the signal $x(n)$ can be estimated from the fundamental frequency DFT of $x(n)$ as follows:

$$\bar{X}_r = \frac{X_c(1)}{\sqrt{2}} = \frac{\sqrt{2}}{N}\sum_{n=0}^{N-1}x(n)cos(n\theta) \quad \text{and} \quad \bar{X}_i = \frac{X_s(1)}{\sqrt{2}} = \frac{\sqrt{2}}{N}\sum_{n=0}^{N-1}x(n)sin(n\theta) \tag{5.38}$$

With the DFT computed considering a window of a full cycle, the estimation method is known as *full cycle DFT phasor estimation*. This estimation method is known to be accurate and immune to harmonics. Though it is not an issue with the protection scheme proposed in this study, high-speed relaying applications requiring estimates in less than a cycle cannot use this technique.

5.7 DFT Phasor Estimates Updates

If relay protection algorithm necessitates phasors estimates, they should be acquired continuously to ensure that the system is continuously protected. This can be achieved by updating the phasors

as newer data samples are obtained. This updating process can be achieved by two methods: non-recursive or recursive methods.

5.7.1 Non-recursive DFT method

Considering the discrete waveform $x(n) = X_m cos(n\theta + \phi)$ with N samples within a data window, the phasor can be estimated using by (5.37). If the window's index is equal to its last sample's index, the first full window with N samples is the $(N-1)^{th}$ window, with the first sample being $x(0)$. Then the phasor estimates can be as follows:

$$\bar{X}^{N-1} = \frac{\sqrt{2}}{N} \sum_{n=0}^{N-1} x(n)[cos(n\theta) - jsin(n\theta)] \tag{5.39}$$

Since the sinusoid $x(n)$ is constant, its phasor $\bar{X}$ does not change. Therefore, the phasor estimated from the N^{th} data window should be the same as the one estimated at $(N-1)^{th}$ window. Considering that the N^{th} window covers also N samples taken from $n = 1$ to $n = N$. The associated phasor is given by

$$\bar{X}^{N} = \frac{\sqrt{2}}{N} \sum_{n=0}^{N-1} x(n+1)[cos(n\theta) - jsin(n\theta)] \tag{5.40}$$

Substituting the samples $x(n+1)$ by $x(n+1) = \sqrt{2}|\bar{X}|cos[(n+1)\theta) + \phi]$ in (5.40) yields

$$\bar{X}^{N} = \frac{2}{N}\bar{X} \left\{ \sum_{n=0}^{N-1} cos[(n+1)\theta) + \phi]cos(n\theta) - j \sum_{n=0}^{N-1} cos[(n+1)\theta) + \phi]sin(n\theta)] \right\} \tag{5.41}$$

Taking $\phi^{'} = \theta + \phi$, the real part of (5.40) becomes

$$\bar{X}_c^N = \frac{2}{N}|\bar{X}| \sum_{n=0}^{N-1} cos(n\theta + \phi^{'})cos(n\theta) = \frac{\bar{X}}{N} \sum_{n=0}^{N-1} cos^2(n\theta)cos\phi^{'} - \frac{1}{2}sin(n\theta)sin\phi^{'} = |\bar{X}|cos\phi^{'}$$

Following the similar process, it can be verified that the imaginary component $\bar{X}_s^N$ is given by $|\bar{X}|sin\phi^{'}$'.

Replacing back $\phi^{'}$ by $\theta + \phi$, the estimated phasor is found

$$\bar{X}^N = \bar{X}_c^N - j\bar{X}_s^N = |\bar{X}^N|e^{-j\phi}e^{-j\theta} \tag{5.42}$$

This equation shows that with a moving window the phasor estimate rotates at a speedof $e^{j\theta}$ per cycle window. This rotation is not acceptable in the computation of the phasor. It can be avoided by indexing the summation starting from the index of the first sample of the corresponding window [46]. With this principle (5.42) can be written as

$$\bar{X}^N = \frac{\sqrt{2}}{N}\sum_{n=1}^{N}[cos(n\theta) - jsin(n\theta)] \tag{5.43}$$

It can be verified that the estimated phasor from this equation is stationary. And similarly, other phasors can be estimated continuously as a new sample is acquired. Since new phasor calculations are performed for each window without using any data from the earlier estimates, this method is known as "non-recursive algorithm". It is numerically stable but requires much computation.

5.7.2 Recursive method

From (5.39) and (5.40) it can be seen that there is redundancy in the calculations of phasor estimates from consecutive windows. There are $(N-1)$ common samples to the two estimates. It can be established that there are then $(N-1)$ multiplication operations by Fourier coefficients that appear in both phasors expressions. The first sample $x(0)$ appears only in the first window while the newest sample $x(N)$ is only in the subsequent window.

Applying this theory to L^{th} and $(L-1)^{th}$ full cycle windows where each window contains N samples of the sinusoid $x(n) = X_m cos(n\theta+\phi)$, the phasor estimates from the L^{th} data window in the complex form is given by

$$\bar{X}^L = \bar{X}^{L-1} + \frac{\sqrt{2}}{N}\Big[(x(L+N)e^{-j(L+N)\theta} - (x(L-N)e^{-j(L-N)}\theta\Big]$$

$$= \bar{X}^{L-1} + \frac{\sqrt{2}}{N}\Bigg[(x(L+N) - x(L-N)\Bigg]e^{-jL\theta} \tag{5.44}$$

This result can be demonstrated and generalised from the non-recursive expressions of phasors

calculated from both data windows based on the discussion in [113]. Applying (5.41) and (5.42), the non-recursive phasors can be expressed in complex form as follows:

$$\bar{X}^{L-1} = \frac{\sqrt{2}}{N} \sum_{n=0}^{N-1} x(n + L - N) e^{-jn\theta} \tag{5.45}$$

$$\bar{X}^{L} = \frac{\sqrt{2}}{N} \sum_{n=0}^{N-1} x(n + L - N + 1) e^{-jn\theta} \tag{5.46}$$

These phasors, $\bar{X}^{L-1}$ and $\bar{X}^{L}$, can be made stationary by rotating them by angles $(L-N)\theta$ and $(L-N+1)\theta$ respectively. This yields

$$\hat{\bar{X}}^{L-1} = e^{-j(L-N)\theta} X^{L-1} = \frac{\sqrt{2}}{N} \sum_{n=0}^{N-1} x(n + L - N) e^{-j(n+L-N)\theta} \tag{5.47}$$

$$\hat{\bar{X}}^{L} = e^{-j(L-N+1)\theta} X^{L} = \frac{\sqrt{2}}{N} \sum_{n=0}^{N-1} x(n + L - N + 1) e^{-j(n+L-N+1)\theta} \tag{5.48}$$

Equivalently, these expressions can be written as follows:

$$\hat{\bar{X}}^{L-1} = \frac{\sqrt{2}}{N} \sum_{n=L-N}^{L-1} x(n) e^{-jn\theta} \quad \text{and} \quad \hat{\bar{X}}^{L} = \frac{\sqrt{2}}{N} \sum_{n=L-N+1}^{L} x(n) e^{-jn\theta} \tag{5.49}$$

The difference between the two expressions in (5.49) is the first term of the sum in first expression, $\frac{\sqrt{2}}{N} x(L-N) e^{-jn(L-N)\theta}$, and the last term of the sum in second expression, $\frac{\sqrt{2}}{N} x(L) e^{-jnL\theta}$. The remaining $(N-1)$ terms are the same in both expressions. Consequently, these common terms can be used to mathematically combine the two expressions into one expression as given in (5.50)

$$\hat{\bar{X}}^{L} - \hat{\bar{X}}^{L-1} = \frac{\sqrt{2}}{N} \Big[x(L) e^{-jnL\theta} - x(L-N) e^{-jn(L-N)\theta} \Big]$$

$$\hat{\bar{X}}^{L} = \hat{\bar{X}}^{L-1} + \frac{\sqrt{2}}{N} \Big[(x(L) - x(L-N)) e^{jN\theta} \Big] e^{-jL\theta} \tag{5.50}$$

The expression in (5.50) gives a generalised update of phasor estimates for any data window length. For the case of a full cycle window $e^{jN\theta} = e^{jN\frac{2\pi}{N}} = e^{j2\pi} = 1$ and the expression becomes

$$\hat{\bar{X}}^{L} = \hat{\bar{X}}^{L-1} + \frac{\sqrt{2}}{N}[(x(L) - x(L-N)]e^{-jL\theta} \tag{5.51}$$

From this expression, the cosine and sine components demarcated as:

$$\hat{X}_c^{L} = \hat{X}_c^{L-1} + \frac{\sqrt{2}}{N}[(x(L) - x(L-N)]cos(L\theta) \tag{5.52}$$

$$\hat{X}_s^{L} = \hat{X}_s^{L-1} + \frac{\sqrt{2}}{N}[(x(L) - x(L-N)]sin(L\theta) \tag{5.53}$$

From expressions (5.52) and (5.53), the phasor $\hat{X}_c^{L}$ is calculated from the preceding phasor $\hat{X}_c^{L-1}$. This has an advantage of using the previous data window to compute the new phasor by only updating the old phasor. This method is known as *recursive technique*. It offers computational efficiency for phasor estimation due to very few operations involved. This efficiency has made it one of the preferred methods for phasor estimation. However, this fast calculation advantage comes at the cost of instability of the algorithm due to the recursive property. For example, if an error occurs in the old phasor estimate, it will always be present in all subsequent phasor estimates. Fortunately, these accumulated errors have been successively avoided using fixed-point data with carefully scaled coefficients [116]. Moreover, [116] suggests a practical solution to eliminate the errors when float-point data are used.

5.8 Phasor Estimation Challenges in Real Power System

So far, the DFT phasor estimation has been performed assuming a sinusoidal function with a constant frequency, and a sampling frequency, multiple of the frequency. However, voltage and current signals, usually of interest for power system protection relaying, could be constant sinusoidal waveform only if the power system was operated in ideal steady state i.e. the power system frequency is continuously equal to the nominal frequency. Practically, it is difficult, even impossible, to achieve such an ideal operational condition, resulting in having the fundamental frequency of voltage and current signals changing narrowly around the nominal frequency. Some of the factors causing change in frequency are: the change in load generation unbalance, unbalanced loading in phases, faults events, and switching events. The latter two factors may cause the frequency to experience very high frequency

deviation from the nominal frequency. Furthermore, in a microgrid, the control response and the switching do cause changes in system frequency.

It is therefore essential to understand the impact of frequency deviation from the nominal frequency on the DFT phasor estimation and how it can be handled to accurately estimate the phasors. The analysis given in this study follows the discussion in [115].

Among techniques practically used for voltage/current phasor estimation in digital protective relays, discrete Fourier transform (DFT) has been the most popular, particularly recursive DFT due to its simplicity [115–117].

Assuming a constant input current sinusoidal signal $i(t)$ given in (5.54) with nominal frequency f_n and sampled at frequency $f_s = Nf_n$, a full-cycle recursive DFT can be applied to extract the fundamental current phasor of the signal samples I_n (given by (5.55)) as in (5.56) [115]:

$$i(t) = I_m cos(2\pi f_n t + \phi) \tag{5.54}$$

$$I_n = I_m cos(n\theta + \phi) \tag{5.55}$$

where $n = 0, 1, 2, 3, ...$

$$\bar{I}_k = \bar{I}_{k-1} + \frac{\sqrt{2}}{N}[I_k - I_{k-N}]e^{\frac{-2\pi j}{N}} \tag{5.56}$$

where N is the number of samples per cycle, and $k = N+1, N+2, N+3, ...$

The cosine and sine terms of (5.56) can be determined as in (5.57) and (5.58) respectively:

$$\bar{I}_{Ck} = \bar{I}_{k-1} + \frac{\sqrt{2}}{N}\cos\left(\frac{2\pi j}{N}\right)[I_k - I_{k-N}] \tag{5.57}$$

$$\bar{I}_{Sk} = \bar{I}_{k-1} + \frac{\sqrt{2}}{N}\sin\left(\frac{2\pi j}{N}\right)[I_k - I_{k-N}] \tag{5.58}$$

From these terms, the fundamental phasor magnitude $\bar{I}_m$ and phase angle ϕ can be calculated:

$$\bar{I}_m = \sqrt{\bar{I}_{Ck}^2 + \bar{I}_{Sk}^2} \tag{5.59}$$

$$\phi = \tan^{-1} \frac{\bar{I}_{Sk}}{\bar{I}_{Ck}} \tag{5.60}$$

While conventional DFT offers simplicity and precision in steady state conditions, when the signal frequency is temporarily or permanently off-nominal the phasor estimation accuracy is affected when the sampling frequency is fixed and keyed to the nominal frequency. This can happen in practice since the frequency varies constantly around the nominal value in a very narrow range ± 0.5 Hz [115]. The situation is more pronounced in islanded systems, particularly in inverter-only microgrids where frequency excursions may reach ± 10 Hz [115] or the system frequency can settle to a frequency different from the nominal one. In practice however, the frequency deviation is controlled and brought back to a value close to the nominal. On the other hand, the phasor measurement units should be accurate for frequency deviation up to ± 5 Hz [115, 118].

In islanded microgrids, the system operating frequency can therefore be different from the nominal value or experience large frequency fluctuations within a large range around the nominal frequency. The analysis of the impact of the frequency deviation on phasor estimation has been studied in detail in [115, 116] and it is briefly discussed in this chapter in relation to the proposed protection strategy.

Considering the signal i(t) in (5.54) with a frequency $f = f_n + \Delta f$, Expression (5.61) gives the relationship between the off-nominal frequency phasor estimates and the true phasors $\bar{I}_k$ and its conjugates $\bar{I}_k^*$ [115, 116]:

$$\bar{I}'_k = P\bar{I}_k e^{\frac{j2\pi\Delta f}{Nf_n}k} + Q\bar{I}_k^* e^{\frac{-j2\pi(2f_n+\Delta f)}{Nf_n}k} \tag{5.61}$$

where

$$P = \frac{sin\left(\frac{\pi\Delta f}{f_n}\right)}{Nsin\left(\frac{\pi\Delta f}{Nf_n}\right)} e^{j\frac{\pi(N-1)\Delta f}{Nf_n}}$$

$$Q = \frac{sin\left(\frac{\pi\Delta f}{f_n}\right)}{Nsin\left(\frac{\pi\Delta f}{f_n}\right)} e^{j\frac{\pi(N-1)\Delta f}{Nf_n}}$$

5.9 Positive Sequence current Phasor Estimation

From phase phasor estimates, positive sequence phasor estimation of a three-phase input signal can be calculated and analysed. Applying Fortescue transform to three phase phasors $\bar{I}'_{ka}$, $\bar{I}'_{kb}$ and $\bar{I}'_{kc}$ of three phase current input samples I_{ka}, I_{kb} and I_{kc} respectively, yields:

$$\begin{bmatrix} \bar{I}'_{k0} \\ \bar{I}'_{k1} \\ \bar{I}'_{k2} \end{bmatrix} = Pe^{\frac{j2\pi\Delta f}{Nf_n}k} \begin{bmatrix} \bar{I}_{k0} \\ \bar{I}_{k1} \\ \bar{I}_{k2} \end{bmatrix} + Qe^{\frac{-j2\pi(2f_n+\Delta f)}{Nf_n}k} \begin{bmatrix} \bar{I}^*_{k0} \\ \bar{I}^*_{k2} \\ \bar{I}^*_{k1} \end{bmatrix} \tag{5.62}$$

where $\bar{I}_{ka}$, $\bar{I}_{kb}$ and $\bar{I}_{kc}$ are the true phasors and $\bar{I}^*_{ka}$, $\bar{I}^*_{kb}$ and $\bar{I}^*_{kc}$ their respective conjugates.

It is important to note that the transformation from phase to sequence components has been done based on Phase A as the phase reference. It can be clearly seen from (5.62) that the positive sequence current phasor estimated using DFT is attenuated by time-invariant complex factor P with the negative sequence current component attenuated by time-invariant complex factor Q.

In ideal steady state conditions balanced three-phase currents do not present the negative sequence current and only P affects the accuracy of the phasor with most noticeable impact on the phase angle. The phase angle experiences an average slope corresponding to $2\pi\Delta ft$ [115]. This slope changes the true phase angle trajectory with even a very small change in frequency. For example a permanent frequency deviation of 0.0001 Hz causes a change in phase angle from 0 to 2π rad in just under three hours unless the relay is regularly reset. In such conditions, the cosine of the phase angle becomes a periodic signal with a frequency equalling to Δf. This means that to accurately measure the current/voltage phase angle using conventional recursive DFT is very challenging in practice even under slight frequency deviation.

With unbalanced currents, the negative sequence component and the coefficient Q do not affect the overall phase angle trajectory as the P coefficient does. The former affects the phase angle instantaneous values by superposing on it a second order harmonic. This harmonic can be filtered out using an average filter [115].

5.10 Conclusions

In this chapter, different ways of estimating phasor magnitude and phasor angle have been discussed in detail. The main approach, which is mainly used in protective relays, is DFT. Practical challenges to this estimation technique such as off-nominal frequency and unbalanced faults have been discussed in this chapter and how one can deal with them.

It is however, essential to note that the operation of a bulk power system is different from a smaller islanded microgrid. In islanded microgrid, the frequency variation is larger and the system may operate at off-nominal frequency. Furthermore, while harmonics are well dealt with full cycle DFT technique, it can be compromised by interharmonics and DC offset. In Chapters 6 and 7, these challenges and others are discussed with respect to the performance of the proposed protection schemes.

Chapter 6

Protection Scheme Using Current Phase Angle Trajectory

6.1 Introduction

This chapter discusses a line protection scheme based on line local and remote-end current measurements and the comparison of binary state outputs of relays at both ends of the line. The operation principle of the proposed protection scheme (fault detection and localisation) is described along with a 3-Bus multi-inverter microgrid used to demonstrate the effectiveness of the scheme. This scheme is mainly relevant for untapped lines. A more complex system will be considered in chapter 7. Its performance is assessed through several simulations scenarios of the 3-Bus microgrid system. As this protection scheme requires a communication channel between line relays, the unlicensed microwave radio communication system is provided as an example of low-cost communication system that can be used with it.

6.2 Protection Operation Principle

Typically, when a fault occurs on a line the current will flow towards the fault point location. If the line is protected by two relays; one at each end, they will register different current direction transitions with respect to the prefault current flow directions in case a fault occurs. With these

transitions completely different i.e. "**change in current flow direction**" or "**no change**", they can be easily converted into binary digit representation; "**one (1)**" or "**zero (0)**". Assuming the change in direction event to be represented by 1 and no-change event by 0, a fault condition leads to the relays registering different bits. So the change in current direction can be a useful indication of a fault on the line. The fault detection under this chapter does not cover tapped lines, which are commonly not used in networks like microgrids under consideration. Otherwise, an extension to the proposed scheme is proposed in the next chapter as an alternative or back-up protection scheme.

Conventionally, current flow direction estimation has been based on the comparison of the voltage and current phase angles. However, with no voltage measurement devices installed at every node in distribution systems, current-only based techniques become necessary. Schemes based on current-only approach proposed in the literature, so far, are only for fault direction estimation [110,119–123]. Research in [119–121] compares prefault and fault current phase angles to determine if a fault is upstream or downstream of the relay. However, this is limited to radial systems where prefault power flow direction is known, and a separate fault detection device is required. On the other hand [110] applies directly the phase comparison approach which requires the exchange of the phase angle values between relays. In [122, 123], the fault direction is estimated at both ends of the line to detect an internal fault. With the approach in [122], the relay at each end of the line detects a fault on a fraction of the line based on an overcurrent principle. This scheme is only effective in grid connected microgrids with the grid providing significantly higher fault current than the DGs. The study in [123] proposes an interesting approach based on fault direction estimation technique proposed in [119–121] by considering the fault direction estimation at both ends of the line. This study, however, has analysed and verified this approach with extra high voltage transmission system data which may not necessarily be consistent with distribution systems.

While the difference between the local prefault and fault current phase angles could be used, as in [123], a clever, yet simple approach to detecting a change in current flow direction keeping the prefault angle as the reference is to calculate the cosine of the angle. When there is a change in direction, the cosine value changes the sign. This approach offers a new simple comparison reference, "zero", as a constant and neutral number. In three-phase systems, the positive sequence current is used. Therefore, for simplicity, the word "current" is subsequently adopted in this study to refer to positive sequence current.

The proposed approach can be equivalent to the principle of phase comparison protection scheme with the difference that, in this work, the compared quantities are measured at one end of the line

at two successive instants and then compare the transition patterns (events) from both ends rather than directly comparing the two quantities measured at the two ends of the line at the same instant. Moreover, the proposed principle is built on full cycle Fourier technique recognised for its inherent immunity to harmonics.

The proposed protection scheme uses "the zero" as the reference for detection of the change in current flow direction by computing the cosine value of the current phase angle. The relay fault detection principle and the phasor computation algorithm are provided in Fig. 6.1. The phasor estimation is based on full cycle DFT due to its deterministic aspect and capability to reject harmonics. Non-Fourier algorithms such as least squares-based algorithms, differential-equations algorithms, Kalman filter algorithms and Walsh functions algorithms suffer from harmonic effect and might not attain the required online speed computation [115, 120]. The update of phasor estimates with time are computed using recursive full cycle technique. This technique offers computational simplicity and provides a stationary phase angle in steady state by default as one of the side benefits.

When a fault occurs on a line, one of the ends of the line experiences a change in current flow direction (i.e. the change of its cosine value sign) while the other does not get affected much. With each line-end relay capturing the current direction transition, the fault on the line is detected by the relays by exchanging their current direction information. When both relays register the same direction transition (no change or a change in current direction) there is no fault detected on that line. On the contrary, if one of the relays registers a change, a fault is detected on the line.

It may happen that there is no current flowing in the line before fault occurrence. In this case, the relay is not able to take a decision on the change of current direction. To tackle this issue, two assumptions are made:

- When the current is zero or very small, its phase angle is set to zero i.e. the cosine is "one".
- While it may not necessarily be the case when the current is flowing in a line prior to fault occurrence, the monitoring directions of relays at both ends of the line must be the same. This means that the current transformers supplying measurements to the relays must be consistently polarized, and both relays consistently installed. This convention allows the definition of the same virtual reference ($\cos(0) = 1$) for the cosine value sign for both relays. Therefore, the relay can virtually decide a change of current direction or a no-change condition.

The latter assumption above does not only solve the direction change issue but also allows correct discrimination of fault from load switching events. Under load switching events, both relays register

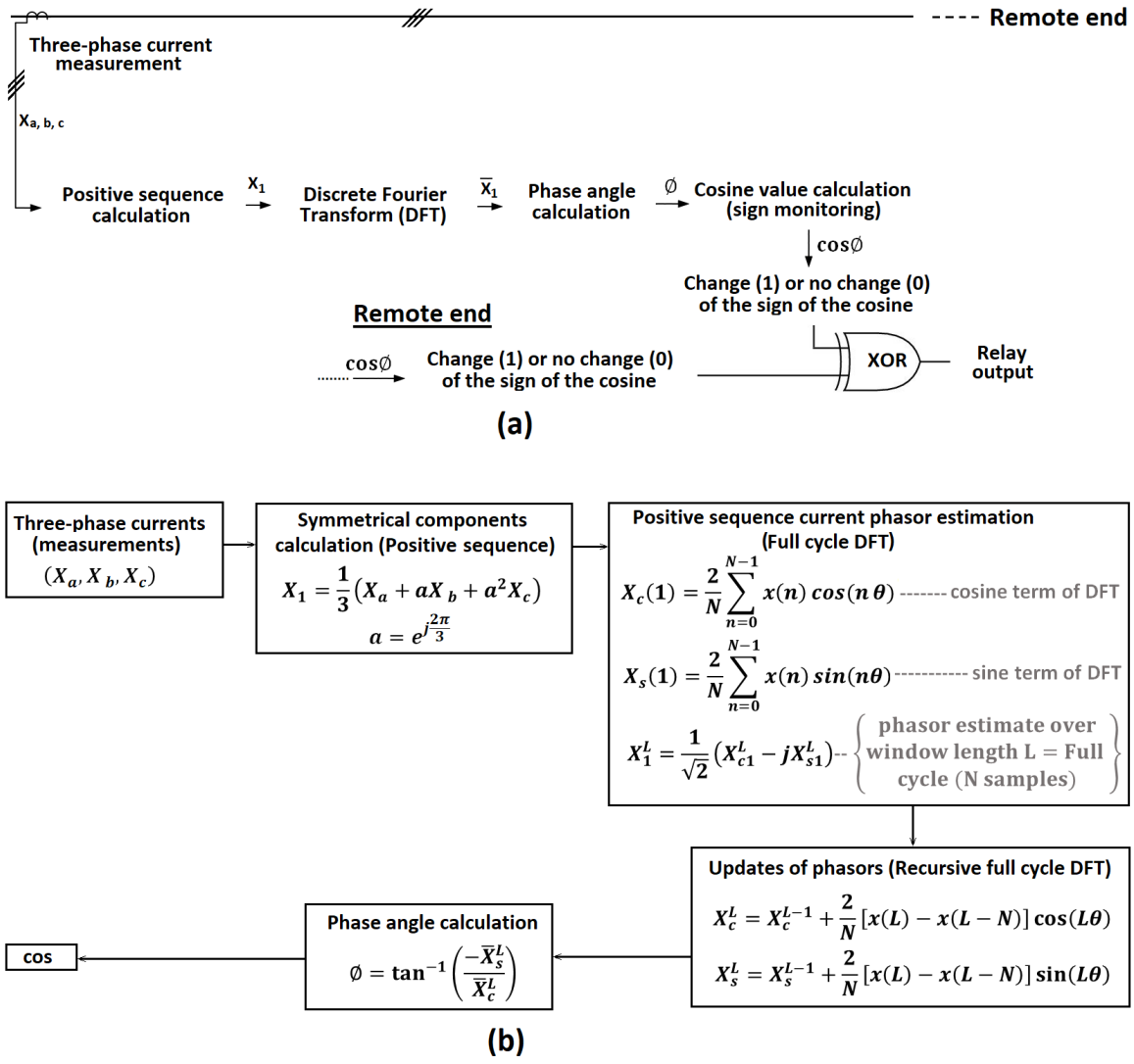


Figure 6.1: Fault detection strategy: (a) principle (b) phasor estimation

the same transition pattern (no change or change of current direction), which is also the case for an external fault.

As previously mentioned, the exchange of information between the line relays requires a communication channel. Conventional communication-assisted protection schemes require high bandwidth communication systems. The high cost of such systems may hinder their adoption in microgrids. With this approach, the current direction transitions (the change or no change) are directly transformed into binary states, "1" or "0" in order to allow the use of simple and low bandwidth (low-cost) communication systems. Moreover, reduced message size offers flexibility in its transmission.

6.3 Low-Cost Communication System

As discussed in the cost driver section of the thesis introduction, unlicensed microwave radio communication technology offers the lowest practical cost among existing communication technologies for power system protection. The two most used spread-spectrum techniques for unlicensed radio communication are frequency hopping spread spectrum (FHSS) and direct-sequence spread spectrum (DSSS). Both techniques can be used for protection applications. The FHSS offers more reliability at low frequency band, typically 902-928 MHz [23].

To ensure low-cost communication system feasibility, the protection scheme should offer flexibility in reducing the message size. On the other hand, the presence of other functions, for example the control signals for master-slave power sharing strategy, which rely on communications may relieve some of the pressure in that respect.

6.3.1 Practical considerations of low-cost communication system with the proposed protection scheme

To analyze the communication requirements, the proposed protection scheme is classified as a teleprotection scheme. Standard practice requires a certain level of reliability of such schemes to adhere to. The standard sets the security as the probability of unwanted command to be between 10^{-4} and 10^{-8}, and the dependability as the probability of missing command to be between 10^{-2} and 10^{-4} [25]. This means that one unwanted trip requires a minimum of 10^{8} noise bursts for a scheme designed with 10^{-8} security [124].

The proposed protection scheme is evaluated for the most stringent requirements among teleprotection schemes i.e. 10^{-8} security. To achieve such a level of security, it is important to ensure that if a distinct message was corrupted, it should not be received as a valid message. It is therefore necessary not to send binary 1 and 0 as they are, because a corrupted binary 1 might become a binary 0 and vice-versa. To tackle this issue, two approaches are usually used i.e. redundant bits, and duplicate messages [124]. However, the former increases the bandwidth requirement affecting the dependability (probability of missing commands) as expressed in (6.1) while the latter approach may require extra memory that might increase the cost and time delay for the fault detection.

$$P_{mc} = 2k(BER) \tag{6.1}$$

where P_{mc} is the probability of missing command, k the number of bits in a message, and BER, the bit error rate defined as the ratio of erroneous bits to total bits transmitted on a digital channel.

Fortunately, the proposed protection scheme, being phasor-based, has an inherent typical delay of one cycle (20 ms for 50 Hz nominal frequency). Despite not usually desirable, this delay can allow the relay to send the same message more than once in a cycle without a memory, thus creating a natural duplicate message approach. Furthermore, it is a standard practice that a protection message is sent two to eight times per cycle [24, 25]. A combination of this natural duplicate message and the bit redundancy approaches offers an opportunity to achieve the required security and dependability with a low bandwidth channel requirement and short transmission time. The total time delay associated with radio communication system can then be evaluated based on the message size, the number of messages exchanged per cycle, the relay processing time, the channel bandwidth capacity, and the allowed communication channel latency [124].

While radios are characterized by high latency, technologies with variable latency are recommended for teleprotection. These types allow for setting changes of some features that require much processing time with no value addition to the scheme application [25]. Such features are forward error correction (up to 5 ms), message acknowledgement, retry or re-transmission, data buffering ($\sim$ 50 ms), and encryption ($\sim$ 10 ms) [25]. This is because the relay sends data continuously allowing the receiving relay to get the right message even when some are corrupted. Practically radio latency of 2 ms is achieved [124]. Currently, unlicensed radios exist with band-width as high as 38400 bps that can achieve the range of 15 to 30 km [24].

To evaluate the feasibility of the whole scheme (fault detection and communication), a simple serial digital to digital bit stream communication protocol is considered. This protocol can use interfaces such as Universal Asynchronous Receiver Transmitter (UART) or Ethernet for message transmission [124, 125]. Taking the UART interface as an example, the message size to be exchanged between relays can be assessed. This interface can allow 1 to 23 bits per data word in addition to an overhead of two bits (typically one start bit and one stop bit) (message) [126]. This gives flexibility in choosing the appropriate word size for some applications. For many applications, the most common data word size is 8 bits. Along with this message size, two others are compared in Table 6.1 in terms of their associated delays: 25-bit, and 16-bit messages.

To obtain the total time required by the proposed scheme to output a decision, the relay delay ($\sim$ 20 ms), and the transmission interface delay ($\sim$2 ms, typically between 1-5 ms) are added to the total communication time delay. This time is about 41.3 ms, 36.4 ms, and 36.7 ms for the 10-bit,

Table 6.1: Comparison of communication system delays of different message sizes

	10 bits	**16 bits**	**25 bits**
Transmission time (ms)	0.26	0.42	0.65
Allowed latency (ms)	2	2	2
Receiving Interface delay (ms)	2	2	2
Relay reporting rate delay (ms)	15	10	10
Total communication delay (ms	**19.26**	**14.42**	**14.65**

16-bit, and 25-bit message sizes respectively. Considering the interface allowable word size range, the scheme requires about 2 cycles. This is typically acceptable for protection applications as it is well below the critical clearing time requirement for microgrids reported in the literature (about 5 cycles) [93, 127]. This assessment has assumed a full duplex communication channel. However, a half-duplex system can be used by automatically switching the channel in both direction [124]. This would further reduce the communication system cost but at the expense of response time. This would add a delay of about a cycle bringing the total response time to about 3 cycles. This time should also be acceptable because circuit breakers can clear the fault in less than 2 cycles.

Also, for any communication-assisted protection scheme, the failure of communication system leaves the system unprotected. It is therefore important to have a back-up protection in place to ensure the system protection in such a situation.

6.4 Simulation Scenarios and Results Discussion

6.4.1 Microgrid study system and assumptions

A medium voltage microgrid system, with loop configuration, is used as a study system as shown in Fig. 6.2. While there are no impediments to using the same or similar technique applied to a more traditional, radial grid with many laterals, the extensive presence of tapped extensions and use of automation would require more in-depth analysis and make the study system more complex. This case does not really apply to rural/small scales microgrids or also the site-based industrial and commercial microgrids with a classical radial configuration. It does apply more to MV microgrids

with various sources dotted around and interconnected together with untapped lines. Nevertheless, this is a reasonable configuration to try the concept as it represents a reliable isolated grid, and a reasonably challenging case to evaluate the effectiveness of the proposed protection scheme.

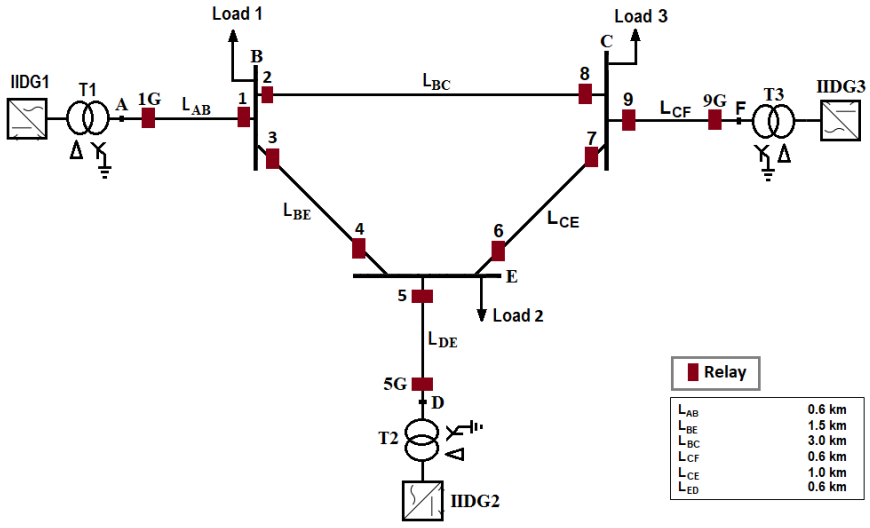


Figure 6.2: Study microgrid system

The configuration of the inverters adopted in this study is a three-phase three-wire topology usually used in medium voltage distribution systems. Each inverter is connected to the rest of the microgrid through an LCL filter. The filter is formed of an LC circuit and a step-up transformer. The microgrid side of the LC circuit is considered as the point of the common coupling (PCC) at which the IIDG is connected to the rest of the microgrid. It is at the PCC that the voltage and current are measured for control and protection of the inverter. This is illustrated by the black background side of Fig. 6.3. It could be possible to consider measurements taken after the transformer, but high voltage level would challenge the cost-effectiveness of voltage measurement. For the simplicity of the control system, constant DC voltage supply to the inverter is assumed.

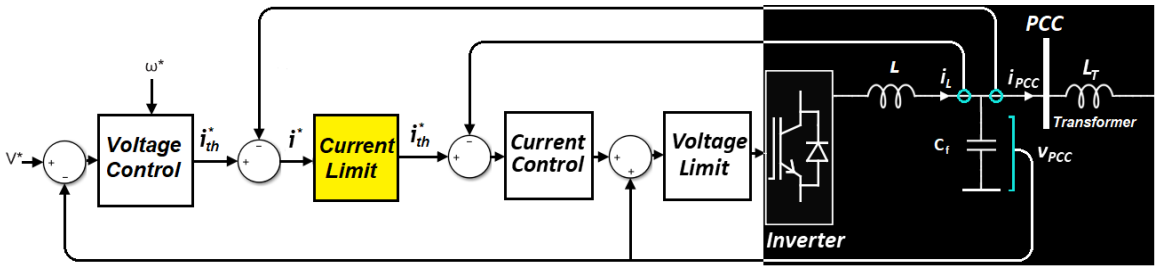


Figure 6.3: Voltage source control

The parameters of the IIDGs, step-up transformers, and power lines are provided in Table 7.1. The IIDG1 adopts the Voltage-Frequency control to form and maintain the voltage and frequency of the system (50 Hz) at reference values while the others are locally controlled as current sources. To ensure appropriate power sharing among IIDGs, the master-slave control is adopted. The IIDG1 operates as the master, and shares its current reference signals to other IIDGs (the slaves). This strategy is chosen due to its simplicity and highest sensitivity to faults. The control process is performed in synchronous reference frame (dq). To limit the fault current generated by IIDGs and overvoltage under unbalanced faults, the latched current limiting strategy (1.2 p.u.), and the instantaneous voltage saturation limit (1.1 p.u.) are respectively adopted. The general structure of the IIDG's control is given by the white background of Fig. 6.3. The signals generated by the VSC under different fault types measured at the filter inductor outputs and at the PCC are shown in Fig. 6.4.

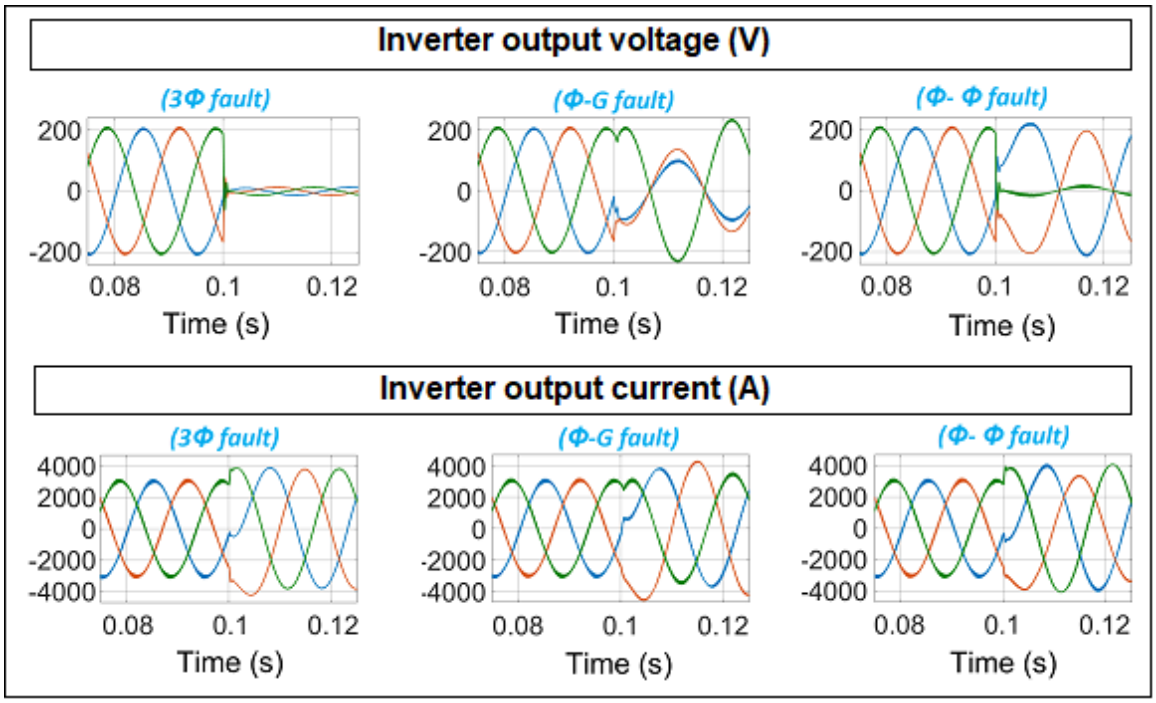


Figure 6.4: Voltage and current signals measured at PCC (at the output of the filter) for different fault conditions (three phase fault (3Φ), single phase to ground fault (Φ-G), and phase to phase fault (Φ-Φ))

Table 6.2: Microgrid system parameters

IIDER Parameters			
	IIDG1	**IIDG2**	**IIDG3**
Rated power (kVA)	1000	1000	1000
Rated voltage (V)	260	260	260
DC bus voltage (V)	500	500	500
Fundamental frequency (Hz)	50	50	50
Switching frequency (kHz)	5	5	5
Filter inductance (mH)	0.04	0.04	0.04
Filter resistance (mΩ)	0.067	0.067	0.067
Filter capacitance (mF)	1.2	1.2	1.2
Damping resistance (mΩ)	28	28	28
Current control proportional	0.248	0.248	0.248
Current control integral	0.42	0.42	0.42
Voltage control proportional	0.748	0.748	0.748
Voltage control integral	0.00	0.00	0.00
Step-up Transformer Parameters			
Rated power (kVA)	1200	1200	1200
Rated primary voltage (kV)	0.260	0.260	0.260
Rated secondary voltage (kV)	20	20	20
Winding configuration	D1Yg	D1Yg	D1Yg
Fundamental frequency (Hz)	50	50	50
Winding inductance (pu)	0.03	0.03	0.03
Winding resistance (pu)	0.001	0.001	0.001
Line Parameters			
Line type	Overhead		
Positive sequence parameters	Resistance (Ω/km)	Reactance (Ω/km)	Susceptance (μS/km)
	0.510	0.366	3.172
Zero sequence parameters	Resistance (Ω/km)	Reactance (Ω/km)	Susceptance (μS/km)
	0.658	1.611	1.280

6.4.2 Simulation scenarios

To validate the effectiveness of the proposed scheme, the model of the study microgrid was developed in Matlab/Simulink environment.

Three scenarios namely Reference Scenario, Scenario 1, and Scenario 2 are assessed under this study.

Reference scenario: This scenario assesses the effectiveness of the protection scheme versus fault type, fault resistance, and fault location. The existence of prefault currents in all branches of the microgrid loop is assumed and ensured by the following load conditions: Load 1 = 0.7 MW; Load 2 = 1.3 MW; Load 3 = 0.2 MW. The fault currents are limited to 1.2 times the value of the rated inverter current, an ideal value to challenge the proposed scheme and even more to conventional scheme. The power factor is set to 0.56 (lagging) i.e. $i^*_{dth} = 0.67\ pu$ and $i^*_{qth} = -1.0\ pu$. These predefined fault current references are assumed to be the same for all three IIDGs in this study. Different types of faults i.e. symmetrical (L-L-L-G) and unsymmetrical faults (L-G and L-L) were simulated on Line L_{BE} (between relays 3 and 4) and Line L_{AB} (between Relays 1G and 1) at time instant $t = 0.1\ s$.

Scenario 1: This scenario evaluates the effectiveness of the proposed protection scheme for different fault inception time instants, and for different reactive current values generated by IIDGs during fault. With the former, a fault on Line L_{BE} at two fault inception instants different from the Reference Scenario's are considered; $t = 0.11\ s$, and $t = 0.116\ s$. On the other hand, different power factors (PF) are considered. It is important to note that the required IIDER response in terms of reactive fault current contribution to support voltage recovery, particularly during unbalanced faults is not clearly defined in most grids codes. To establish the effectiveness of the proposed scheme in situations of generators with different PFs, the following three current PF values reflecting the range of reactive current contributions are adopted:

- The fault current references for all IIDGs are limited to 1.2 pu with a power factor of 0.85 (lagging) i.e. $i^*_{dth} = 1.02\ pu$ and $i^*_{qth} = -0.63\ pu$.
- The fault current references for all IIDGs are limited to 1.2 pu with a power factor of 0.2 (lagging)i.e. $i^*_{dth} = 0.24\ pu$ and $i^*_{qth} = -1.17\ pu$.
- The fault current references for all IIDGs are limited to 1.2 pu with different power factors. The power factor of IIDG1 (PF 1) = 0.85; PF 2 = 0.56, and PF 3 = 0.2.

Other than the fault inception time instants, and fault current references, the parameters and conditions under Scenario 1 are the same as in the Reference Scenario.

Scenario 2: This scenario assesses the performance of the proposed protection scheme in case of load switching. This scenario has been undertaken considering two cases:

- the performance of the scheme when there is current flowing in a line prior to fault occurrence; and
- the performance of the scheme when there is no current flowing through at least one of the loop lines prior to fault occurrence.

Since the fault events are comprehensively covered in the previous scenarios when there is current flowing in the lines prior to fault, the first case under this scenario will only consider load switching event. The initial loading under this case is such that Load 1 = 0.5 MW, Load 2 = 0.8 MW, and Load 3 = 0.2 MW. At t = 0.1 s a an additional load of 0.5 MW is switched on at Bus B.

The second case on the other hand, considers both load switching and fault events. This is because it is a special case not covered in the previous scenarios. Initially, all loads at the nodes are set to 0.5 MW. With such loading, there is no current flowing in the loop as the IIDGs can satisfy their respective local loads. To assess the performance of the scheme, at t = 0.1 s a three phase fault is simulated on Line L_{BE}. For the load switching events, with the same loading condition, an additional load of 0.6 MW is connected at Bus B at t = 0.1 s. With this additional load kept in the system, the 0.6 MW are switched off from the system at t = 0.15 s in order to verify the effectiveness of the scheme when a considerable load is suddenly disconnected from the system.

Other than the loading parameters, other simulation parameters are the same as those of the Reference scenario.

6.4.3 Simulation results and discussion

The cosine values computed by each relay over time for a three-phase solid fault are provided in Fig.6.5. It is clear that only Relay 4 registers a change in the cosine value sign just after the fault inception time. With the rest of relays registering a no-change direction state, the fault is detected between Relays 3 and 4 as it is the only relay pair to register different cosine sign transitions.

This case is reflected in Fig. 6.6 illustrating the current flow direction in the study system before and during the fault (note that due to line styles used to demarcate the cosine values computed by different relays in the figure, some values seem to be greater than one while they are actually not). A full picture of the simulation results is provided in Tables 6.3, 6.4, and 6.5. The results demonstrate the effectiveness of the proposed protection scheme for all simulated scenarios.

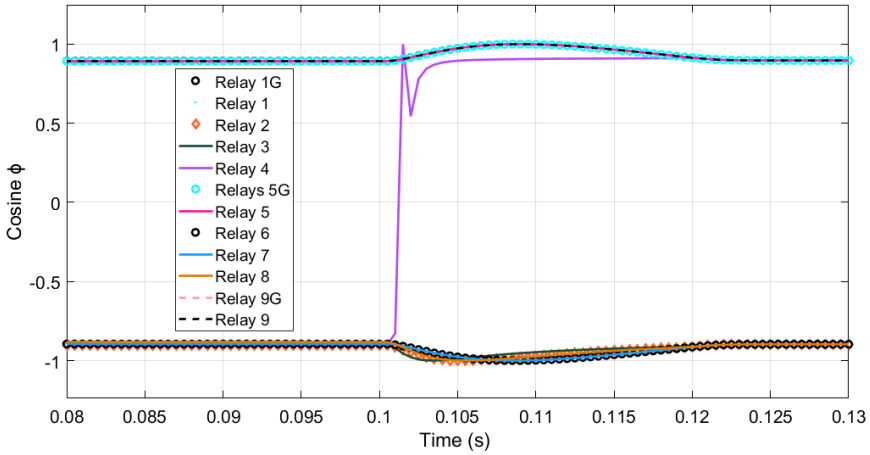


Figure 6.5: The cosine values computed by relays for a three-phase fault on Line L_{BE}

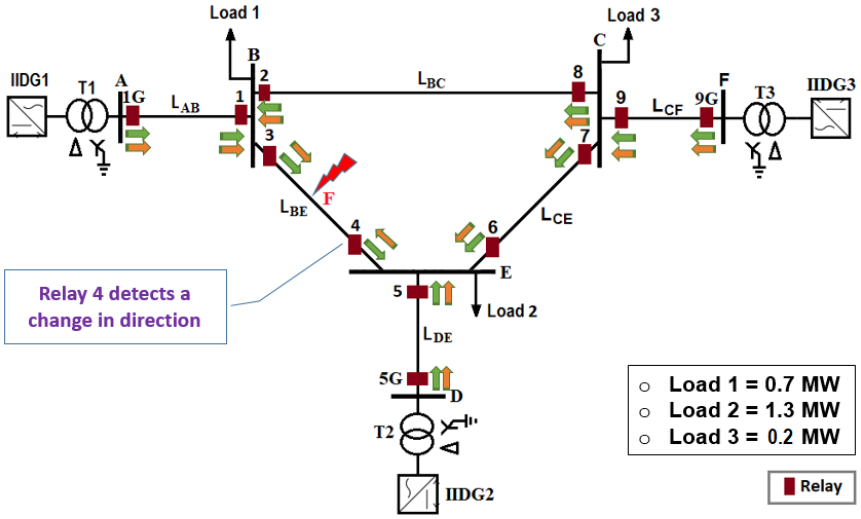


Figure 6.6: The illustration of current flow direction through the lines before and after a three-phase fault on Line L_{BE}

Table 6.3: Performance of the proposed protection scheme for the Reference Scenario

Positive sequence current phase angle (degree)												
Event type		**1G**	**1**	**2**	**8**	**3**	**4**	**5**	**5G**	**6**	**7**	**9**	**9G**
Prefault		26.7	26.7	-154.5	-151.5	-153.6	-154.7	27	27	-153.5	-153.5	26.8	26.8
Fault on Line L_{BE} (between Relays 3 and 4)													
$R_f = 0\ \Omega$	L-L-L-G	-26.3	-26.3	153.7	153.7	153.7	-26.3	-26.2	-26.2	153.7	-153.7	-26.3	-26.3
	L-G	-39.2	-39.2	135	135.5	133.2	-49.4	-39.1	-39.1	139.2	139.2	-39.2	-39.2
	L-L	-39	-39	136.3	136.8	134.6	-47.6	-38.8	-38.8	140	140	-38.8	-38.8
$R_f = 10\Omega$	L-L-L-G	-26.5	-26.5	153.5	153.5	153.5	-26.53	-26.5	-26.5	153.5	-153.5	-26.5	-26.5
	L-G	-38.2	-38.2	136.7	138.3	135	-47.6	-38	-38	140.5	140.5	-38.1	-38.1
	L-L	-38.1	-38.1	137.3	137.8	135.7	-46.5	-38	-38	140.7	140.7	-38.1	-38.1
Fault on Line L_{AB} (between Relays 1G and 1)													
$R_f = 0\ \Omega$	L-L-L-G	-26.3	153.6	153.7	153.7	-26.4	-26.4	-26.3	-26.3	153.8	-153.8	-26.3	-26.3
	L-G	-39.2	121.3	133.4	133.6	-50	-50	-39.1	-39.1	144	144.1	-39.2	-39.2
	L-L	-38.9	124.5	135	135.1	-48	-47.9	-38.7	-38.7	144	144	-38.8	-38.8

- R_f refers to fault resistance in ohms (Ω).

Table 6.4: Performance of the proposed protection scheme for Scenario 1

Positive sequence current phase angle (degree)												
Event type		**1G**	**1**	**2**	**8**	**3**	**4**	**5**	**5G**	**6**	**7**	**9**	**9G**
Prefault		26.7	26.7	-154.5	-151.5	-153.6	-154.7	27	27	-153.5	-153.5	26.8	26.8
Fault on Line L_{BE} (between Relays 3 and 4)													
$t = 0.110\ s$	L-L-L-G	-26.3	-26.3	153.7	153.7	153.7	-26.3	-26.2	-26.2	153.5	153.5	-26.3	-26.3
	L-G	-39.2	-39.2	135.1	135.6	133.3	-49.3	-39.1	-39.1	139.3	139.3	-39.1	-39.1
$t = 0.116\ s$	L-L-L-G	-26.3	-26.3	153.7	153.7	153.7	-26.3	-26.2	-26.2	153.7	-153.7	-26.3	-26.3
	L-G	-39.2	-39.2	135.1	135.5	133.2	-49.2	-39.1	-39.1	139.2	139.3	-39.2	-39.2
PF = 0.85	L-L-L-G	-1.9	-1.9	178.1	178.1	178	-1.9	-1.8	-1.8	178.1	178.1	-1.9	-1.9
	L-G	-14.7	-14.7	160.2	160.7	158	-25.1	-14.7	-14.7	164.7	164.8	-14.7	-14.7
PF = 0.20	L-L-L-G	-48.5	-48.5	131.4	131.4	131.4	-48.6	-48.5	-48.5	131.5	131.5	-48.5	-48.5
	L-G	-61.3	-61.4	113.7	114.1	111.4	-71.7	-61.3	-61.3	118.1	118.2	-61.3	-61.3
Different PFs	L-L-L-G	-1.9	-1.9	125.8	125.8	164.4	-33.5	-26.2	-26.2	134.9	134.9	-48.5	-48.5
	L-G	-8	-8	86.3	86.4	157.8	-66.1	-38.9	-38.9	113	113	-71.3	-71.3

- PF and t refer to the power factor of fault reference currents of IIDGs, and fault inception time (in seconds) respectively.
- Different PFs refers to $PF\ 1 = 0.85, PF\ 2 = 0.56, PF\ 3 = 0.20$

Table 6.5: Performance of the proposed protection scheme for Scenario 2

Positive sequence current phase angle (degree)												
Event type		**1G**	**1**	**2**	**8**	**3**	**4**	**5**	**5G**	**6**	**7**	**9**	**9G**
Load 1 = 0.5 MW, Load 2 = 0.8 MW, Load 3 = 0.2 MW													
Event: { Load switching: Load connection = 0.7 MW at Node B at t = 0.1 s; Fault: Three-phase fault on Line L_{BE} at t = 0.1 s													
Same direction	Prefault	27.4	27.4	-154.7	-150.7	-152.6	-154.6	27.3	27.4	-153.2	-153	27.3	27.4
	Load	26.7	26.7	-153.8	-152.8	26.6	27	26.9	26.9	-153.6	-153.3	26.8	26.9
	Fault	-26.3	-26.3	153.7	153.7	153.7	-26.3	-26.3	-26.3	153.7	153.7	-26.3	-26.3
Different direction	Prefault	26.4	26.3	-153.7	-150.7	-152.6	25.4	27.3	27.4	-153.2	-153	27.3	27.4
	Load	26.7	26.7	-153.8	-152.8	26.6	-153	26.9	26.9	-153.6	-153.3	26.8	26.9
	Fault	-26.3	-26.3	153.7	153.7	153.7	153.7	-26.3	-26.3	153.7	153.7	-26.3	-26.3
Load 1 = Load 2 = Load 3 = 0.5 MW													
Event: { Load switching: Load connection = 0.6 MW at Node B at t = 0.1 s; Fault: Three-phase fault on Line L_{BE} at t = 0.1 s													
Prefault		27.4	27.3	0	0	0	0	27.3	27.4	0	0	27.3	27.4
Same direction	Load	26.9	26.9	-154	-152.5	26.6	27	26.9	26.9	-154.4	-153.1	26.9	26.9
	Fault	-26.3	-26.3	153.7	153.7	153.7	-26.3	-26.3	-26.3	153.7	153.7	-26.3	-26.3
Different direction	Load	26.9	26.9	-154	-152.5	26.6	-153	26.9	26.9	-154.4	-153.1	26.9	26.9
	Fault	-26.3	-26.3	153.7	153.7	153.7	153.7	-26.3	-26.3	153.7	153.7	-26.3	-26.3

- Direction refers to relay monitoring direction.

From the tables, the first case ($R_f = 0\,\Omega$) under the Reference scenario shows that the scheme is effective for all types of fault. For any type of fault on line L_{BE}, consistency in results is observed whereby only Relay 4 registers a change in the cosine value sign (the angle changing from -159.4° to a value of 4$^{\text{th}}$ quadrant) as marked in red. With Relay 3 registering no change in cosine value sign, a fault is detected on the line protected by relay pair (3,4). Each of the other relay pairs, (1G,1), (2,8), (5,5G), (6,7), and (9,9G), registers the same transition states, which indicates that there is no fault on their lines. Furthermore, the same consistency in results is obtained for the cases of faults with large range of resistance. For example, Fig. 6.7 shows that simulation results of a solid line to ground fault and the same type of fault with a fault resistance of 100 Ω are consistently the same.

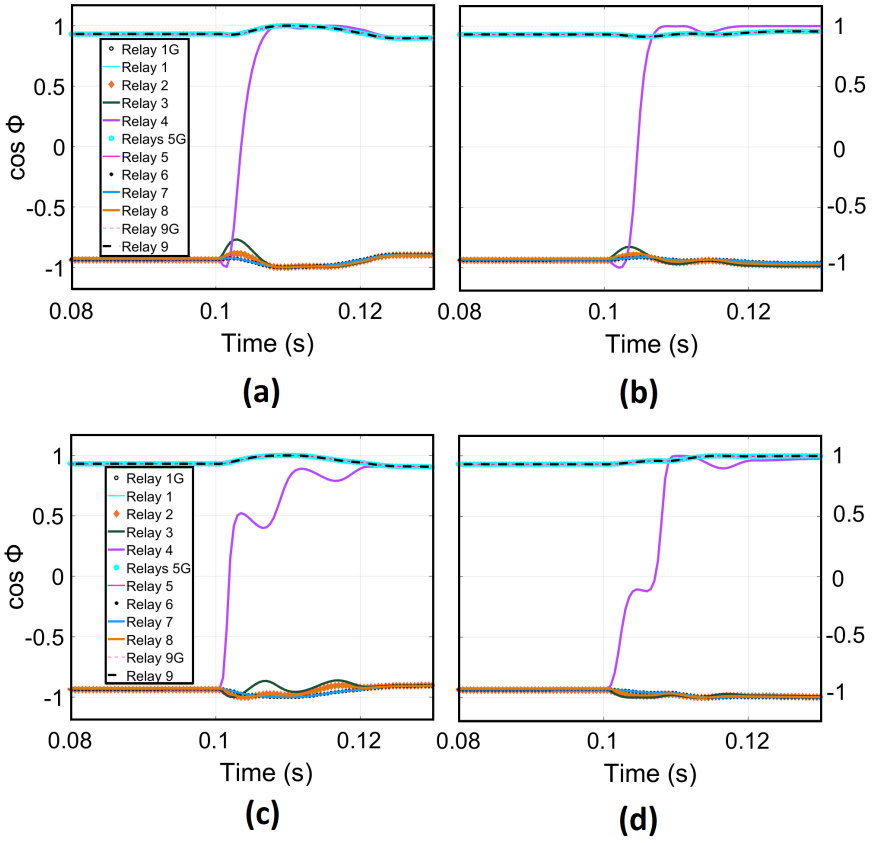


Figure 6.7: The cosine values computed by relays with a fault on Line L_{BE}: (a) solid line to ground fault; (b) line to ground fault with a fault resistance of 100 Ω; (c) solid line to line fault; (d) line to line fault with a fault resistance of 100 Ω

The results registered under all the cases of Scenario 1, as provided in Table 6.4, are also as consistent as those in Reference case. The consistency is clearly obtained for different fault inception time instants, when IIDGs have the same fault currents references as well as when they have different

fault current references (i.e. different power factors) as shown in the table.

The results on the discrimination of faults from load switching events are presented in Table 6.5. In the previous scenarios, results clearly show the effectiveness of the proposed protection approach in detecting faults when the current flows in the faulted line prior to the fault occurrence. The discrimination of fault from load switching event in the previous scenarios is straight-forward as any change in current direction due to load switching event is seen by both relays protecting the line. This is clearly demonstrated with both Relays 3 and 4 registering the change. However, when there is no current flowing in the faulted line prior to fault occurrence depending on the system loading, as explained in the scheme working principle, the relay pair monitoring directions should be the same to discriminate a fault from load switching.

The state of the system prior to fault or load switching event, as provided in Table 6.5, shows that there is no current flowing in Lines L_{BE} and L_{BE} due to initial system loading. When the load is switched into the system at Bus B at the time instant $t = 0.1\ s$, the cosine values computed by Relays 2, 8, 6, and 7 change the sign. However, as they are in pairs i.e (2,8) and (6,7), there is no fault detected. The same situation happens when the load is later disconnected from the system. On the other hand, when a three-phase fault occurs on Line L_{BE}, Relay 3 registers a change as well. This clearly indicates a fault on the line as the remote relay sees no change.

The slight difference obtained in the angle values throughout the simulation results from relay pairs is not an issue as the sign of the cosine value is rather consistent. This shows that the proposed scheme does not require high precision in the phasor estimates to perform effectively. Furthermore, due to the two-end state comparison approach, erroneous phasor estimates that may be caused by IIDGs generating off-nominal frequencies or unbalanced fault contribution during unsymmetrical faults do not affect the effectiveness of the scheme. This is because the line relay pair experience almost the same effects from the frequency deviation or unbalance. This is shown in Fig. 6.8 presenting the results from the simulation of a line to ground fault on Line L_{BE} with a wide range of off-nominal frequencies (45 Hz, 49 Hz, 51 Hz, and 55 Hz) of IIDGs.

From the figure, it is clear that when the fault occurs, Relay 4 registers a change contrary to its counterpart (Relay 3) in all cases. Other than the frequency, other simulation parameters are the same as the ones in reference scenario.

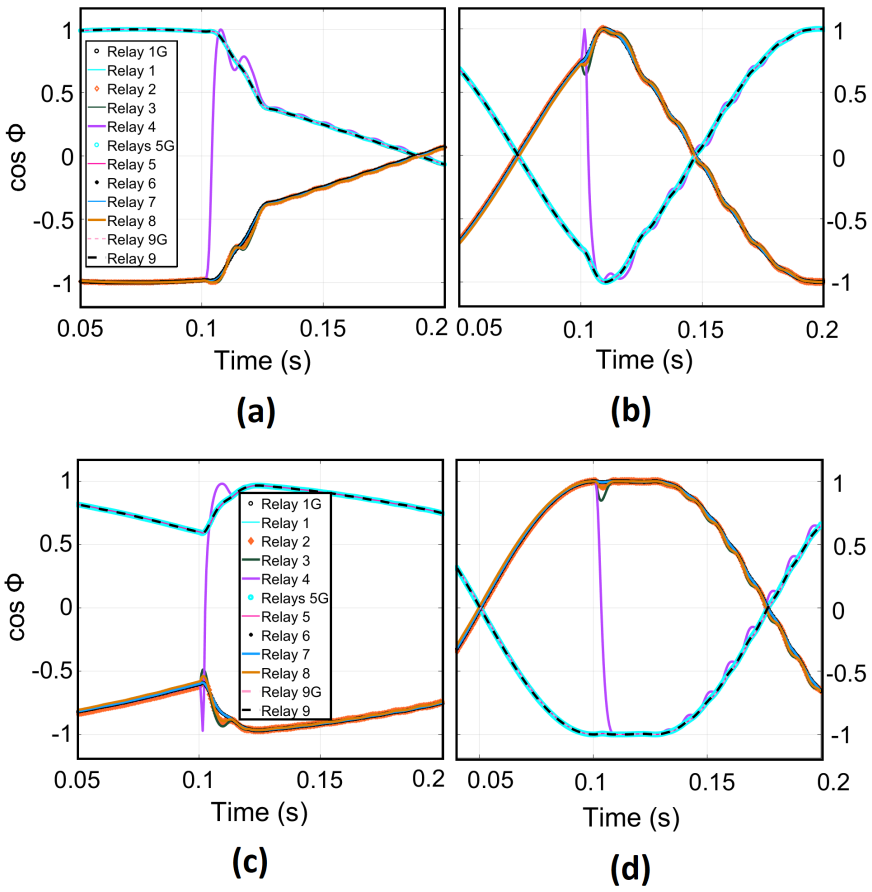


Figure 6.8: The cosine values computed by relays with a line to ground fault on Line L_{BE} at $t = 0.1\,s$ with: (a) IIDGs frequency of 49 Hz; (b) IIDGs frequency 45 Hz; (c) IIDGs frequency of 51 Hz; (d) IIDGs frequency 55 Hz

6.5 Conclusions

In this chapter, a line protection scheme based on line local and remote end current measurements for fault detection and the comparison of binary state outputs of relays at both ends of the line has been investigated. For the sake of simplicity a 3-Bus microgrid system was used to assess the performance of the scheme. Since this scheme only relies on the two line end information, a grid feeder, with tapped lines, operating as microgrid would require relays around the tap point in order to use this scheme. The proposed microgrid protection relay was derived from an analysis of inverter-based microgrids behavior and allows the use of a low-cost communication system. Its performance demonstrates the effectiveness in all fault conditions and immunity to the inverter fault signature effect as verified by simulations on the microgrid study system.

Chapter 7

Protection Scheme Using Phase Angle Trajectory and ROCOSP

7.1 Introduction

Digital relays can integrate both the primary and back-up protection algorithms into one relay unit. This integration offers cost reduction advantage that can attract the use of such relays in distribution systems embedded with IIDGs. Despite the cost reduction advantage that may be offered by these relays, however, the cost of the communication channel is relatively expensive for microgrids, let alone the cost of both the primary and redundant back-up communication systems. The integration of main and back-up protection functions has inspired the proposed protection scheme in this chapter that can work as the main or a back-up protection by sharing the same communication means with the main or back-up. In this chapter, the operational principle of the proposed scheme as well as the assumptions associated with it are presented. A study microgrid system used to test the effectiveness of the scheme through simulations is also discussed with the simulation results.

The proposed protection strategy is based on the following key assumptions:

- The line protection relays are available at both ends of the line.
- The relays are digital type protective relays.
- A communication channel exists between the local and remote line relays. The two relays

protecting a line, are also referred to as relay counterparts in this work.

- Communication channels exist between neighbouring relays protecting lines connected to a common busbar (neighbouring relays around the busbar).
- In normal operating conditions, the power flowing in the line connecting the distributed generator to the loop is always from the generator to the loop. Otherwise power flow direction detection device is required.

7.2 Disturbance Detection

Typically, the occurrence of a disturbance such as a fault in a power system causes changes in power system parameters such as voltage and current magnitudes and the phase angles of current and voltage phasors, etc. As voltage measurement devices might not be available at each bus at distribution voltage levels, changes in current signal are investigated, particularly the phase angle as the fault currents generated by IIDGs are limited and could be inappropriate to use the magnitude for fault detection. In three-phase systems, the phase angle of positive sequence current phasor is used for simplicity and accuracy.

From the analysis done in Chapter 5, Section 5.8, it can be established that in steady state conditions, the slope "S" of the phase of the current phasor is directly proportional to the local frequency deviation and can be expressed as the rate of change of the phase angle over a cycle as follows:

$$S = \frac{f_n}{2\pi}(\phi_k - \phi_{k-N}) \tag{7.1}$$

where f_n is the nominal frequency, N the number of samples in a cycle, and ϕ_k and ϕ_{k-N}, the values of the phase angle estimates of positive sequence current from two consecutive cycles.

This means that any change in trajectory of the phase angle over a cycle can be reflected in the value of the slope of the phase angle of (7.1).

On the other hand, relays with identical hardware and algorithms should yield the same phasor estimates under all conditions [115]. This means that despite the loss of accuracy in phase angle estimation using conventional recursive DFT, it can still be used for protection and monitoring purposes (decision making and disturbance detection) as long as the relay's estimates are not required for control or measurements purposes that requires accurate estimates.

This work exploits this avenue by proposing a relay coordination strategy using the cosine of the positive sequence current phase angle and communication channels to monitor the phase angle trajectory of relays with respect to the others for decision-making. This coordination and associated details are discussed in the next section.

The expression in (7.1), in this study, forms the basis for the detection of the occurrence of a disturbance in the system. This can be a fault or a severe switching event such as a sudden loss or connection of a generator or a large load. However, switching events as well as faults on busbar, are considered as external disturbances to the proposed line protection scheme. This means that significant change in the slope of the phase angle could serve only as an alarm, signalling a potential fault in the system. It is the coordination of the relays that determines whether the disturbance detected is a fault and whether it occurred in the relay zone of protection.

Recognising that an islanded microgrid can operate at off-nominal frequency, a change in slope values may not accurately reflect a disturbance as it would if the system was operating at nominal frequency. For example if the frequency varies from 52 Hz to 48 Hz and the acceptable operating frequency range is ± 5 Hz around 50 Hz (the nominal frequency) i.e. 45 - 55 Hz, then such disturbance cannot be detected based on the change in the phase angle slope value. To detect such a disturbance, the rate of change of the slope of the phase angle (ROCOSP) over a cycle is adopted. This can be expressed as follows:

$$ROCOSP = \frac{f_n^2}{2\pi}(\phi_k - 2\phi_{k-N} + \phi_{k-2N}) \tag{7.2}$$

where f_n is the nominal frequency, N the number of samples in a cycle, and ϕ_k, ϕ_{k-N} and ϕ_{k-2N} are estimates of phase angle from three consecutive cycle windows.

During normal operation, regardless of the operating frequency, the average value of the ROCOSP over a cycle is zero. Any change in the local frequency or the occurrence of disturbance (transient conditions) in the microgrid causes ROCOSP to deviate significantly from zero. A threshold value for the ROCOSP can then be defined and set at any value different from zero to detect a disturbance in the microgrid. The threshold should be set at a value that allows the detection of any disturbance, even small ones to ensure high reliability of the protection scheme as the relay coordination proposed in this study has the capability of discriminating a fault in the zone of the protection scheme from non-fault and external fault events.

It is important to note, however, that such deductions on ROCOSP are only correct when the

current flow direction in a line does not change. The change in current flow direction, which is not necessarily caused by a disturbance, causes significant step change in the phase angle (close to 180^0) which in turn causes significant change in phase angle slope and in the ROCOSP.

Taking the 180^0 phase angle difference following a certain event in the system such as a fault or a switching event, and applying (7.1) and (7.2), one can find that the associated values of the phase angle slope and ROCOSP are 25 Hz and 1250 Hz/s. These theoretical values can be obtained by a relay if the fundamental frequency of current signal is equal to the nominal frequency. Otherwise values close to these can be considered. This is demonstrated in simulation results of the case study in Fig. 7.8.

Since the current flowing through the line connecting directly the IIDG to the busbar, seen by a relay at the line end close to the busbar, changes its direction only when a fault occurs between the generator and the busbar. This relay is ideal for disturbance detection in the microgrid and a fault on its own line based on ROCOSP. It is important to highlight that such a relay detects a disturbance regardless of its location in the microgrid. Such relays are, in this study, referred to as *"master relays"*. The relays protecting other lines connected to the same busbar as the master relay's line are the *"slaves"*. With an appropriate coordination between master relays and their respective slaves, the identification of faulted line and its isolation can be achieved. The proposed coordination is described in next section.

7.3 Identification of the Faulted Line

Once a disturbance is detected in the system by the master relays, the directionality comparison feature can be used to determine the faulted line. For example, assuming that the positive flow direction of the current is from the line to the bus, it can be determined that when a fault occurs on a line in the system both relays protecting the line will register negative directions. Equivalently, when an external fault to the line occurs, one of the relays of the pair sees a positive current flow direction. Therefore, if all relays around the busbar have the same monitoring direction (from the line to the bus or from the bus to the line) it is easier to ensure the effective comparison of the outputs of slave relays with their respective master relays and establish the fault location. Otherwise, care must be taken to ensure correct comparison of relays' outputs.

The directionality comparison can be achieved by applying the cosine concept discussed in the

previous chapter. In this case, the sign of the cosine value computed by the slave relay is compared to that of the value computed by the master relay. Assuming that the relay monitoring directions of both the master and its slave are the same, it can then be established that after a fault on a line protected by a slave relay, the cosine values calculated by the relay and its master are of opposite signs as the current flowing in the faulted line flow towards the fault from the busbar. Equivalently, when one of the relays of the slave pair sees a current flowing from the line to the busbar (the case for the master relay line current), the line is healthy i.e. there is no fault on that particular line.

As outlined in the previous section, the coordination and communication between the microgrid relays is based on the master-slave strategy. The master relay detects the occurrence of a disturbance in the microgrid. When a disturbance is detected, the master relay sends a potential fault signal (alarm) to its respective slaves as well as the sign of the computed cosine value. Conversely, when a fault is on the master relay line, the concerned master relay sends a blocking signal as the master relay already detected a fault on its line. In case two or more DGs are connected to a common busbar, the blocking signal from one of the master relays overrides the disturbance signal received by the slave relays from other master relays. In such a situation, when a fault occurs on one of the DGs'lines, only the concerned master relay registers a change in cosine value sign and sends a blocking signal to the slave relays, which are common to all master relays around the busbar. Recalling that the proposed scheme is for islanded multi-inverter-based microgrids, each of the slave relays in the microgrid receives either a fault or a blocking signal from its master relay. In summary, the slave relay will receive one of the following signals from its master relay when a disturbance is detected:

- A blocking signal from the master relay
- A fault signal with the same sign of the cosine value as the master relay's
- A fault signal with the opposite sign of the cosine value to the master relay's

For the first two cases, the slave relay has a confirmation that a disturbance is external to its line. Therefore the relay sends in turn a blocking signal to its remote counterpart to prevent the line isolation from the remote end. On the other hand, the third case indicates a potential fault on the relay line. Therefore, if the slave relay does not receive a blocking signal from its counterpart, a fault is assumed on its line and should send a trip signal to the relevant circuit breaker.

With this relay coordination and communication approach, when the primary line protection experiences a communication channel failure between the two relays protecting the concerned line, this

scheme will effectively operate using the blocking signals sent through the remaining and healthy communication channels of the healthy lines. This scheme, however, does not cover situations where any of the other line communication channels fail at the same time as the one of the faulted line.

It may happen that there is a tapped line in the loop. In this case, the point of connection is considered as the tap point. Fig. 7.1 illustrates an example of such a case. In this example, Relays 1 and 4 are master relays while Relays 2 and 3 are their slaves respectively.

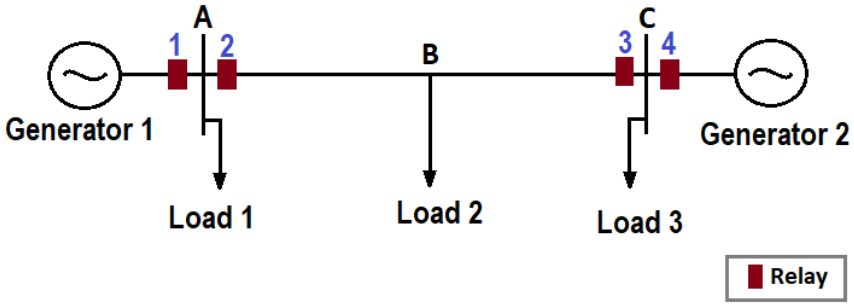


Figure 7.1: Example of a case with a tapped line (tap point B)

Three possibilities can be considered under this case.

- Load 2 is larger than Loads 1 and 3
- Load 3 is larger than Loads 1 and 2
- Load 1 is larger than Loads 2 and 3

For the first case, the prefault currents seen by Relays 2 and 3 flow from the busbars A and C to the tap point B. This is illustrated in Fig. 7.2. As shown in the figure, when a fault occurs on the line, there is no change in current flow directions with respect to the prefault currents.

Based on the proposed coordination principle, and assuming that the slave relays are installed with the same monitoring direction as their respective master relays, each master relay will detect the fault and send a fault signal with the cosine value sign (opposite sign due to opposite current flow direction seen by the slaves) to their respective slave relays. A potential fault is so far confirmed by each slave relay; and since there is no blocking signal from either slave relay to its counterpart, a fault on the line is confirmed and tripping signals, with a reasonable delay, will be issued by slave relays to their respective circuit breakers to isolate the line. On the other hand, for the other two cases (load at Bus A or C is the largest in the system), the prefault current flow direction seen by

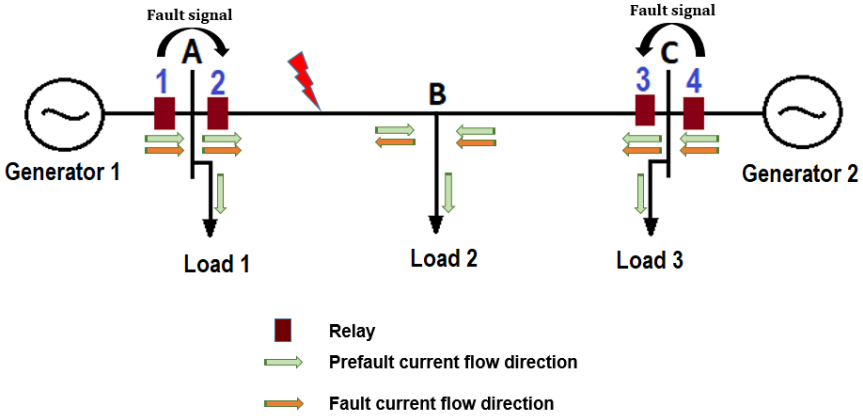


Figure 7.2: Coordination of Relays with the largest load at the tap point B

one of the slave relays is towards the busbar. After a fault occurrence on the line, the situation becomes consistent with the previous case due to a change in current flow direction registered by either Relay 2 or Relay 3. This is illustrated in Fig. 7.3 with the largest load connected at Bus A.

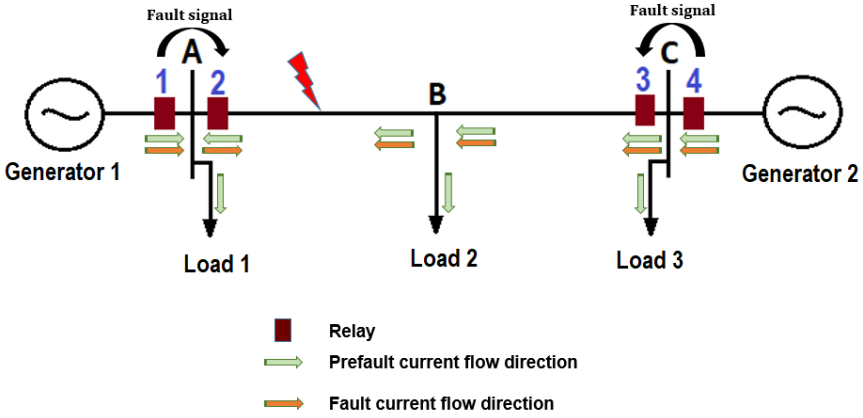


Figure 7.3: Coordination of Relays with the largest load at Bus A

As mentioned above, it may be possible that a load is connected to or disconnected from the system and leads to a change in current flow directions. For example considering the previous case (the largest load at Bus A), if an additional load (Load 4) is connected to Bus C so that the total load at Bus C becomes larger than the load at A, the slave relays (2 and 3) will register a change in current flow direction as shown in Fig. 7.4. However, since the slave relays are only activated by a signal from their respective master relays, there will be no operation of the protection system as there is no fault to be detected by the master relays. However, even if the switching event was severe enough to cause large ROCOSP values (detected as fault condition by master relays), it would be considered as

an external disturbance and no line would be isolated. The case of a fault on the busbar is described in the subsequent sections.

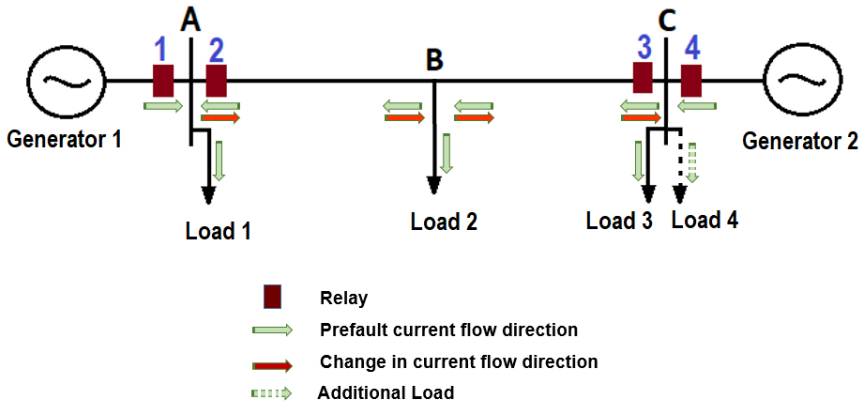


Figure 7.4: Relay coordination for load switching event causing change of current flow direction seen by Relays 2 and 3

It is important to note that complex and large meshed microgrids, time accumulation of the communication between relays should be taken into account to ensure that the time clearance requirement is met. Also, microgrid generation mix can affect the fault clearance time as some generation technologies such as small gas turbine, internal combustion based generators, etc. generate higher fault currents than IIDGs, and the fault might be required to be cleared faster. Moreover, a microgrid can provide less constant frequency operation if gas turbine is the only type of generation, or dominates the generation mix.

7.4 Study Microgrid and Simulation Results

The proposed protection scheme is tested using four-bus loop-based microgrid system given in Fig. 7.5. The general control structure of inverter interfaced generator (IIDG) is shown in the white background of Fig. 6.3, duplicated as Fig. 7.6 for ease of reference. The black background of the figure shows the circuit with the main elements of the IIDG including the inverter, the LC filter, and the step-up transformer. The study microgrid adopted in this Chapter presents a tapped line to the microgrid used in Chapter 6. As highlighted in Chapter 6, there are no impediments to using a more complex system such as the CIGRE MV network benchmark, but more in-depth analysis would be required.

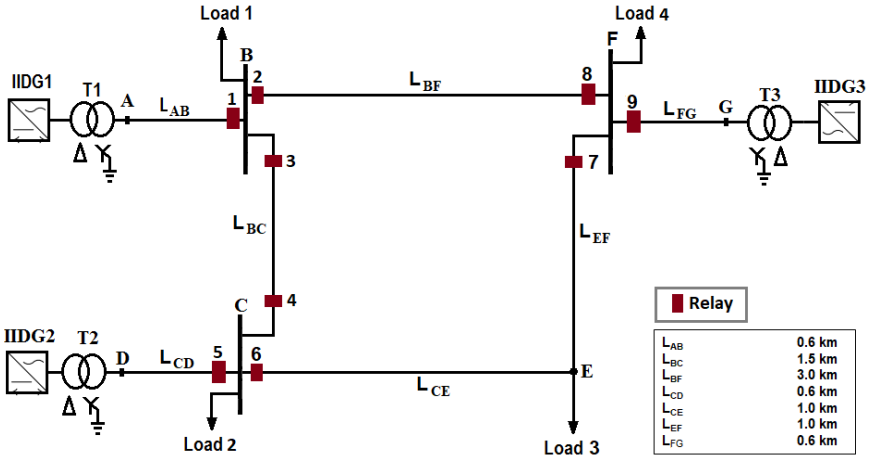


Figure 7.5: Four-bus loop-based microgrid

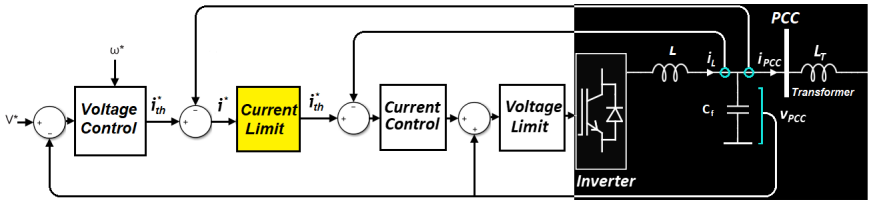


Figure 7.6: IIDG control structure

The study system was implemented and simulated in MATLAB/SIMULINK environment. The parameters of the system elements are given in Table 7.1. Each of the IIDGs is controlled in the synchronous reference frame using PI controller. A master-slave power sharing control strategy is adopted whereby the IIDG 1 is the master that forms the voltage and frequency of the microgrid, and share the current references i_{ref} generated by its voltage controller to the current controllers of the slave IIDGs. The current reference of each IIDG is limited to 120% of the rated current based on latched limiting strategy as one of the most popular inverter limit strategies [108].

Once a fault occurs, the references from the master IIDG's voltage controller are replaced by pre-defined current references $i_{ref}^{'}$ chosen such that converter's power factor (PF) during fault is 0.56 lagging ($I_q = -1.0$ and $I_d = 0.67$). This PF is used just as an example. Case studies with different PF values have been extensively investigated in Chapter 6. The positive sequence current phasor angle of the fundamental frequency (50 Hz) were estimated using conventional recursive discrete Fourier transform (DFT) over a power cycle window (20 ms). This method is the basis of the proposed scheme and has been chosen as it is very well understood phasor estimation technique and prevalent in protective relays due to its immunity to harmonics, computational simplicity and

efficiency [128].

Four simulation scenarios are considered: a fault on a line protected by a master relay; a fault on a line protected by slave relays; a fault on a tapped line; and a fault on a busbar. The latter case represents an external fault to the proposed scheme's protection zone. For each of all scenarios under this study, a permanent fault is initiated at time instant t = 0.15 s with a simulation period of 0.3 s. Fig. 7.7 provides the IIDGs output voltages and currents during different fault types on Line L_{AB}.

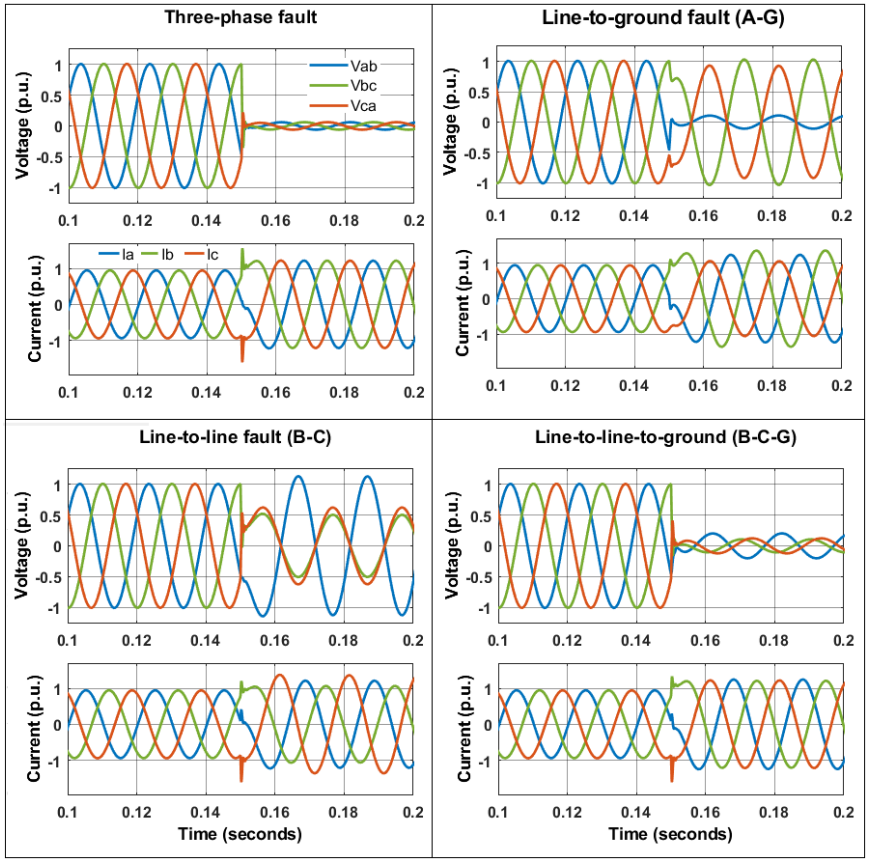


Figure 7.7: IIDGs voltage and current output during different types of fault

It can be seen that the IIDGs generate nearly balanced fault currents for unbalanced faults. This means that the configuration of the transformer interfacing the IIDG to the network has an impact on the currents supplied to the fault and the voltage waveform. The proposed scheme has been tested for all configurations during the study. The case presented in this study considered a Delta-Wye configuration as it is usually used to prevent multiple sources of ground fault currents.

Simulation results for a three phase, single phase to ground fault and phase to phase faults are

Table 7.1: Study microgrid parameters

IIDG Parameters			
	IIDG 1	**IIDG 2**	**IIDG 3**
Rated power (kVA)	1000	1000	1000
Rated voltage (V)	260	260	260
DC bus voltage (V)	500	500	500
Fundamental frequency (Hz)	50	50	50
Switching frequency (kHz)	5	5	5
Filter inductance (mH)	0.0264	0.0264	0.0264
Filter resistance (mΩ)	0.067	0.067	0.067
Filter capacitance (mF)	2.4	2.4	2.4
Damping resistance (mΩ)	15.5	15.5	15.5
Current control proportional	0.1658	0.1658	0.1658
Current control integral	0.4199	0.4199	0.4199
Voltage control proportional	1.4965	1.4965	1.4965
Voltage control integral	0.00	0.00	0.00
Step-up Transformer Parameters			
Rated power (kVA)	1200	1200	1200
Rated primary voltage (kV)	0.260	0.260	0.260
Rated secondary voltage (kV)	20	20	20
Configuration (vector group)	D1Yg	D1Yg	D1Yg
Fundamental frequency (Hz)	50	50	50
Winding inductance (pu)	0.03	0.03	0.03
Winding resistance (pu)	0.001	0.001	0.001
Line Parameters			
Line type	Overhead		
Positive sequence parameters	Resistance (Ω/km)	Reactance (Ω/km)	Susceptance (μS/km)
	0.510	0.366	3.172
Zero sequence parameters	Resistance (Ω/km)	Reactance (Ω/km)	Susceptance (μS/km)
	0.658	1.611	1.280

considered for different cases. However, it is impossible to exhaustively simulate all faults for each case in this chapter.

7.4.1 Detection of disturbance occurrence in the microgrid

As above discussed, the local ROCOSP is used to detect a disturbance in the microgrid and to discriminate a fault on a line protected by a master relay from a fault elsewhere in the microgrid network. To provide a clear understanding on this, a load switching event was simulated in the system on Bus B. For the simulation purposes, the system loading is shared as follows: initially, the system was simulated with Load 1 = 0.5 MW, Load 2 = 0.7 MW, Load 3 = 0.2 MW, and Load 4 = 0.2 MW. After 0.15 s, an additional load of 1.2 MW was then connected to bus B. This load is more than a third of the total system load capacity and is used to ensure that an appreciable load is used to see the effect of the event on the ROCOSP. Simulation results, as given in Fig. 7.8, show that the phase angle difference between phase angles measured before and during the event, the slope, and ROCOSP maximum absolute values estimated by all master relays stay relatively small ($\leq$ 40 degrees, 6 Hz and 40 Hz/s respectively) for both 50 Hz (Fig. 7.8 (b), (c), (d)) and 52 Hz (Fig. 7.8 (f), (g), (h)) operating frequencies compared to Relay 4 that registered significantly larger maximum absolute values (close to 180 degrees, 25 Hz and greater than 1000 Hz/s respectively). Knowing that the large values estimated by Relay 4 are due to the change in current flow direction after the additional load in the system, it can be seen that simulation results are close to theoretical values previously calculated.

Furthermore, the calculation of the average values of angle difference, phase angle slope and ROCOSP over a cycle provides steady increase towards the maximum values rather than instantaneous step change from zero to the maximum value after a cycle. This means that a change in current flow direction can be detected before the values reach the maximum value. This threshold can be set at half the maximum values to ensure faster detection (half a cyle). In this study, change in current flow direction in the lines protected by master relays is set at a ROCOSP value of 600 Hz/s.

On the other hand, when a fault is external to a relay line, the master relays are expected to detect the disturbance based on ROCOSP as well. However, the threshold for a fault detection is far less than that of change in current flow direction in the master relay line. So any threshold value other than zero can be used. This is because even a severe switching event (generator disconnection or large load connection/disconnection) is discriminated by the protection scheme as an external disturbance to the scheme zone of protection. In this study a 50 Hz threshold is set to reduce

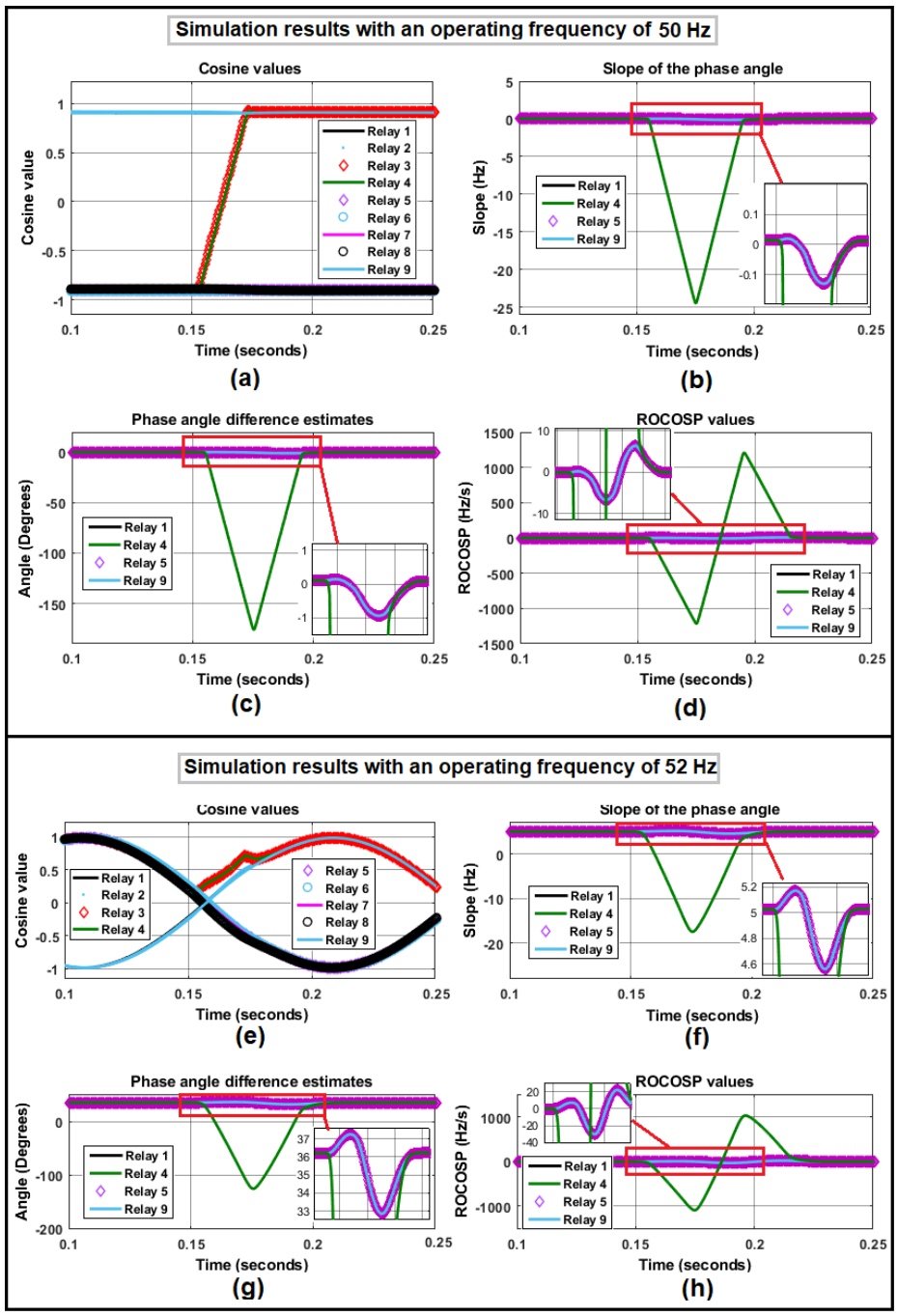


Figure 7.8: Simulation results for two different operating frequencies (50 and 52 Hz) for a load switching event at Bus B causing a change in current flow direction in the line protected by Relay 4: (a & e) cosine values computed by all relays; (b & f) phase angle difference between the two consecutive cycle estimates (degrees); (c & g) slope of the positive sequence current phasor angle (Hz); and (d & h) rate of change of the phase angle slope (ROCOSP in Hz/s)

frequent false disturbance alarms.

A three-phase fault is simulated on Line L_{AB}. The loads at the buses are distributed as follows: Load 1 = 0.8 MW, Load 2 = 1.3 MW, Load 3 = 0.2 MW, and Load 4 = 0.5 MW. This is considered as the reference case. Simulation results, as presented in Fig. 7.9 (b), (d), and (f) provide the values local ROCOSP estimated by master relays 1, 5 and 9. It can be clearly seen that all master relays detected the disturbance occurrence in the system with Relay 1 registering the largest ROCOSP value due to the change in current flow direction in its line.

7.4.2 Identification of the faulted line

Once the disturbance is detected in the system by the master relays, the directionality feature is used to determine the faulted section. It is important to note that for the sake of simplicity, all relays around the busbar have the same monitoring direction, from the line to the bus, under all simulation scenarios to ensure effective comparison of the cosine values signs of slave relays with their respective master relay. Otherwise, care is required to ensure correct comparison.

Fault on a line protected by master relays: The fault on Line L_{AB} discussed in the previous section represents this case. Contrary to slave relays, master relays will always see the current flowing from the DG to the busbar during normal operation. So when the current flow direction seen by a master relay changes, the fault is identified to be on the line it protects.

Taking the case of a fault on Line L_{AB}, as explained in details in the previous subsection the fault was identified on the master relay line L_{AB}. Regarding the cosine value signs by different relays as shown in Fig. 7.9 (a), (c), and (e), it can be clearly seen that despite the operating frequency (nominal or off-nominal), before the fault Relays 1, 2, and 9 yields cosine values with opposite sign to those of Relays 3, 4, 5, 6, 7, and 8. After the fault, Relays 1, 5, 6, 7, and 8 register cosine values with opposite signs to the ones of Relays 2, 9, 3, and 4.

By applying the proposed scheme principle as above described, the output of other relays are as follows:

- Relay 1 sends blocking signals to Relays 2 and 3, which in turn send blocking signals to their remote line relay counterparts, 8 and 4 respectively to overturn the disturbance signals received from their respective master relays 9 and 5. Thus, Lines L_{BF} and L_{BC} are kept connected.

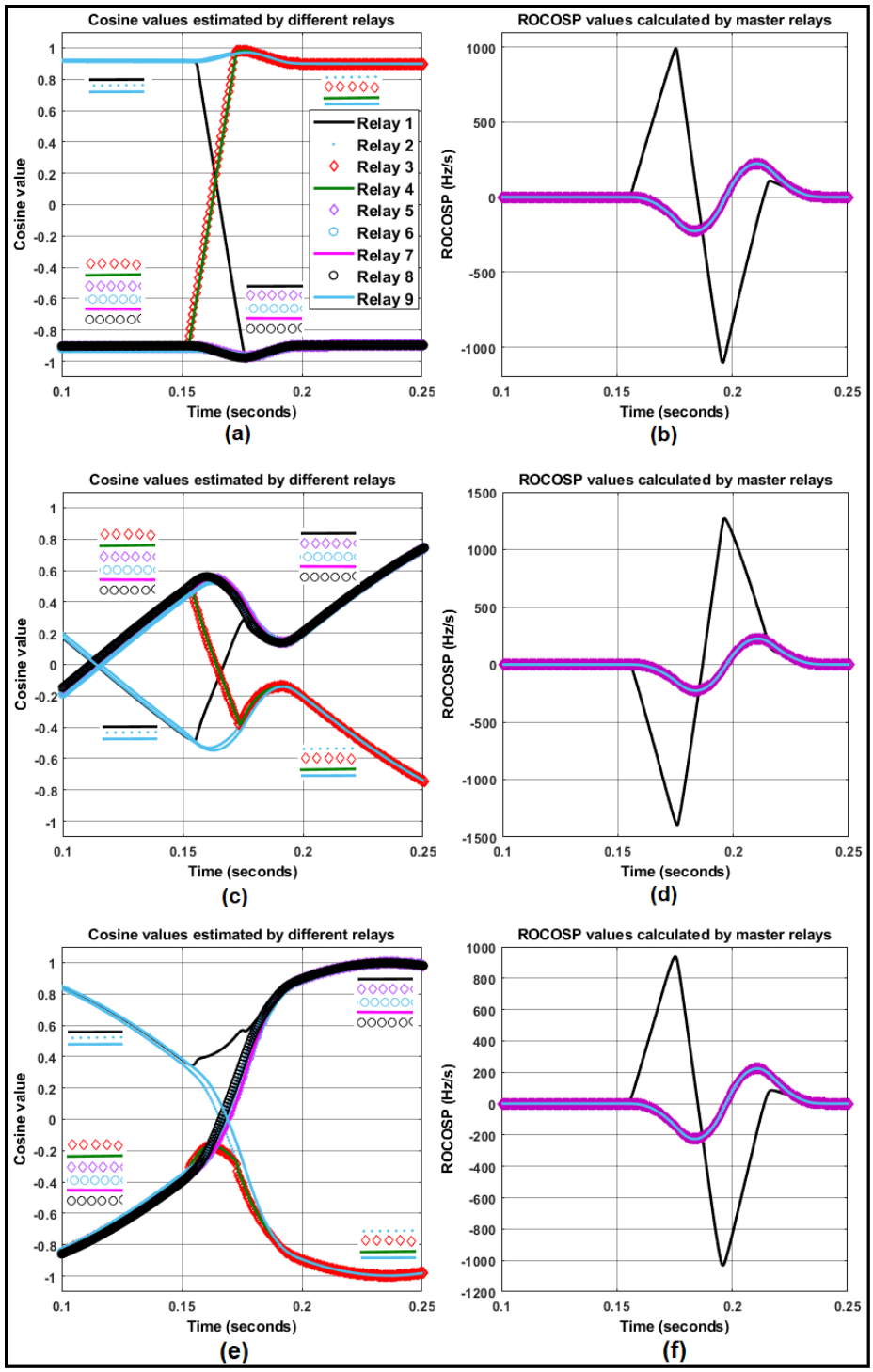


Figure 7.9: Simulation results for a three-phase fault on Line L_{AB}: Cosine and ROCOSP values estimated by relays with operating frequency of: (a & b) 50 Hz; (c & d) 52 Hz; (e & f) 48 Hz

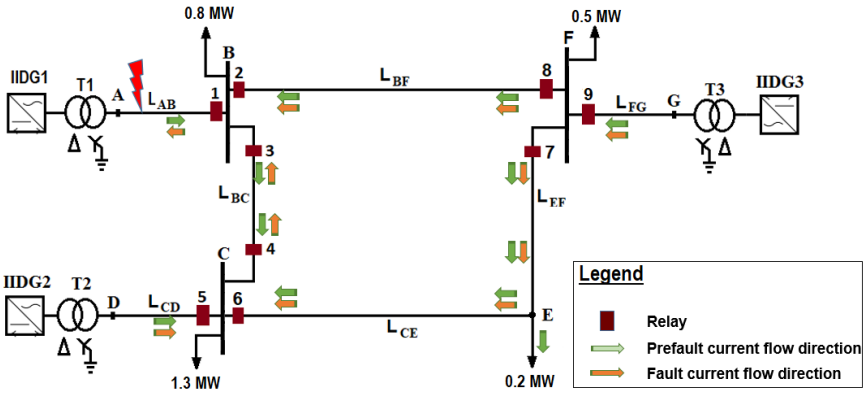


Figure 7.10: Current flow direction during normal operation (green) and during a fault on line L_{AB} (Orange)

- Relays 6 and 7 have received a fault signal with the cosine value signs from their master relays 5 and 9 respectively. The simulation results show that the cosine values of Relay 6 and its master relay 5 are the same while they are opposite for Relay 7 and its master relay 9. So Relay 6 sends a blocking signal to Relay 7 (its remote line relay counterpart) as the fault is external to their line, Line L_{CF}.

The combination of proposed relay coordination strategies has identified a fault on Line L_{AB}, since at least one relay of each of the other lines relays received a blocking signal indicating an external fault to their lines. The reflection of the results to the study system is illustrated in Fig. 7.10. The prefault current flow directions are based on the loading system while the fault current flow directions are derived from the simulation results.

Fault on a line protected by slave relays: A single phase to ground fault (Phase A to ground) is initiated in the middle of Line L_{BC}. The loads used are the same as those for the fault simulated previously on Line L_{AB}. The current flow directions in all lines of the system before and during the fault are shown in Fig. 7.12. These directions are derived from the cosine values as provided from simulation results in Fig. 7.11 (a) where clearly only Relay 4 registers a change in cosine value sign.

After the fault is detected by the master relays 1, 5, and 9, a as shown in Fig. 7.11 (b), the faulted line is identified as follows:

- Relays 2, 3, 4, 6, 7, and 8 receive fault signals from their respective master relays (1, 5, and 9) along with the signs of cosine values.

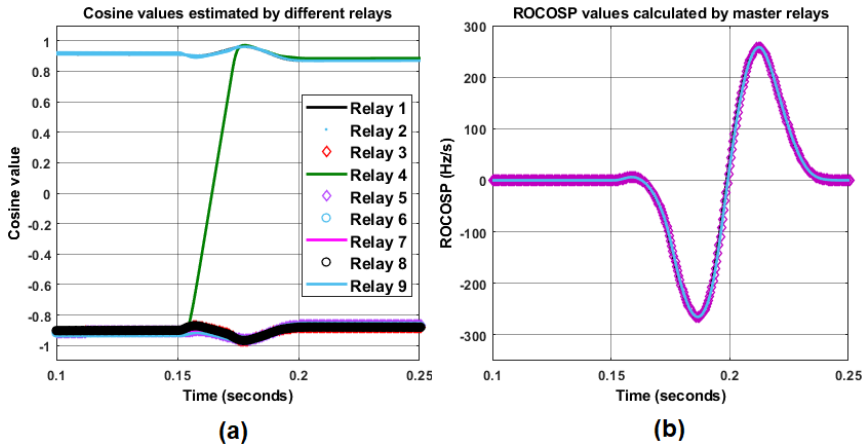


Figure 7.11: Simulation results for a Phase A to ground fault on Line L_{BC}: (a) Cosine values estimated by all relays; (b) ROCOSP values estimated by master relays

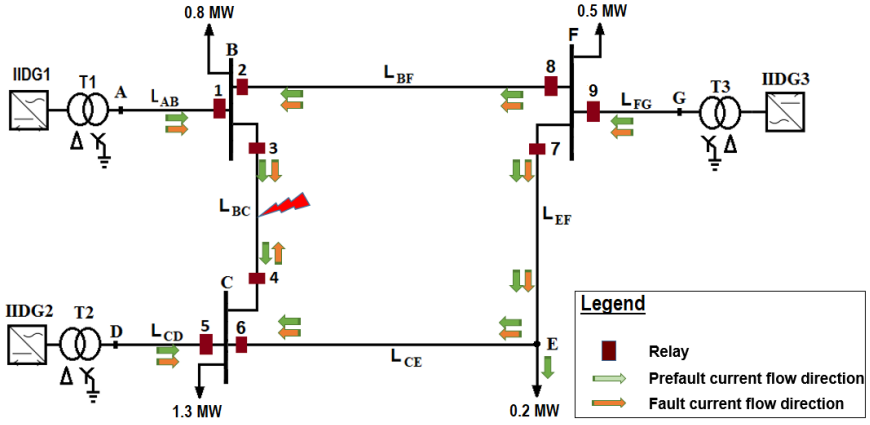


Figure 7.12: Current flow direction during normal operation (green) and fault (orange) on Line L_{BC}

- The slave relays compare the received value signs with theirs. Relays 2 and 6 output the same signs as their master relays 1 and 5 respectively, indicating an external fault to Lines L_{BF} and L_{CF}. So Relays 2 and 6 send blocking signals to Relays 8 and 7 respectively. The rest of the slave relays 3, 4, 7, and 8 register opposite cosine value signs to their master relays.

It can be seen that with exception to Relays 3 and 4, at least one of the other line relay pairs received a blocking signal. So, the Line L_{BC} protected by the pair (3,4) is identified as the faulted line to be isolated.

Fault on a tapped line: A phase to phase fault was simulated on Line L_{CF} on its part L_{EF} keeping other system parameters as in the reference case. As expected, the fault is detected by master relays using ROCOSP estimates as given in Fig. 7.13 (b). Also simulation results in Fig. 7.13 (a) show that there is no change in current flow direction in any of the lines protected by the master relays 1, 5 and 9 as illustrated in Fig. 7.14. Therefore, the fault is on one of the loop lines. The identification of the faulted line is as follows:

- Relays 2, 3, 4, 6, 7, and 8 receive fault signals from their respective master relays (1, 5, and 9) along with the signs of the cosine values.
- The comparison of the received cosine signs from the master relays with the one of slaves shows that only Relays 4 and 8 register the same sign as their master relays. Consequently, the fault is external to Lines L_{BC} and L_{BF}. So Relays 4 and 8 send blocking signals to Relays 3 and 2 respectively.

With only Relays 6 and 7 having not received a blocking signal, the fault is confirmed on the line they are protecting, Line L_{CF}.

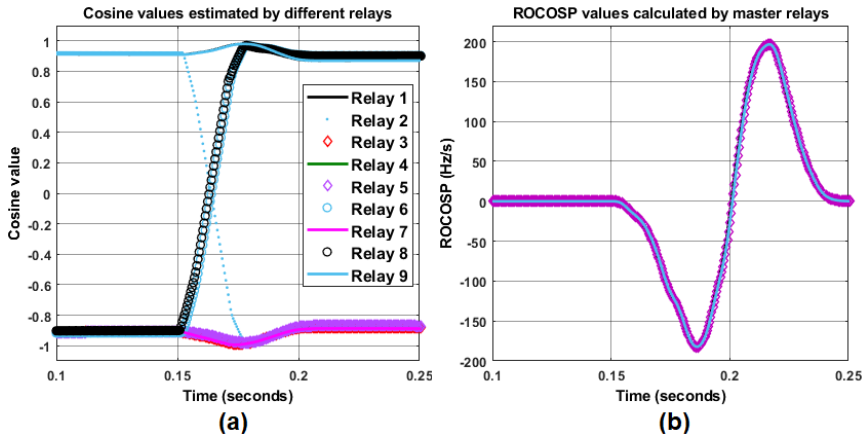


Figure 7.13: Simulation results for a fault on Line L_{EF}: (a) Cosine values estimated by all relays; (b) ROCOSP values estimated by master relays

Fault on a bus: A fault on a bus is external to all lines. So all relays are expected to keep their lines connected as busbars are considered out of the proposed scheme's protection zone. To verify how the scheme responds to such a fault, a single phase to ground fault was initiated on Bus B with other simulation conditions kept the same as the reference case. The associated simulation

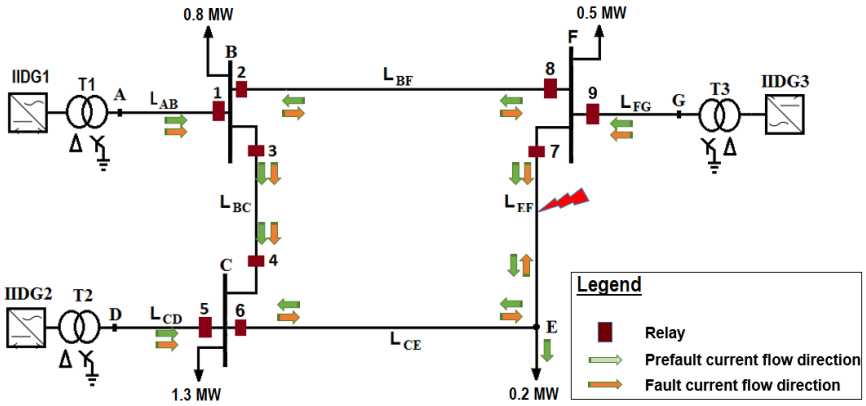


Figure 7.14: Current flow direction during normal operation (green) and fault (orange) on Line L_{EF}

results for this scenario are given in Fig. 7.15 (a) with the positive sequence current flow directions illustrated in Fig. 7.15 (c).

Under the same simulations conditions, synchronous generators with the same capacity as the IIDGs were used instead of the IIDGs. The corresponding simulation results are provided in Fig. 7.15 (b). These results are consistent with those in Fig. 7.15 (a) as expected with the only difference in cosine and ROCOSP values due to difference in fault response.

To verify the effectiveness of the proposed scheme with different type of loads and DGs, Loads 1 and 2 were changed from purely resistive loads, 0.8 MW and 1.3 MW respectively, to loads consuming both active and reactive power, 0.8 MVA (P = 0.65 MW and Q = 0.45 MVAr) and 1.3 MVA (P = 1.1 MW and Q = 0.7 MVAr) respectively. With a single phase to ground fault on Bus B at time instant t = 0.35 s (the fault time instant was changed in this case to ensure that the fault occurs when the control system is stable), simulation results with IIDGs and synchronous DGs as given in (d) and (e) parts of Fig. 7.15 were consistent with the ones with loads consuming only active power.

A simple discussion on this scenario's simulation results is sufficient, since the results are the same as the ones for a fault on Line L_{BC} discussed in III.B.c with one exception. The only difference is the change of current flow direction registered by both Relays 3 and 4 rather than by only Relay 4 as it is for the scenario with a fault on Line L_{BC}. Therefore the sign of the cosine value calculated by Relay 3 is of the same sign as the one of its master relay, Relay 1. This leads to Relay 3 sending a blocking signal to Relay 4 to keep the line L_{BC} connected. Consequently, no line is isolated as all lines are kept connected by their relays.

This situation is the same as the one for the load switching event shown in Fig. 7.8 except that

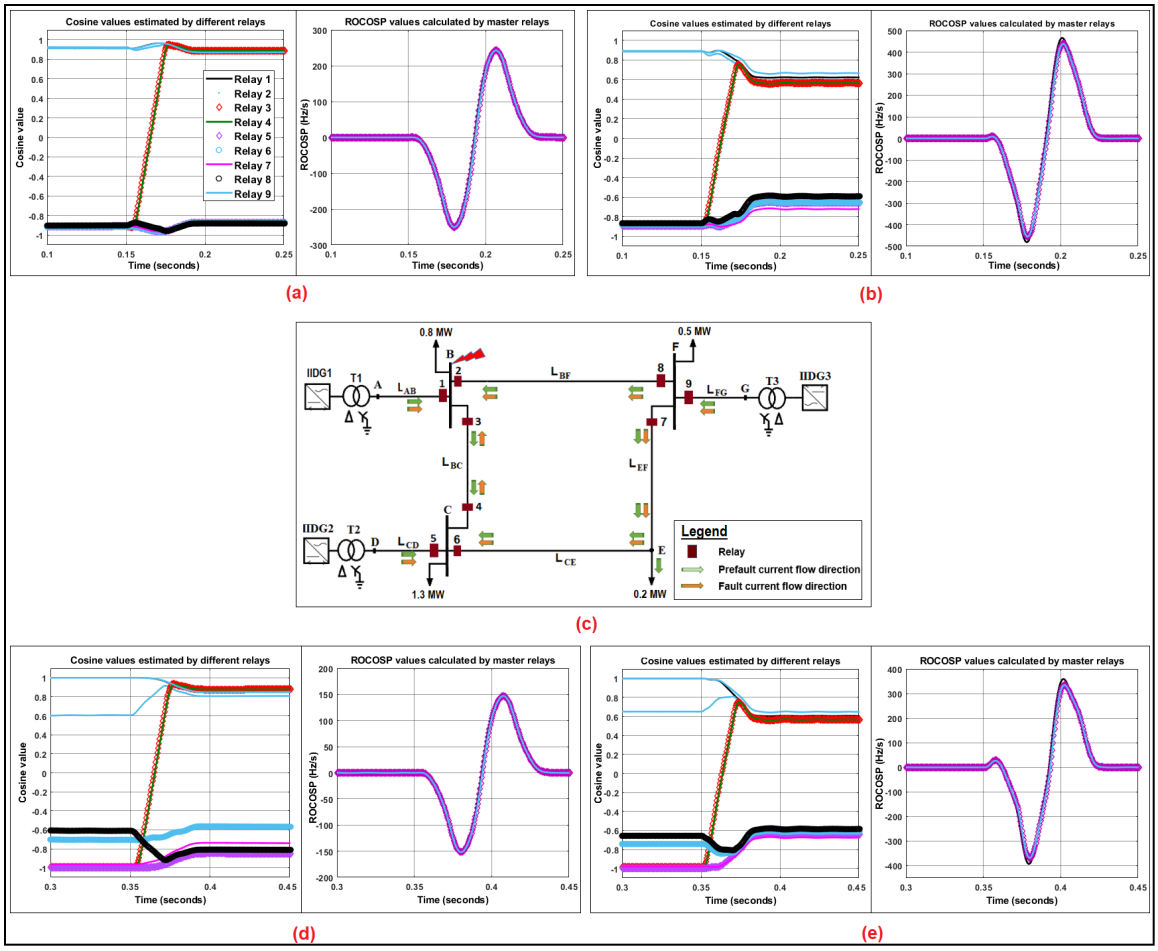


Figure 7.15: Cosine and ROCOSP values for a fault on Bus B in the microgrid constituting of: (a) purely resistive loads and only IIDGs; (b) purely resistive loads and only synchronous-based DGs; (d) inductive loads and only IIDGs; (e) inductive loads and only synchronous-based DGs; (c) Illustration of current flow direction during normal (green) and fault operating conditions (orange)

the disturbance detection threshold was not reached. However, assuming that the threshold was set lower, still the relay coordination based on cosine value sign would see it as an external disturbance. This is to say that any disturbance occurring on the busbar such as generator/load connection/disconnection or a fault is effectively discriminated from a fault on a line. This clearly shows the effectiveness of the proposed scheme to external faults. Yet, this can also indicate a possibility of extending the scheme to busbar protection. However, this is out of the scope of this study.

It is also important to recognise that the performance of a microgrid, particularly during faults

depends on many factors such as generation technology mix, control parameters of the IIDGs' controllers, step-up transformer configuration, type of loads supplied by the microgrid, and still need to be investigated in detail as they may have impacts on the operation of the proposed protection scheme, particularly in situations with interharmonics-rich waveforms.

Considering the latter, an indication of the effect of interharmonics on the proposed protection scheme is provided. While the interharmonic voltage limits are defined based on flickers in IEEE and IEC standards, it is suggested that for issues similar to harmonics, the limits should be similar to those of harmonics, specifically, the next higher even harmonic [129]. Following this approach, [129] recognises that even harmonic current limits for systems rated 120 V to 69 kV are more complicated as they depend on the frequency and the ratio of the short-circuit to load current in the range of 0.075% (high frequency harmonic ($\geq 35^{th}$ harmonic) and low short circuit ratios (≤ 20)) and 3.75% (low frequency ($\leq 11^{th}$ harmonic) and high short circuit ratios (≥ 1000)). One would expect therefore that the interharmonic current limits in multi-inverter microgrids to be lower than 3.75% due to low short circuit ratio in the microgrid and low frequencies due to lowpass filter in protective relays. Preliminary results have indicated that interharmonic currents below 3.75% of the line current do not affect the proposed scheme. However, in practice, this limit can be exceeded. In such a case, the effectiveness of the proposed scheme applied to the study microgrid may be compromised for interharmonic (below the 2^{nd} harmonic) current levels roughly above 6%.

7.5 Conclusions

A robust and low-bandwidth communication-assisted protection scheme based on current directionality feature estimated using the cosine of the current phase angle and ROCOSP has been investigated. With a fault detected in less than a cycle (around half a cycle), recalling that the total communication delay of less than a cycle, as established in the previous chapter, can be achieved, the proposed scheme can allow a fault detection in about three cycles. As a blocking scheme, this protection strategy may as well be used as a back-up protection to any line protection scheme using a communication means between the line terminals, such as differential protection, to save the cost of the back-up communication infrastructure as it can utilize the communication means of the healthy lines when the one for the faulted line fails. Considering the complexity that may exist in a microgrid, such as generation technology mix, control parameters of the inverters, type of loads, that may result in more complex practical situations beyond what has been reported in this work, further investigation can be undertaken to ensure that the scheme can be applied to any microgrid.

Chapter 8

Conclusions and Future Work

8.1 Summary of the Work

This study has highlighted the capability of the phasors in fault detection due to fault information they contain, particularly in distribution microgrids dominated by IIDGs where the application of transmission-based protection relays not only are costly but also fails in many cases. The behaviour of IIDGs mainly characterised by limited and controlled fault currents, distribution systems characterised by short lines and relatively low voltage levels as well as a departure from traditional radial topology of feeders due to DGs have been revealed to be at the origin of the failure of conventional distribution and transmission-based protection schemes. Effective protections of inverter-based microgrids requires relays that can overcome these challenges. Technically, it has been acknowledged that differential relays can overcome the challenges among other transmission and distribution system-based protection schemes. However, despite being technically satisfactory, differential relays are not economically viable due to their significantly high communication costs. The work in this report had two main aims:

- To find a parameter that can be appropriate for multi-inverter based microgrids considering their fundamental fault characteristics such as low and controlled short circuit current contributions. The positive sequence current phase angle has been identified for that purpose.
- To use the identified parameter to develop a protection strategy for multi-inverter based microgrids. Two protection schemes were proposed using the sign of the cosine of the positive

sequence current phase angle and the ROCOSP to estimated the change in current flow direction for fault detection and localisation. Expressing the directionality using the cosine and ROCOSP concepts provides a simple way of deriving low bandwidth information from the current phasors to allow the use of low-cost communication systems for line protection.

8.2 Future Work

8.2.1 Microgrid protection using current phase angle trajectory without communication system

In Chapter 7, it has been shown that the cosine concept can be enhanced by the ROCOSP into a more powerful protection scheme. More enhancement can still be brought to the scheme to eliminate the need for the communication channels between line relays. This can be achieved by finding a feature whose intensity varies with a fault location. This can then be used to detect the fault direction. A transient monitor, a parameter that is usually used to evaluate the quality of phasor estimate, has shown a potential with preliminary results being promising. The challenge, however, is to to find a normalisation technique of the transient monitor values for the protection scheme to be applied to all microgrid topologies and operation modes.

8.2.2 Protection speed improvement using fractional cycle DFT estimation technique

Protection schemes discussed in Chapters 6 and 7 are based on full cycle DFT phasor estimation technique. Though the full cycle provides immunity to harmonics and noise, the investigation of viability of fractional cycle DFT needs to be considered taking into account the speed it can provide. This would allow the extension of the protection technique to high voltage transmission lines and critical feeders that require fast fault clearance. However, the severe impact harmonics have on fractional DFT based phasor estimation should be carefully considered among others.

8.2.3 The impact of energy resources variation on the behaviour of power electronic based power sources

In Chapter 3, simulations have been provided with respect to the literature review on the behaviour of inverters during fault conditions. Most of these studies, as it is the case in this work, a DC source is considered constant. However, in real operation, the fuel availability variation, particularly with the renewable energy resources, may directly affect the behaviour of the generator and the system stability. A detailed investigation of the impact of energy resource variation on the fault behaviour of the Power Electronic-based Power Sources and the system will be carried out in the future.

8.2.4 Performance of current phase angle trajectory considering distribution automation systems

Feeder automation strategies, such as reclosers, sectionalizers, capacitor banks whose purpose may be related to protection, separation of the feeder into energized islands and faulted region, loss minimization, feeder restoration following major outages have not been covered under this scope as the focus has been on addressing the major issue of change of type of protection. The extension of the proposed approaches in such cases makes a potential interesting research work as more distribution feeders may be operated as microgrids in the future.

Bibliography

[1] A. Hooshyar and R. Iravani, "Microgrid protection," in *Proceedings of the IEEE*, vol. 105, no. 7, pp. 1332–1353, Jul. 2017.

[2] S. M. Brahma, J. Trejo, and J. Stamp, "Insight into microgrid protection," in *IEEE PES Innovative Smart Grid Technologies Europe,* Istanbul, 2014, pp. 1-6.

[3] N. Hatziargyriou, "MICROGRIDS – Large Scale Integration of Micro-Generation to Low Voltage Grids," in Proc. CIGRE Gen. Session, Paris, France, Paper no. C6-309, 2006, no. Lv, pp. 1–24.

[4] M. A. Zamani, T. S. Sidhu, and A. Yazdani, "A protection strategy and microprocessor-based relay for low-voltage microgrids," IEEE Trans. Power Deliv., vol. 26, no. 3, pp. 1873–1883, 2011.

[5] S. Chouhan, D. M. Barrett, H. Inan, A. Feliachi, and H. Mayfield, "Model based design of West Virginia Super Circuit(WVSC) microgrid system," in 2017 North American Power Symposium (NAPS), 2017, pp. 1–6.

[6] U. Tamrakar, D. Shrestha, M. Maharjan, B. Bhattarai, T. Hansen, and R. Tonkoski, "Virtual Inertia: Current Trends and Future Directions," Appl. Sci., vol. 7, no. 7, p. 654, 2017.

[7] CIGRE JWG B5/C6.26/CIRED, ""Protection of Distribution Systems with Distributed Energy Resources,"" 2015.

[8] H. Laaksonen, S. Zubic, and J. Ylinen, "Distributed Energy Resources Protection Requirements in Future Distribution Grids," pp. 1–10, 2017.

[9] A. Mazloomzadeh, M. H. Cintuglu, and O. A. Mohammed, "Islanding detection using synchronized measurement in smart microgrids," 2013 IEEE PES Conf. Innov. Smart Grid Technol. ISGT LA 2013, 2013.

[10] T. Loix, T. Wijnhoven, and G. Deconinck, "Protection of microgrids with a high penetration of inverter-coupled energy sources," 2009 CIGRE/IEEE PES Jt. Symp. Integr. Wide-Scale Renew. Resour. Into Power Deliv. Syst., pp. 1–6, 2009.

[11] A. R. Haron, A. Mohamed, H. Shareef, and H. Zayandehroodi, "Analysis and solutions of overcurrent protection issues in a microgrid," PECon 2012 - 2012 IEEE Int. Conf. Power Energy, no. December, pp. 644–649, 2012.

[12] X. Liu, M. Shahidehpour, Z. Li, X. Liu, Y. Cao and W. Tian, "Protection Scheme for Loop-Based Microgrids," in *IEEE Transactions on Smart Grid,* vol. 8, no. 3, pp. 1340-1349, May 2017.

[13] Z. Chmiel, S.C. Bhattacharyya, 'Analysis of off-grid electricity system at Isle of Eigg (Scotland): lessons for developing countries', Renew. Energy, 2015, 81, pp. 578–588, issn: 09601481, doi: 10.1016/j.renene.2015.03.061.

[14] K. Hirose, "Behavior of the Sendai microgrid during and after the 3.11 great east Japan disaster," in Proc. 35th IEEE Int. Telecommun. Energy Conf. (INTELEC), Hamburg, Germany, Oct. 2013, pp. 1–6.

[15] S. Tselepis, "12 years operation of the Gaidouromantra Microgrid in Kythnos island", COI-3869, 2014.

[16] L. Tao, C. Schwaegerl, S. Narayanan and J. H. Zhang, "From laboratory Microgrid to real markets — Challenges and opportunities," 8th International Conference on Power Electronics - ECCE Asia, Jeju, Korea (South), 2011, pp. 264-271.

[17] D. E. Olivares et al., "Trends in microgrid control," IEEE Trans. Smart Grid, vol. 5, no. 4, pp. 1905–1919, 2014.

[18] G. Lammert et al., "Activities of the Joint Working Group CIGRE C4 / C6 . 35 / CIRED: Modelling and Dynamic Performance of Inverter Based Generation in Power System Transmission and Distribution Studies," in 1st International Conference on Large-Scale Grid Integration of Renewable Energy in India, 2017.

[19] "Microgrid Protection Systems," Working Group C30, Subcommittee C of the Power System Relaying and Control Committee, July 2019.

[20] E. Casagrande, W. L. Woon, H. H. Zeineldin, and D. Svetinovic, "A Differential Sequence Component Protection Scheme for Microgrids With Inverter-Based Distributed Generators," in *IEEE Transactions on Smart Grid,* vol. 5, no. 1, pp. 29–37, Jan. 2014.

[21] H. H. Zeineldin, N. H. Kan'an, E. Casagrande, and W. L. Woon, "Data mining approach to fault detection for isolated inverter-based microgrids," in *IET Generation, Transmission Distribution,* vol. 7, no. 7, pp. 745-754, July 2013.

[22] S. Kar, S. R. Samantaray, and M. D. Zadeh, "Data-Mining Model Based Intelligent Differential Microgrid Protection Scheme," in *IEEE Systems Journal,* vol. 11, no. 2, pp. 1161-1169, June 2017.

[23] S. V Achanta, B. Macleod, E. Sagen, H. Loehner, and S. E. Laboratories, "Apply Radios to Improve the Operation of Electrical Protection," *SEL J. Reliab. Power,* vol. 1, no. 2, pp. 1–12, 2010.

[24] E. O. Schweitzer, D. Finney, and M. V. Mynam, "Applying radio communication in distribution generation teleprotection schemes," in *2012 65th Annual Conference for Protective Relay Engineers*, 2012, pp. 310–320.

[25] "Using Spread Spectrum Radio Communication for Power System Protection Relaying Applications," *IEEE PES PSRC Working Group H2 to the Power System Relaying Committee*, 2005.

[26] MEF, "Microwave Technologies for Carrier Ethernet Services," 2011.

[27] "High Penetration of Power Electronic Interfaced Power Sources (HPoPEIPS) - ENTSO-E Guidance document for national implementation for network codes on grid connection", ENTSO-E, 2017.

[28] S. Bhagavathy, N. Pearsall, G. Putrus, and S. Walker, "Performance of UK Distribution Networks with single-phase PV systems under fault", *International Journal of Electrical Power Energy Systems,* Volume 113, December 2019, Pages 713-725.

[29] H. Urdal, et. al "Future System Challenges in Europe - Contributions to Solutions from Connection Network Codes", 2016 CIGRÉ USNC International Colloquium.

[30] A. J. Roscoe, A. Dyśko, B. Marshall, M. Lee, H. Kirkham and G. Rietveld, "The Case for Redefinition of Frequency and ROCOF to Account for AC Power System Phase Steps," *2017 IEEE International Workshop on Applied Measurements for Power Systems (AMPS),* Liverpool, 2017, pp. 1-6.

[31] "Technical Report on the events of 9 August 2019", National Grid ESO, 2019.

[32] "GB power system disruption on 9 August 2019", Energy Emergencies Executive Committee (E3C): Final report, Department for Business, Energy and Industrial Strategy, 2020.

[33] EURAMET , "Evaluation report on the problem of ROCOF measurement in the context of actual use cases and the 'wish list' of accuracy and latency from an end-user point of view", 2018, Available online at: http://www.ROCOFmetrology.eu/wp-content/uploads/sites/21/2018/10/ROCOF-Uses-Cases-and-Test-Conditions-V1.pdf, Accessed 15th October 2019.

[34] M. Braun, C. Hachmann and J. Haack, "Blackouts, Restoration, and Islanding: A System Resilience Perspective," in IEEE Power and Energy Magazine, vol. 18, no. 4, pp. 54-63, July-Aug. 2020.

[35] "Black Start from Non-Traditional Generation Technologies," National Grid ESO, 2019.

[36] J. Shiles et al., "Microgrid protection: An overview of protection strategies in North American microgrid projects," *2017 IEEE Power Energy Society General Meeting*, Chicago, IL, 2017, pp. 1-5.

[37] J. MacDowell et al., "A Journey Through Energy Systems Integration: Trending Grid Codes, Standards, and IEC Collaboration," *in IEEE Power and Energy Magazine,* vol. 17, no. 6, pp. 79-88, Nov.-Dec. 2019.

[38] J. Matevosyan et al., "Grid-Forming Inverters: Are They the Key for High Renewable Penetration?" *in IEEE Power and Energy Magazine,* vol. 17, no. 6, pp. 89-98, Nov.-Dec. 2019.

[39] C. Roggatz, M. Power and N. Singh, "Power System Restoration: Meeting the Challenge to Resiliency from Distributed Generation," *in IEEE Power and Energy Magazine,* vol. 18, no. 4, pp. 31-40, July-Aug. 2020.

[40] A. Cagnano, E. De Tuglie, L. Cicognani, "Prince — Electrical Energy Systems Lab: A pilot project for smart microgrids," *Electric Power Systems Research,* Volume 148, 2017, Pages 10-17.

[41] X. Wang, J. M. Guerrero, and Z. Chen, "Control of grid interactive AC microgrids," IEEE Int. Symp. Ind. Electron., pp. 2211–2216, 2010.

[42] Y. Wang, X. Yin, D. You, T. Xu, and H. Xiang, "Development of wide area current differential protection IED based on IEC 61850," Transm. Distrib. Expo. Conf. 2008 IEEE PES Powering Towar. Futur. PIMS 2008, no. 2005, pp. 1–9, 2008.

[43] J. Rocabert, A. Luna, F. Blaabjerg, and P. Rodríguez, "Control of power converters in AC microgrids," *IEEE Trans. Power Electron.,* vol. 27, no. 11, pp. 4734–4749, 2012.

[44] A. D. Paquette and D. M. Divan, "Virtual Impedance Current Limiting for Inverters in Microgrids With Synchronous Generators," *in IEEE Transactions on Industry Applications,* vol. 51, no. 2, pp. 1630-1638, March-April 2015.

[45] F. Blaabjerg,"Control of power electronic converters and systems," vol. I (Academic Press-Elsevier, London, UK, 2018).

[46] P. S. A. Soman, Digital Protection of Power Systems, 2012.

[47] H. Bevrani, B. Francois, and T. Ise, Microgrid dynamics and control. Hoboken, NJ, USA: John Wiley Sons, Inc., 2017.

[48] H. Han, X. Hou, J. Yang, J. Wu, M. Su, and J. M. Guerrero, "Review of power sharing control strategies for islanding operation of AC microgrids," IEEE Trans. Smart Grid, vol. 7, no. 1, pp. 200–215, 2016.

[49] Y. Zhou and C. Ngai-Man Ho, "A review on Microgrid architectures and control methods," 2016 IEEE 8th Int. Power Electron. Motion Control Conf. IPEMC-ECCE Asia 2016, pp. 3149–3156, 2016.

[50] S. M. Kaviri, M. Pahlevani, P. Jain, and A. Bakhshai, "A review of AC microgrid control methods," 2017 IEEE 8th Int. Symp. Power Electron. Distrib. Gener. Syst. PEDG 2017, 2017.

[51] Y. Li and Y. W. Li, "Power management of inverter interfaced autonomous microgrid based on virtual frequency-voltage frame," IEEE Trans. Smart Grid, vol. 2, no. 1, pp. 18–28, 2011.

[52] F. Blaabjerg, R. Teodorescu, M. Liserre, and A. V. Timbus, "Overview of control and grid synchronization for distributed power generation systems," IEEE Trans. Ind. Electron., vol. 53, no. 5, pp. 1398–1409, 2006.

[53] N. Bottrell and T. C. Green, "Comparison of current-limiting strategies during fault ride-through of inverters to prevent latch-up and wind-up," *in IEEE Transactions on Power Electronics,* vol. 29, no. 7, pp. 3786–3797, 2014.

[54] I. Sadeghkhani, M. E. Hamedani Golshan, A. Mehrizi-Sani, J. M. Guerrero and A. Ketabi, "Transient Monitoring Function–Based Fault Detection for Inverter-Interfaced Microgrids," *in IEEE Transactions on Smart Grid,* vol. 9, no. 3, pp. 2097-2107, May 2018.

[55] D. N. Zmood and D. G. Holmes, "Stationary frame current regulation of PWM inverters with zero steady-state error," *in IEEE Transactions on Power Electronics,* vol. 18, no. 3, pp. 814-822, May 2003.

[56] Z. Ali, N. Christofides, L. Hadjidemetriou, et al., "Design of an advanced PLL for accurate phase angle extraction under grid voltage HIHs and DC offset," *IET Power Electron.,* 2018, 11, (6), pp. 995–1008.

[57] M. Bobrowska-Rafal, K. Rafal, M. Jasinski, and M. P. Kazmierkowski, "Grid synchronization and symmetrical components extraction with PLL algorithm for grid connected power electronic converters - A review," Bull. Polish Acad. Sci. Tech. Sci., vol. 59, no. 4, pp. 485–497, 2011.

[58] N. Guerrero-Rodriguez, A. B. Rey-boué, A. Rigas, and V. Kleftakis, "Review of Synchronization Algorithms used in Grid-Connected Renewable Agents," Int. Conf. Renew. Energies Power Qual., vol. 1, no. 12, pp. 8–13, 2014.

[59] X.-Q. Guo, W.-Y. Wu, and H.-R. Gu, "Phase locked loop and synchronization methods for grid-interfaced converters: a review," PRZEGLAD ELEKTROTECHNICZNY (Electrical Rev., vol. 87, no. 4, pp. 33–2097, 2011.

[60] N. Jaalam, N. A. Rahim, A. H. A. Bakar, C. K. Tan, and A. M. A. Haidar, "A comprehensive review of synchronization methods for grid-connected converters of renewable energy source," Renew. Sustain. Energy Rev., vol. 59, pp. 1471–1481, 2016.

[61] Y. Yang, L. Hadjidemetriou, F. Blaabjerg, and E. Kyriakides, "Benchmarking of phase locked loop based synchronization techniques for grid-connected inverter systems," 9th Int. Conf. Power Electron. - ECCE Asia "Green World with Power Electron. ICPE 2015-ECCE Asia, pp. 2167–2174, 2015.

[62] V. Kaura and V. Blasko, "Operation of a phase locked loop system under distorted utility conditions," in IEEE Transactions on Industry Applications, vol. 33, no. 1, pp. 58-63, Jan.-Feb. 1997.

[63] S. Golestan, J. M. Guerrero and J. C. Vasquez, "Three-Phase PLLs: A Review of Recent Advances," in IEEE Transactions on Power Electronics, vol. 32, no. 3, pp. 1894-1907, March 2017.

[64] Z. Ali, N. Christofides, L. Hadjidemetriou, E. Kyriakides, Y. Yang, and F. Blaabjerg, "Three-phase phase-locked loop synchronization algorithms for grid-connected renewable energy systems: A review, Renewable and Sustainable Energy Reviews," Volume 90, 2018, Pages 434-452.

[65] P. Rodriguez, J. Pou, J. Bergas, J. I. Candela, R. P. Burgos and D. Boroyevich, "Decoupled Double Synchronous Reference Frame PLL for Power Converters Control," in IEEE Transactions on Power Electronics, vol. 22, no. 2, pp. 584-592, March 2007.

[66] Z. Ali, N. Christofides, K. Saleem,A. Polycarpou, K. Mehran, "Performance Evaluation and Benchmarking of PLL Algorithms for Grid-Connected RES Applications," *IET Renew. Power Gener.* 2019, 14, 52–62.

[67] L. Hadjidemetriou, E. Kyriakides and F. Blaabjerg, "A New Hybrid PLL for Interconnecting Renewable Energy Systems to the Grid," in IEEE Transactions on Industry Applications, vol. 49, no. 6, pp. 2709-2719, Nov.-Dec. 2013.

[68] A. Cagnano, E. De Tuglie, and P. Mancarella, "Microgrids: Overview and guidelines for practical implementations and operation," *Applied Energy,* Volume 258, 2020, 114039.

[69] S. M. A. Solar and T. Ag, "Technical Information Short-Circuit Currents Information on short-circuit currents of SMA PV inverters 1 Response to Voltage Dips," pp. 1–5.

[70] C. Vaucourt, "Choosing Inductors and Capacitors for DC/DC Converters Large-Signal vs Small-Signal Response," no. February, p. 6, 2004.

[71] J. Keller and B. Kroposki, "Understanding Fault Characteristics of Inverter-Based Distributed Energy Resources," January, 2010.

[72] M. Brucoli, T. C. Green and J. D. F. McDonald, "Modelling and Analysis of Fault Behaviour of Inverter Microgrids to Aid Future Fault Detection," *IEEE International Conference on System of Systems Engineering,* 2007, pp. 1-6.

[73] Z. Shuai, C. Shen, X. Yin, X. Liu and Z. J. Shen, "Fault Analysis of Inverter-Interfaced Distributed Generators With Different Control Schemes," *in IEEE Transactions on Power Delivery,* vol. 33, no. 3, pp. 1223-1235, June 2018.

[74] C. A. Plet, M. Brucoli, J. D. F. McDonald, and T. C. Green, "Fault models of inverter-interfaced distributed generators: Experimental verification and application to fault analysis," *IEEE Power Energy Soc. Gen. Meet.,* pp. 1–8, 2011.

[75] S. Conti, "Protection issues and state of the art for microgrids with inverter-interfaced distributed generators," in *Clean Electrical Power (ICCEP), 2011 International Conference on Clean Electrical Power (ICCEP)*, June 2011, pp. 643–647.

[76] S. Mirsaeidi, X. Dong, S. Shi, and B. Wang, "AC and DC Microgrids: A Review on Protection Issues and Approaches," *J. Electr. Eng. Technol.*, vol. 12, no. 6, pp. 2089–2098, 2017.

[77] L. Yashen, et al., "Research Roadmap on Grid-Forming Inverters" *Golden, CO: National Renewable Energy Laboratory,* NREL/TP-5D00-73476, 2020.

[78] N. Tummasit, S. Premrudeepreechacharn, and N. Tantichayakorn, "Adaptive overcurrent protection considering critical clearing time for a microgrid system," Proc. 2015 IEEE Innov. Smart Grid Technol. - Asia, ISGT ASIA 2015, 2016.

[79] F. Coffele, C. Booth, and A. Dyśko, "An Adaptive Overcurrent Protection Scheme for Distribution Networks," IEEE Trans. Power Deliv., vol. 30, no. 2, pp. 561–568, 2015.

[80] P. Mahat, Z. Chen, B. Bak-Jensen, and C. L. Bak, "A simple adaptive overcurrent protection of distribution systems with distributed generation," IEEE Trans. Smart Grid, vol. 2, no. 3, pp. 428–437, 2011.

[81] H. Laaksonen, D. Ishchenko, and A. Oudalov, "Adaptive protection and microgrid control design for Hailuoto Island," IEEE Trans. Smart Grid, vol. 5, no. 3, pp. 1486–1493, 2014.

[82] G. Buiges, A. Dysko, I. Zamora, and E. Fernandez, "Microgrid Protection: Technical challenges and existing techniques," Int. Conf. Renew. Energies Power Qual., vol. 11, no. 11, pp. 1–6, 2013.

[83] M. Dewadasa, R. Majumder, A. Ghosh, and G. Ledwich, "Control and protection of a microgrid with converter interfaced micro sources," 2009 Int. Conf. Power Syst. ICPS '09, no. 1, pp. 25–30, 2009.

[84] M. Dewadasa, "Protection of microgrids using differential relays," *Univ. Power Eng. Conf. (AUPEC),* 2011 21st Australas., no. January, pp. 1–6, 2011.

[85] T. Shono et al., "Next generation protection system over ethernet," 10th IET Int. Conf. Dev. Power Syst. Prot. (DPSP 2010). Manag. Chang., pp. 83–83, 2010.

[86] M. P. Nthontho, S. P. Chowdhury, S. Winberg, and S. Chowdhury, "Protection of domestic solar photovoltaic based microgrid," 11th IET Int. Conf. Dev. Power Syst. Prot. (DPSP 2012), pp. P94–P94, 2012.

[87] E. Sortomme, S. S. Venkata, and J. Mitra, "Microgrid protection using communication-assisted digital relays," *IEEE Trans. Power Deliv.,* vol. 25, no. 4, pp. 2789–2796, 2010.

[88] J. Tang and P. G. McLaren, "A wide area differential backup protection scheme for shipboard application," 2005 IEEE Electr. Sh. Technol. Symp., vol. 2005, no. 3, pp. 219–224, 2005.

[89] E. Sortomme, J. Ren, and S. S. Venkata, "A differential zone protection scheme for microgrids," *2013 IEEE Power Energy Society General Meeting*, Vancouver, BC, 2013, pp. 1-5.

[90] M. Xu, G. Zou, C. Xu, W. Sun, and S. Mu, "Positive sequence differential impedance protection for distribution network with IBDGs," *2016 IEEE International Conference on Power System Technology (POWERCON),* Wollongong, NSW, 2016, pp. 1-5.

[91] X. Yin, Z. Zhang, Z. Li, X. Qi, W. Cao, and Q. Guo, "The research and the development of the wide area relaying protection based on fault element identification," Prot. Control Mod. Power Syst., vol. 1, no. 1, p. 12, 2016.

[92] T. Alexopoulos, M. Biswal, S. M. Brahma and M. El Khatib, "Detection of fault using local measurements at inverter interfaced distributed energy resources," *2017 IEEE Manchester PowerTech,* Manchester, 2017, pp. 1-6.

[93] A. H. K. Alaboudy and H. H. Zeineldin, "Critical clearing time for isolating microgrids with inverter and synchronous based Distributed Generation," in *IEEE PES General Meeting*, 2010, pp. 1–6.

[94] "Microgrid protection: Advancing the State of the Art," SANDIA REPORT SAND2019-3167, March 2019.

[95] M. A. Zamani, A. Yazdani and T. S. Sidhu, "A Communication-Assisted Protection Strategy for Inverter-Based Medium-Voltage Microgrids," in *IEEE Transactions on Smart Grid,* vol. 3, no. 4, pp. 2088-2099, Dec. 2012.

[96] E. Dehghanpour, H. Kazemi Karegar, R. Kheirollahi and T. Soleymani, "Optimal Coordination of Directional Overcurrent Relays in Microgrids by Using Cuckoo-Linear Optimization Algorithm and Fault Current Limiter," *in IEEE Transactions on Smart Grid,* vol. 9, no. 2, pp. 1365-1375, March 2018.

[97] H. M. Sharaf, H. H. Zeineldin and E. El-Saadany, "Protection Coordination for Microgrids With Grid-Connected and Islanded Capabilities Using Communication Assisted Dual Setting Directional Overcurrent Relays," *in IEEE Transactions on Smart Grid,* vol. 9, no. 1, pp. 143-151, Jan. 2018.

[98] . Yazdaninejadi, S. Golshannavaz, D. Nazarpour, S. Teimourzadeh and F. Aminifar, "Dual-Setting Directional Overcurrent Relays for Protecting Automated Distribution Networks," *in IEEE Transactions on Industrial Informatics,* vol. 15, no. 2, pp. 730-740, Feb. 2019.

[99] A. M. Tsimtsios and V. C. Nikolaidis, "Towards Plug-and-Play Protection for Meshed Distribution Systems With DG," *in IEEE Transactions on Smart Grid,* vol. 11, no. 3, pp. 1980-1995, May 2020.

[100] H. Karimi, G. Shahgholian, B. Fani et al. "A protection strategy for inverter-interfaced islanded microgrids with looped configuration," *Electr Eng 101,* 1059–1073 (2019).

[101] K. A. Saleh and A. Mehrizi-Sani, "Harmonic Directional Overcurrent Relay For Islanded Microgrids With Inverter-Based DGs," *in IEEE Systems Journal,* 2020.

[102] A. Soleimanisardoo, H. Kazemi Karegar and H. H. Zeineldin, "Differential Frequency Protection Scheme Based on Off-Nominal Frequency Injections for Inverter-Based Islanded Microgrids," in *IEEE Transactions on Smart Grid,* vol. 10, no. 2, pp. 2107-2114, March 2019.

[103] X. Wang et al., "Studies on fault analysis and protection configuration schemes in an isolated micro-grid," *2014 IEEE PES General Meeting — Conference Exposition,* National Harbor, MD, 2014, pp. 1-5.

[104] S. T. P. Srinivas and K. S. Swarup, "Optimal relay coordination and communication based protection for microgrid," *2017 IEEE Region 10 Symposium (TENSYMP),* Cochin, 2017, pp. 1-5.

[105] A. Yazdani, and R. Iravani, Voltage-Sourced Converters in Power Systems: Modeling, Control, and Applications, John Wiley Sons Inc., Hoboken, New Jersey, 2010.

[106] B. Mahamedi and J. E. Fletcher, "The Equivalent Models of Grid-Forming Inverters in the Sequence Domain for the Steady-State Analysis of Power Systems," *in IEEE Transactions on Power Systems,* vol. 35, no. 4, pp. 2876-2887, July 2020.

[107] "Benchmark Systems for Network Integration of Renewable and Distributed Energy Resources," Task Force C6.04.02, CIGRE, 2014.

[108] I. Sadeghkhani, M. E. Hamedani Golshan, J. M. Guerrero and A. Mehrizi-Sani, "A Current Limiting Strategy to Improve Fault Ride-Through of Inverter Interfaced Autonomous Microgrids," in IEEE Transactions on Smart Grid, vol. 8, no. 5, pp. 2138-2148, Sept. 2017.

[109] P. Kundur, Power System Stability and Control. New York: McGrawHill, 1994.

[110] W. Li, J. He, D. Zhang, and Q. Zhang, "Directional pilot protection based on fault current for distribution network with Distributed Generation (DG)," in *The Journal of Engineering,* vol. 2017, no. 13, pp. 1327-1331, 2017.

[111] H. Gao, J. Li, and B. Xu, "Principle and Implementation of Current Differential Protection in Distribution Networks With High Penetration of DGs," in *IEEE Transactions on Power Delivery,* vol. 32, no. 1, pp. 565-574, Feb. 2017.

[112] B. S. I. S. Publication, "Short-circuit currents in three-phase a. c. systems Part 0: Calculation of currents," 2016, p. BS EN 60909-0:2016.

[113] Arun G. Phadke and James S. Thorp, Computer Relaying for Power Systems, 2nd ed. John Wiley Sons Ltd, 2009.

[114] E. Oran Brigham, "The Fast Fourier Transform and its Applications," 1998.

[115] A. G. Phadke, and J. S. Thorp, "Synchronized Phasor Measurements and Their Applications", Springer Science & Business Media, LLC, 2008.

[116] H. A. Darwish and M. Fikri, "Practical Considerations for Recursive DFT Implementation in Numerical Relays," *in IEEE Transactions on Power Delivery,* vol. 22, no. 1, pp. 42-49, Jan. 2007.

[117] M. M. Begovic, P. M. Djuric, S. Dunlap and A. G. Phadke, "Frequency tracking in power networks in the presence of harmonics," *in IEEE Transactions on Power Delivery,* vol. 8, no. 2, pp. 480-486, April 1993.

[118] IEEE/IEC International Standard - Measuring relays and protection equipment - Part 118-1: Synchrophasor for power systems - Measurements, in *IEC/IEEE 60255-118-1:2018 ,* vol., no., pp.1-78, 19 Dec.

[119] A. K. Pradhan, A. Routray, and S. Madhan Gudipalli, "Fault Direction Estimation in Radial Distribution System Using Phase Change in Sequence Current," in *IEEE Transactions on Power Delivery,* vol. 22, no. 4, pp. 2065-2071, Oct. 2007.

[120] A. Ukil, B. Deck, and V. H. Shah, "Current-Only Directional Overcurrent Relay," in *IEEE Sensors Journal,* vol. 11, no. 6, pp. 1403-1404, June 2011.

[121] "Fault Direction Parameter Indicator Device And Related Methods," by A. Ukil, B. Deck, and V. H. SHAH (2016, June 14). Patent US 9,366,715 B2.

[122] C. Zhou, G. Zou, J. Yang and X. Lu, "Principle of Pilot Protection based on Positive Sequence Fault Component in Distribution Networks with Inverter-interfaced Distributed Generators," *2019 IEEE PES GTD Grand International Conference and Exposition Asia (GTD Asia)*, Bangkok, Thailand, 2019, pp. 998-1003.

[123] Q. Li, H. Gao, D. Yu, and B. Xu, "Analysis and verification of a novel current comparison pilot protection," *2017 IEEE Conference on Energy Internet and Energy System Integration (EI2)*, Beijing, 2017, pp. 1-5.

[124] I. E. O. Schweitzer, K. Behrendt, and T. Lee, "Digital Communications for Power System Protection: Security , Availability , and Speed," *SEL J. Reliab. Power,* vol. 1, no. 1, 2010.

[125] D. P. Dickinson, "So Many Wireless Technologies ... Which Is the Right One for My Application?," 2015.

[126] Vernon Goler, ""Using the Universal Asynchronous Receiver Transmitter (UART) eTPU Function,"" 2004.

[127] A. H. Kasem Alaboudy, H. H. Zeineldin, and J. Kirtley, "Microgrid stability characterization subsequent to fault-triggered islanding incidents," in *IEEE Transactions on Power Delivery,*, vol. 27, no. 2, pp. 658–669, 2012.

[128] A. Ukil, B. Deck, and V. H. Shah, "Current-Only Directional Overcurrent Protection for Distribution Automation: Challenges and Solutions," *IEEE Transactions on Smart Grid,* vol. 3, pp. 1687-1694, 2012.

[129] Michael B. Marz, "Interharmonics: What they are, Where they come from and What they do", [Online] Available: https://ccaps.umn.edu/documents/CPE-Conferences/MIPSYCON-Papers/2016/Interharmonics.pdf.